POLITECNICO DI MILANO
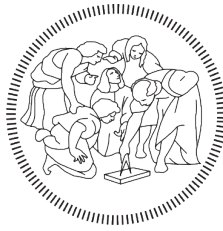
School of CIVIL, ENVIRONMENTAL AND LAND MANAGEMENT
ENGINEERING

Master degree in CIVIL ENGINEERING

POLITECNICO

MILANO 1863

ANALYSIS, DESIGN AND MODELING OF UNBONDED POST-TENSIONED CONCRETE SHEAR WALLS IN SEISMIC AREAS

Advisor: Prof. Franco MOLA
Co-Advisor: Jeffrey I. KEILEH, PE, SE, LEED AP BD+C

Candidates:
Stefano GEROSA   Matr. 817395
Beatrice MERONI   Matr. 819944

Academic Year 2014-2015

Abstract

In the seismic engineering philosophy it is becoming more and more important to realize structures that not only prevent the collapse but that can be cost-efficient as well, in terms of structural and non-structural repair and in terms of loss of business operation after the earthquake. The self-centering system is a lateral resisting system that could achieve the afore-mentioned enhancement, proving a restoring force that pulls the structure back to its undisplaced configuration. Particular self-centering systems are the unbonded post-tensioned hybrid concrete walls whose behavior is based on the possibility to have a gap opening at the joint between wall and foundation, combined with the presence of vertical unbonded post-tensioned tendons that provide a clamping force. The damping system is composed by steel bars debonded for a certain length inside the concrete that dissipate energy yielding in tension and compression. For this kind of structures the common code-based design procedures do not give correct results, because they do not take into account the unique behavior of these systems under seismic loads. On the contrary, the Direct Displacement-Based Design method starts from the definition of a target displacement that represents the expected performance of the building and takes into account the typical displacement profile and hysteresis rule of the structure from the very beginning. The strength design carried out with this method for an unbonded post-tensioned con-

crete wall, must be verified. Analytical models already present in literature used softwares that are not usually present in structural firms and therefore their results are not so easily applicable to real case studies. For this reason, the modeling of this particular structures is developed using a well-known and commercially available finite element software, ETABS 2015. All these considerations are applied to a real case study, the New Long Beach Civic Center, comparing different seismic design procedures and different configurations for the shear wall.

Sommario

Il seguente elaborato intende studiare particolari pareti a taglio in calcestruzzo con sistema di ricentraggio. A partire dagli agli '90 l'ingegneria sismica ha iniziato a studiare sistemi resistenti ad elevate prestazioni sismiche che potessero sopportare terremoti di progetto con danni e spostamenti differenziali residui limitati, in modo da ridurre le derivanti perdite economiche. Si é quindi cercato di prevenire la plasticizzazione delle componenti strutturali attraverso il formarsi di un meccanismo di apertura tra diversi elementi, in modo da smorzare la risposta strutturale. Trefoli post-tesi inseriti lungo tutta l'altezza della parete di taglio esercitano una forza in grado di riportare la struttura nella posizione verticale, minimizzando lo spostamento laterale residuo in seguito ad un evento sismico. La capacitá di ricentramento conferisce a questi nuovi sistemi il nome di *sistemi laterali ricentranti*. Questo comportamento puó essere definito come oscillante e necessita l'accoppiamento con sistemi di dissipazione, in modo da poter smorzare la risposta globale della struttura e conferirle duttilitá. Tipici sistemi dissipativi consistono in barre d'armatura lenta che dissipano energia tramite il loro allungamento, o in appositi dispositivi come gli smorzatori viscosi. Nel presente lavoro sono state considerate pareti a taglio in calcestruzzo con sistema di pretensione formato da cavi non aderenti e con sistema dissipativo composto da barre d'armatura lenta, le cosiddette *pareti di taglio ibride*. La figura mostra la

tipica elevazione di una parete di taglio ibrida post-tesa.
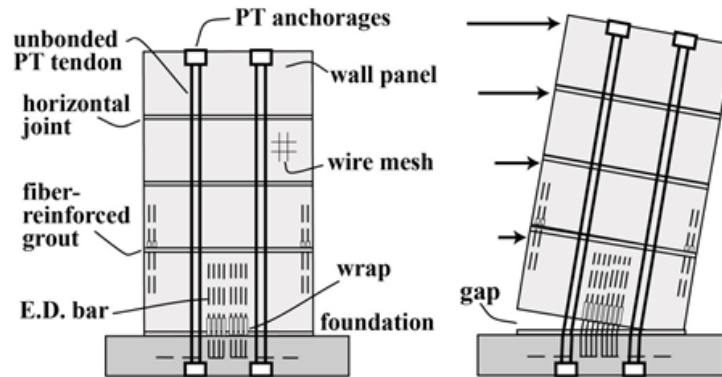
Il termine ibrido riflette il fatto che la connessione alla base del muro sviluppa resistenza laterale grazie a una combinazione di acciaio da post-tensione e di armatura lenta ordinaria. Quando si viene a formare l'apertura alla connessione tra muro e fondazione durante un terremoto, i cavi pretesi si allungano e le deformazioni si distribuiscono per tutta la lunghezza dei trefoli, essendo questi a fili non aderenti. I cavi sono progettati per rimanere elastici in modo tale da fornire la forza di ricentraggio in grado di riportare il muro nella configurazione indeformata quando l'azione sismica viene rimossa. Le barre d'acciaio ordinario invece si snervano a trazione e compressione essendo cosí fonte di dissipazione energetica attraverso la loro deformazione. Normalmente le barre sono svincolate rispetto al calcestruzzo lungo il muro per una certa lunghezza in modo tale da ridurre le deformazioni nel calcestruzzo e prevenire fratture dello stesso durante il loro allungamento. Esse vanno fin dentro la fondazione e risultano cosí ancorate ad essa ed alla zona di ancoraggio nel muro. Il maggior vantaggio di questo sistema é dovuto al fatto che se da un lato la risposta sismica di un muro ibrido é fondamentalmente diversa da quella di una parete tradizionale in calcestruzzo armato, le sue componenti costruttive sono convenzionali e standardizzate, senza la necessitá di utilizzare speciali dispositivi come gli smorzatori viscosi,

vii

che possono influire negativamente nell'economia dell'opera. Lo svantaggio
invece che comporta questo sistema é legato al fatto che le barre d'acciaio
non sono facilmente riparabili o sostituibili in caso di rottura, come lo sono
invece dispositivi esterni come gli smorzatori.

Come é noto, i terremoti inducono forze e spostamenti sulle strutture.
Tradizionalmente la progettazione strutturale sismica si é basata sulle forze
seguendo quanto fatto per altri tipi di carichi, come quelli permanenti ed
accidentali. In questo modo, le diverse normative per le progettazione si-
smica si basano sul metodo delle forze (Force-Based Design, FBD). Secondo
questo approccio, il periodo fondamentale stimato e la massa totale della
struttura sono la base per la determinazione del taglio di progetto alla base
della struttura, incorporando l'influenza dell'intensitá sismica in termini di
accelerazione spettrale. La procedura progettuale codificata parte da una sti-
ma iniziale delle rigidezza della struttura ipotizzando una prima valutazione
delle dimensioni dei vari elementi. Nell'analisi é presa in considerazione la
rigidezza elastica degli elementi e nel caso di strutture in calcestruzzo arma-
to, viene considerata una rigidezza ridotta che tiene conto delle fessurazioni
che compaiono nel calcestruzzo e la cui entitá varia da codice a codice. La
capacitá di spostamento laterale della parete compare invece come verifica
finale, in quanto prodotto del processo di progettazione. La duttilitá neces-
saria stimata per il sistema viene tenuta in conto riducendo la forza con cui
viene condotto il dimensionamento attraverso un parametro chiamato fattore
di struttura, il cui valore dipende dal tipo di struttura in esame.

Alcuni punti critici sono stati individuati nel sopracitato metodo delle
forze. Essi sono principalmente legati alla stima di rigidezza iniziale, chia-
ramente legata alle dimensioni degli elementi le quali peró possono essere
individuate con esattezza come risultato finale delle progettazione, ed alla

definizione di un unico fattore di struttura che possa rappresentare la duttilitá di un intero sistema strutturale. Si puó vedere per esempio, come pile o colonne con diversa lunghezza presentino un fattore di duttilitá molto diverso. Alla luce di queste considerazioni, un metodo di progettazione alternativo basato sugli spostamenti (Direct Displacement-Based Design, DDBD) é stato sviluppato da Priestley con l'intento di risolvere le varie lacune presenti nella metodologia considerata nelle normative odierne. La differenza fondamentale é basata sul fatto che il DDBD caratterizza la struttura attraverso una struttura equivalente ad un grado di libertá che ne rappresenti la prestazione allo spostamento di picco. L'approccio usato é quindi quello di progettare una struttura in grado di raggiungere una data prestazione in termini di spostamento durante uno specifico evento sismico. Il metodo degli spostamenti introduce fin dall'inizio in comportamento non-lineare dell'opera, definendo quindi una rigidezza secante equivalente al massimo spostamento di progetto ed uno smorzamento viscoso equivalente che corrisponde all'energia assorbita durante il terremoto, invece di caratterizzare la struttura attraverso le sue proprietá elastiche come nel FBD. La definizione della rigidezza effettiva risulta da quella di un certo livello di spostamento che stabilisce il periodo naturale effettivo della struttura, a sua volta basato sull'intensitá sismica in termini di spostamento spettrale. Dalla definizione di tutti questi parametri puó essere calcolato il valore del taglio alla base agente sull'elemento strutturale come prodotto tra il livello di spostamento laterale di progetto e la rigidezza effettiva. É stato dimostrato come tipicamente il metodo basato sugli spostamenti produca un valore di taglio alla base minore rispetto a quello ottenuto con il metodo basato sulle forze, riducendo cosí i costi della struttura.

Analizzando i due metodi presentati precedentemente, si puó notare co-

me se da un lato il primo consideri fattori di duttilitá generali per strutture particolari, il secondo invece incorpori nella sua procedura comportamento e legge dissipativa specifici della struttura che analizza. Nel caso di pareti di taglio ibride post-tese attraverso cavi di pretensione, il metodo degli spostamenti sembrerebbe riuscire a considerare il reale comportamento dell'elemento resistente tenendo conto del suo spostarsi come un corpo rigido e della legge isteretica caratteristica di questa tipologia strutturale. Essendo peró questo metodo basato su considerazioni sperimentali, necessita di una validazione analitica.

Per questo motivo uno degli obiettivi principali del seguente elaborato é quello di sviluppare un modello ad elementi finiti in grado di riprodurre il comportamento non lineare dei muri ricentranti durante un terremoto. In questo modo si é in grado di discernere quale metodologia di progettazione sismica tra FBD e DDBD risulti essere piú efficiente nel garantire il raggiungimento di un certo livello prestazionale della struttura imposto in fase di progettazione. Dal momento che non vi é la possibilitá di verificare la correttezza del dimensionamento e dei risultati analitici ottenuti tramite sperimentazione, inizialmente si é cercato di creare un modello analitico che riproducesse i risultati ottenuti in studi precedenti. Si é visto che molti di questi hanno utilizzato software non di comune utilizzo in studi di progettazione, rendendo la loro applicazione limitata al campo della ricerca. Dal punto di vista applicativo invece, le pareti di taglio ibride che sono state realizzate non presentano una procedura di modellizzazione dettagliata in ogni aspetto eseguendo tale operazione attraverso l'utilizzo di programmi ad elementi finiti con altissime potenzialitá. I software utilizzati in quest'ultimo caso risultano sconvenienti nella fase iniziale di concezione della struttura, in termini di tempo necessario per la modellazione e di successivo ottenimento

dei risultati.

La piú importante ricerca in questo ambito é la fase culminante di un programma di ricerca durato anni negli Stati Uniti e denominato *PRESSS (PREcast Seismic Structural Systems) research program*, che aveva l'obiettivo di sviluppare linee guida per l'utilizzo di strutture prefabbricate in zona sismica e di scoprire nuovi materiali e nuove tipologie strutturali in grado di sfruttare le peculiaritá delle strutture prefabbricate in calcestruzzo. In particolare nell'ultima fase, iniziata nel 1999, un edificio multipiano prefabbricato é stato progettato, costruito ed infine testato simulando le condizioni di carico di un evento sismico. La progettazione dell'edificio é stata realizzata confrontando i risultati ottenuti con le procedure FBD e DDBD affinché lo spostamento orizzontale al tetto dell'edificio fosse minore del 2% dell'altezza quando soggetto a un terremoto di design. Tale ricerca risulta interessante ai fine di questo lavoro in quanto l'edificio presenta in una direzione un sistema di resistenza laterale costituito da muri ricentranti. In questa fase inoltre, é stato sviluppato un modello ad elementi finiti che riproduca il comportamento di questi muri i cui risultati sono stati confermati sperimentalmente. Vista l'ampia documentazione disponibile per questa ricerca, si é cercato di riprodurre i risultati da loro ottenuti cosí da poter sviluppare una procedura di modellazione applicabile per altre configurazioni di muri con sistema di ricentraggio. Contrariamente a quanto sviluppato finora in letteratura, nel presente lavoro di ricerca la struttura é stata modellizzata utilizzando ETABS 2015, software di immediata applicazione e largamente usato negli studi di progettazione. Esso viene utilizzato nello studio di progettazione *Skidmore, Owings and Merrill LLP (SOM)*, societá di ingegneria riconosciuta a livello mondiale che ha collaborato nello sviluppo del seguente elaborato.

Il modello creato nel programma di ricerca PRESSS é stato analizzato

nel dettaglio per comprendere come sono stati riprodotti i comportamenti tipici del sistema ricentrante da loro utilizzato, come l'apertura alla base, il comportamento rigido dei pannelli in calcestruzzo, la dispersione di energia dovuta al sistema dissipativo utilizzato e la forza stabilizzante dovuta all'allungamento dei trefoli e al peso proprio. Una volta sviluppata una metodologia di modellazione, si ' visto come essa riproduca in maniera soddisfacente i risultati attesi. Sono state eseguite analisi statiche non-lineari e analisi dinamiche non-lineari in cui la struttura é stata soggetta ad eccitazioni sismiche simulate. Si é stati cosí in grado di modellare pareti di taglio ricentranti generiche, adattando con minime variazioni quanto é stato sviluppato a tipologie strutturali differenti, come per esempio ai muri ibridi precedentemente descritti. É stato cosí possibile verificare se il dimensionamento eseguito consentisse alla struttura di rispettare i limiti normativi e, dove presenti, i limiti prestazionali richiesti dal committente.

I metodi di progettazione sismica, il dimensionamento sviluppato e la procedura di modellazione precedentemente descritti sono stati tutti impiegati a un vero caso di studio, il progetto *New Long Beach Civic Center*, situato a Long Beach, California, USA. Il progetto consiste in 2 edifici multipiano uguali e regolari in pianta con fondazioni comuni per la cui progettazione é stato incaricato *Skidmore, Owings and Merrill LLP (SOM)*. Situato in una zona ad alto rischio sismico, tale edificio é considerato essenziale per la cittá e perció deve garantire prestazioni sismiche elevate in modo tale da non presentare interruzioni operazionali in seguito ad un terremoto. Infatti é richiesto che i danni subiti dall'edifico siano minimi, che la rioccupabilitá sia garantita in una settimana e la piena funzionalitá dell'edificio entro 30 giorni dal terremoto di progetto. In questo modo si minimizzano le perdite economiche causate da un terremoto. Per questo motivo le pareti di taglio convenziona-

li risultano inadeguate per il raggiungimento delle prestazioni richieste e le pareti di taglio ibride possono essere un'alternativa progettuale interessante. Infatti, tale tipologia di pareti di taglio concentra la nonlinearitá dell'elemento resistente nell'apertura alla base, garantendo che il calcestruzzo non si fessuri e non presenti quindi danni permanenti. Inoltre il sistema di precompressione a cavi non aderenti fornisce una forza ricentrante che rende trascurabili gli spostamenti residui dovuti a un terremoto. La duttilitá si sviluppa unicamente nell'armatura lenta appositamente introdotta e dimensionata, concentrando cosí i danni permanenti in questo componente che puó essere facilmente sostituito.

Una parete del *New Long Beach Civic Center* é stata presa in considerazione singolarmente, trascurando per il momento gli effetti torsionali dovuti all'accoppiamento di sistemi resistenti in direzioni ortogonali. Innanzitutto la procedura di analisi sismica DDBD eśtata applicata al caso di studio per calcolare le forze agenti alla base del muro, confrontando i risultati ottenuti con il metodo FBD. Esse sono state poi utilizzate per il dimensionamento della sezione alla base del muro, che risulta essere la piú critica, cosí da determinare i quantitativi di armatura e il numero di trefoli necessari per un corretto comportamento strutturale della parete di taglio ibrida. Il dimensionamento cosí ottenuto é stato verificato grazie ad un modello ad elementi finiti che segue le linee guida sviluppate precedentemente. Per far questo, sono state eseguite analisi statiche non-lineari, cicli isteretici e analisi dinamiche non-lineari sotto eccitazioni sismiche simulate.

La presente ricerca apre spunti interessante per futuri sviluppi. Infatti, una volta studiato il comportamento di una singola parete, essa puó essere studiata all'interno di un edificio come elemento componente il sistema resistente laterale. In questo caso l'interazione tra i diversi elementi costituenti

l'edificio, come altre pareti o solai, deve essere ulteriormente investigata. Altri aspetti fondamentali da indagare per il corretto funzionamento del sistema riguardano la progettazione del confinamento alla base, la prevenzione di slittamento a taglio e l'influenza del comportamento delle fondazioni sulla risposta della parete di taglio. Inoltre, si possono indagare ulteriori configurazioni oltre a quelle qui considerate, come per esempio quella che vede la presenza di un dispositivo ("bearing") alla base della parete che ne permette le rotazioni in tutte le direzione e ne blocca gli spostamenti. Tale configurazione puó essere accoppiata a dispositivi di dissipazione come smorzatori viscosi posti ai lati del muro. I vantaggi legati ad essa consistono nella possibilitá di un posizionamento piú eccentrico dei cavi che garantisce una maggiore capacitá di ricentramento ed nella eliminazione di problematiche legate a congestionamento della sezione alla base.

Contents

Chapter 1

Introduction

1.1 Historical Considerations

Earthquakes induce forces and displacements in structures. Traditionally, seismic structural design was based on forces. The reasons for this approach are historical, and linked to how we design for other actions, such as dead and live loads. Few structures were specifically designed for seismic actions before the 1930's [20]. After the occurrence of several major earthquakes in the 1920's and early 1930's (Japan, 1925 Kanto earthquake; USA, 1933 Long Beach earthquake; New Zealand, 1932 Napier earthquake), it was noted that structures with lateral force resisting systems performed better during these ground motions. As a result, the design for lateral inertia forces started to be specified in design codes for structures in seismic regions. Typically, the application of a vertically distributed lateral force vector equivalent to the 10 percent of the building weight was specified.

During the 1940's and 1950's, the importance of structural dynamic characteristics was recognized, leading to period-dependent design lateral force levels in most seismic design codes in the 1960's. Also during these years, seis-

mic response became better understood and inelastic time-history analysis
was developed. These developments helped to realize that many structures
had survived during seismic events even if their structural strength was many
times lower then the inertia forces induced by the earthquake. To explain the
survival of these structures with inadequate strength, the concept of ductility
was introduced. It has been recognized for some considerable time that well-
designed structures possess ductility and can develop inelastic response up to
the levels of deformation required by the earthquake without loss of strength.
This implies damage, but not collapse. For this reason we normally design
structures for force levels lower than those induced by elastic behavior and
we accept the possibility of damage under seismic actions as economically
acceptable, taking advantages from the decrease of the construction costs as-
sociated with the reduced design levels. The inelastic deformation capacity
of structural components was generally expressed in terms of displacement
ductility capacity. Relationships between this indicator of ductility and the
force-reduction factor were developed to determine the appropriate lateral
force design levels.

Ductility considerations became a fundamental part of the design and dur-
ing the 1960's and 1970's key text books that remain the pillars for seismic
design, were written. Later, during the 1970's and 1980's, the determination
of the available ductility capacity of different structural systems became the
objective of many researches. In order to quantify the available ductility
capacity, the value of the safe maximum displacement of different structural
systems under cyclically imposed displacement was established through ex-
tensive experimental and analytical studies. As we said previously, the re-
quired strength was then determined from a force-reduction factor linked to
the ductility capacity of the structural system and the material chosen for

the design. The displacement capacity was the final stage of the design and the design process was still carried out in terms of required strength. Also during this era the concept of "capacity design" was introduced. In fact, in New Zealand, in 1976 Park and Paulay developed the principles of capacity design after the realization that the distribution of strength in a building was more important than the absolute value of the design base shear [14]. It was recognized that a frame building would perform better during the seismic event if the formation of plastic hinges would take place in the beams rather than in the columns (weak beam/strong column mechanism) and if the shear strength of members was larger enough to inhibit shear failure. Displacement capacity was felt as less important than ductility, though they were clearly related.

In the 1990's, the seismic design of concrete and masonry structures became widely based on textbooks with more emphasis on displacement considerations and capacity design, and the concept of *performed-based seismic design*, based on displacement considerations, became the subject of research attention. It is possible to see from this brief description of the history of seismic design, that initially design was purely based on strength, or force, but then as the importance of displacement has come to be better appreciated, a number of new design methods, or improvements to existing methods, have been recently developed.

1.2 Development of a Displacement-Based Design Method

Lacks in the force-based method of seismic design have been recognized for some time, as the importance of deformation, rather than strength, in the seismic behavior of structures. This led to better appreciate the seismic performance and to some development in seismic engineering. The first attempts were to improve existing force-based design. These can be characterized as *force-based/displacement-checked*, where an attempt on a realistic determination of displacement demand for structures designed to force-based procedures was introduced. Such methods include the selection of more realistic member stiffness for deformation definition, and the possibility to use inelastic time-history analysis, or pushover analysis, to determine peak deformation and drift demand. In general, with these methods no attempt is made to achieve uniform risk of damage, or collapse for structures.

A further version of the "force-based/displacement-checked" approach links the detailing of critical sections to the local deformation demand, and can thus be termed *deformation-calculation based design*. In this version, strength is related to a force-based design procedure through specified force-reduction factors. Local deformation demands, typically expressed in the form of member end rotations or curvature are established by analytical tools, such as inelastic pushover analysis or inelastic time-history analysis. Transverse reinforcement details are then evaluated from known relationships between transverse reinforcement details and local deformation demand. The approach here described cannot produce structures with uniform risk of damage, even if it has the potential of producing structures with uniform risk of collapse.

Recently, the shortcomings in force-based approaches previously discussed led to the development of a number of design approaches in which the aim is to design structures that achieve a specified deformation state under the design-level earthquake, rather than achieve a displacement that is smaller than a specified displacement limit. These approaches appear more satisfying than those previously described. This is because designing structures to achieve a specified displacement limit means designing for a specified risk of damage, in which damage can be directly related to deformation and it seems to be compatible with the idea of uniform risk applied to determine the design level of seismic actions. Different procedures have been developed to reach this aim. The most basic difference between them is the choice of stiffness characterization for design. Some methods follow the conventional force-based design and adopt the initial pre-yield elastic stiffness. Other approaches, instead, utilize the "substitute structure" characterization, i.e. the secant stiffness to maximum displacement and an equivalent elastic representation of hysteretic damping at maximum response. Generally these methods give the possibility to directly design the structure to achieve the specified displacement with few or no iterations, and they are hence known as Direct Displacement-Based Design (DDBD) methods. The DDBD method will be discussed in detail in Chapter 2.

By the end of the twentieth century, while ductility was still central in earthquake engineering, its limits were also recognized because it implies damage. That led to find new technologies to allow a building or other construction to undergo strong earthquake without sacrificing portions of itself to inelastic behavior. A result of these researches are the precast structural systems with prestressing tendons, here subject of the present study.

1.3   Unbonded Post-Tensioned Precast Concrete Shear Wall

As briefly discussed, the displacement-based design method starts from the target lateral displacement linked to the required performance of the building during the seismic phenomenon. In this way, the design base shear is related to the particular structure that we are considering, in contrast with what happens in force-based seismic design: in fact, the force-reduction factor is specified by the design codes for the different type of structure, and not calculated each time for the structure under consideration. This approach is convenient for common and well-known structures, but it is a bad estimator of the post-elastic structural behavior in the case of special structures.

In recent years, seismic engineering has developed not only in preventing building collapse after the design earthquake for the safety of the occupants, but to design cost-efficient structures. For these reasons the aim is to limit permanent damage and to ensure as fast as possible building reoccupation after the seismic event. Common structures and common design methods could achieve it, but the size of the lateral system members shouldn't be acceptable from the architectural point of view, as well as from the prospective of costs. Recent studies proposed precast structural systems with prestressing tendons, like unbonded post-tensioned precast wall, which have good seismic characteristics such as a small residual displacement, as a result of the self-centering capability. The main disadvantage of these walls is the small energy dissipation, which increases lateral displacements. In literature different types of dissipating system are applied to the shear wall, like shear connectors, mild steel reinforcement or damping devices.

The PRESSS (PREcast Seismic Structural Systems) research program

conduced a significant amount of analytical and test studies on precast concrete wall systems for seismic regions of the United States. In particular, it was designed, built and tested under simulated seismic loading a five-story precast test building with a jointed precast wall as lateral resisting system. This type of wall is composed by two precast panels secured to the foundation using unbonded prestressed bars and connected to shear plates, which dissipate energy, in the horizontal direction.

1.4   Scope of Research

The aim of this research is to study, design and model an unbonded post-tensioned concrete shear wall. The interest in this kind of structures comes from the concern in the seismic engineering field to realize structures that not only prevent the building collapse but that can be cost-efficient as well, in terms of structural and non-structural repair and in terms of loss of business operation after the earthquake. The proposed lateral resisting system provides a self-centering capacity pulling back the structure to its undisplaced configuration. This behavior fits well with precast concrete, since it is necessary that the single structural members are not tied and a gap could occur between them. However, it can be adapted also to cast-in-place walls providing the gap opening at the wall base that is guaranteed by jointing the connection between the wall and the foundation. The gap opening at the base of the wall combined with the self-centering capacity given by the post-tensioned tendons and the weight of the wall allows displacement of the system as a rigid body remaining essentially in the elastic field with only cracks at the base. Therefore, this rocking behavior is essentially elastic and needs to be combined with an energy dissipation system, which can be

composed by debonded mild reinforcement or damping devices like viscous dampers. In the present work a single unbonded post-tensioned concrete shear wall was taken into consideration and studied in details, evaluating its global behavior and different possible design options already present in literature.

Studying this kind of walls, it was realized that they can be designed following two different seismic design approaches: the well-known Force-Based Design (FBD) method, present in worldwide building codes, and the Direct Displacement-Based Design (DDBD) method, developed for the first time by Priestley. For this reason, it was decided to apply this two methods to the proposed lateral resisting system combined with the well known system of energy dissipation composed by mild reinforcement with the aim of understanding which of the two design procedures catches the behavior of the wall in the best way and allows a design optimization. These two methods define the required strength of the wall that then leads the design of the wall sections. Since the wall with unbonded prestressing tendons and debonded rebar does not follow the conventional behavior of a reinforced concrete wall because the perfect adherence between concrete and steel is no more respected, it was necessary to look for an alternative design procedure. Thus, another objective of the present work is to define a proper way to size the required material quantities. Finally, the need to validate the results found with all these procedures brought to the creation of an analytical model that could represent the expected behavior of the wall. Since there is no possibility to verify the design results with a test building, some models already present in literature are studied in details with the attempt to reproduce their results. The aim is to create a model using a commercially available finite elements software, like ETABS 2015 that is widely used in engineering firms, in order

to make this structural technology of easy application in the construction field. Once all the design and modeling procedures are validated, their application to other wall configurations and combinations with other energy dissipation system will be possible.

In Chapter 2, the FBD and DDBD methods will be described in details, showing their procedures and potentialities especially for the case of concrete shearwalls. In Chapter 3 self-centering lateral resisting systems with prestressing tendons will be studied considering different configurations, describing their expected behavior and a possible design procedure. In Chapter 4 a modeling procedure of these peculiar structures will be performed with a commercially available finite elements software, ETABS 2015, reproducing the experimental results of the PRESSS (PREcast Seismic Structural Systems) research program in order to verify the computations. In Chapter 5, all the preceding considerations will be applied to the preliminary design of the lateral load resisting system of a real case study. Skidmore, Owings and Merrill LLP (SOM), one of the leading civil engineering firm in the world which collaborates in this research, has been involved in the design of the New Long Beach Civic Center, located in Long Beach, California. Long Beach is located in a high seismic region and the owner required to SOM to design the structure to reach very strict performance levels, for example fully reoccupation of the new facility within a week. For these reasons the self-centering lateral resisting system could be an optimal design option and in Chapter 5 it will be applied to the New Long Beach Civic Center, comparing the results to a conventional reinforced concrete shearwall. Moreover, the results of the FBD method and the DDBD method will be compared. Finally, in Chapter 6 conclusions and future developments will be presented with an initial exploration of a different wall configuration composed by a

bearing at the center of the wall base and by viscous damping devices.

Chapter 2

Seismic Design Methods

2.1 Introduction

The present research studies the design and the properties of an unbonded
post-tensioned precast concrete shear wall in seismic regions. The design
of the proposed lateral resisting system is conduced with two methods in
order to investigate their applicability to this particular kind of structure
and to understand which one leads to better results in terms of optimization
of the design. These two methods are the Force-Based Design (FBD) and
the Direct Displacement-Based Design (DDBD). As it is said in Chapter
1, the traditional approach to seismic design is force-based and therefore it
is widely used in worldwide design codes. In this approach, the estimated
fundamental period and total mass of the structure are the basis for the
computation of the design base shear, incorporating the influence of seismic
intensity in terms of spectral acceleration. In codified force-based design
procedures, displacement capacity is the final stage of the design and it is
only an output of the design process.

In contrast, a target displacement that represents the expected perfor-

mance of the building is used in DDBD as starting point. This method defines an equivalent single-degree-of-freedom system (SDOF) representing the structure and a target displacement that prescribes the structure's required effective natural period, based on the seismic intensity in terms of spectral displacement. The effective period and the effective mass of the equivalent SDOF system, obtained from the total mass of the building, are then used to calculate the effective stiffness of the building [14]. Finally, the design base shear is evaluated from the product between the target lateral displacement and the effective stiffness. It is demonstrated in Priestley [16] that the DDBD approach typically produces a smaller design base shear than the one obtained from the force-based design approach thus reducing the cost of the structure. This aspect will be seen in Chapter 5, where FDB and DDBD are applied to our case study. The procedures of the two methods are presented in this Chapter in order to better understand their differences and benefits.

2.2 Force-Based Seismic Design

In this section the force-based design procedure is presented as currently applied in modern seismic codes, with particular reference to American and European codes. The sequence of operations necessitated in the design is summarized in Fig. 2.1.

Here below, each operation of the design procedure is explained in detail following the order proposed in Priestley, Calvi and Kowalsky's textbook.

1. Evaluation of the structural geometry, including member sizes. In many cases non-seismic loads lead the definition of the geometry.

2. Estimation of member elastic stiffness, based on the estimated members size. Different seismic codes make different assumptions on the
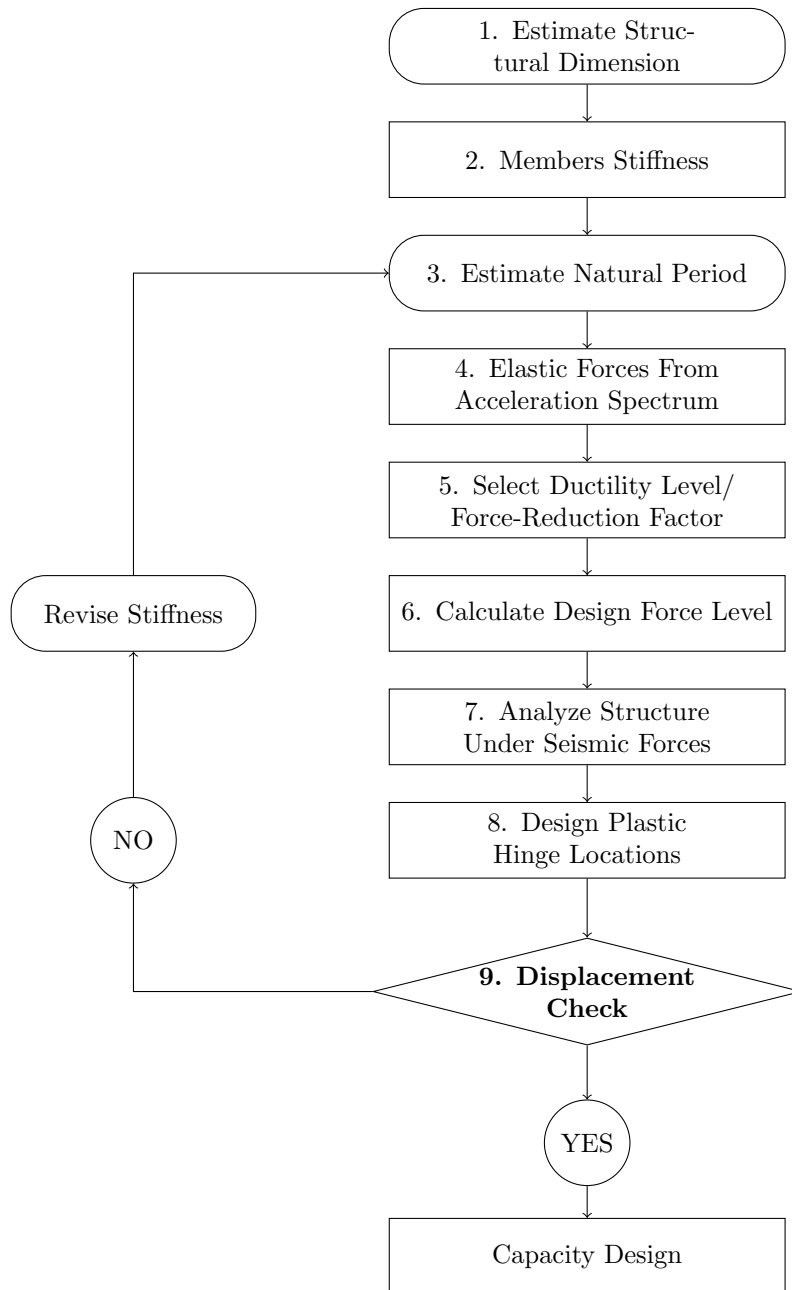
Figure 2.1: Sequence of operations for FBD methodology

appropriate stiffness for reinforced concrete and masonry members. In some cases I_g (stiffness of the uncracked section) is used, while in other cases I_{red} (stiffness of the reduced section) is taken into account to reflect the softening caused by cracks that appear when the yielding response is approached.

3. Calculation of the fundamental period from the assumed members stiffness. For a SDOF representation of the structure it is given by:

$$T = 2\pi\sqrt{\frac{m_e}{K}} \tag{2.1}$$

where m_e is the effective seismic mass.

In Eurocode 8 [31], it is specified that the fundamental period of a building can be determined through expressions based on structural dynamics methods (e.g Rayleigh's method). Alternatively, for building tall less than 40 meters it is possible to use a height-dependent fundamental period, independent from members stiffness, mass distribution or structural geometry. The typical form presented for this approximated period, is given by:

$$T = C_t(H_n)^{0.75} \tag{2.2}$$

where C_t depends on the structural system, and H_n is the building height.

In the American building code (ASCE 7-10, [30]), a similar approach is proposed to determine an approximated building period T_a as an alternative to performing a direct analysis to determine the period T. The difference is that T_a can be calculated according the following equation:

$$T = C_t(H_n)^x \qquad (2.3)$$

where both C_t and x depend on the structural system.

Alternatively, for structure not exceeding 12 stories above the base, where the seismic force-resisting system is based on concrete or steel moment resisting frames and the average story height is at least 3 meters, it is permitted to determine the approximate fundamental period with the following equation:

$$T = 0.1N \qquad (2.4)$$

where N is the number of stories above the base.

These codes propose other possible ways for computing the approximate period for specific building but they are not taken into account in this research.

4. The design base shear $V_{base,E}$ for the structure corresponding to elastic response in each of the horizontal directions in Eurocode 8 is given by an equation of the form:

$$V_{base,E} = S_d(T)m\lambda \qquad (2.5)$$

where $S_d(T)$ is the value of the design acceleration spectra corresponding to the period T, m is the total mass of the building above the foundations or a rigid basement and λ is a corrective coefficient whose value is between 0.85 and 1 depending on the number of stories of the building.

In the American code the same idea is expressed in the following way:

$$V_{base,E} = S_{DS} I_e W \tag{2.6}$$

where S_{DS} is the design spectral response acceleration parameter in the short period range, I_e is an importance factor reflecting different levels of acceptable risk for different structures and W is the effective seismic weight.

5. Selection of the appropriate force-reduction factor R corresponding to the estimated ductility capacity of the structural system and materials. Generally it is specified by the design code and is not a design choice, even if the designer may use a lower value than the one specified in the code. This is what happens in the American code.

    In Eurocode 8, instead, the ductility capacity of the structure is taken into account through a reduction of the response spectrum through the parameter q, called structural parameter. The value of q is specified and given for different structural systems and materials according to their class of ductility. This value cannot be the same in the two horizontal directions of the structure, even if the ductility classification has to be the same in each direction. Referring to the force-reduction factor, we use Fig. 2.2 to understand the relationship between R and ductility which depends on the fundamental period of the structure. Inelastic time-history analysis show that many structures with high fundamental period (normally greater than 0.5 seconds) have very similar maximum seismic displacements of elastic and inelastic systems with the same initial stiffness and mass. The assumption of equal stiffness but different strength is compatible with properties of sections with equal dimensions. This leads to establish the *Equal Displacement Approximation*
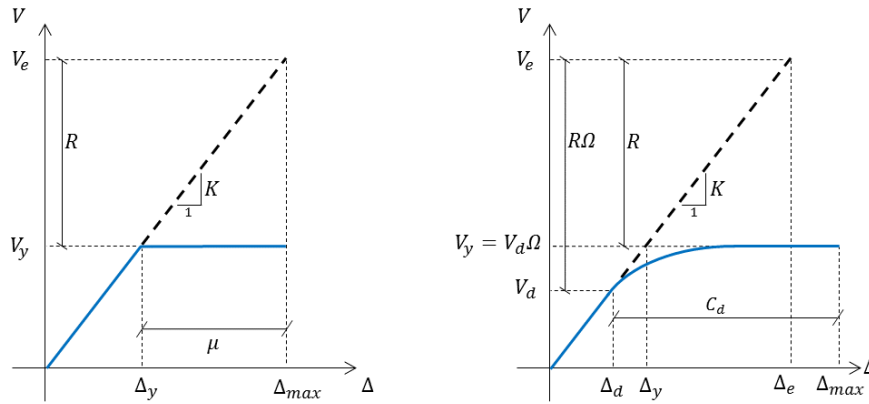
Figure 2.2: Simplified force-displacement response of elastic and inelastic systems under seismic excitation

that we can see in Fig. 2.2 on the left. For a structure with linear elastic response to the design earthquake, the maximum force developed at peak displacement is V_e. We can design the structure for reduced ultimate strength level of V_y. This strength is related to the elastic response level by the force-reduced factors:

$$V_y = \frac{V_e}{R} \tag{2.7}$$

Ductility is a measure of deformation and is the ratio of maximum to effective yield deformation. In the case of Fig. 2.2, lateral displacement is the measure of deformation, and the displacement ductility for the inelastic system is thus:

$$\mu = \frac{\Delta_{max}}{\Delta_y} = \frac{V_e}{V_y} = R \tag{2.8}$$

Therefore, for the equal displacement approximation, the ductility factor and the force-reduced factor assume the same value.

In the 1960's and 1970's problems arose from this approach because of the inappropriateness of the equal displacement approximation for

short period structures (normally with a fundamental period between 0.1 and 0.5 seconds), since for these structures there is a conservation of the maximum force and so there is no benefits from ductility. For these kind of structures the *Equal Energy Approximation*, shown in Fig. 2.2 on the right, was more appropriated. In this case the ductility factor is no more equal to the force-reduced factor and the relationship between them is more complex. Anyway, the design base shear is still defined though Eq. (2.7).

6. As explained above, the design base shear force is calculated from:

$$V_{base} = \frac{V_{base,E}}{R} \qquad (2.9)$$

This force is then used to compute the distribution of horizontal forces along the structure's height. The first step is to calculate the building's fundamental mode shape in the horizontal direction of analysis using structural dynamics methods. In a simplified way, the fundamental mode shape may be approximated by horizontal displacements increasing linearly along the height of the building. Then it is possible to determine the forces distribution that is normally proportional to the product between the mass and the corresponding displacement in the fundamental mode shape. Hence, the seismic action effects are determined by applying horizontal forces F_i to any story, as defined in Eurocode 8 through the following equation:

$$F_i = V_{base} \cdot \frac{s_i m_i}{\sum s_j m_j} \qquad (2.10)$$

where s_i, s_j are the displacements of story diaphragms in the fundamental modal shape and m_i, m_j are the story masses. When the displacement shape of the preferred inelastic mechanism can be approximated
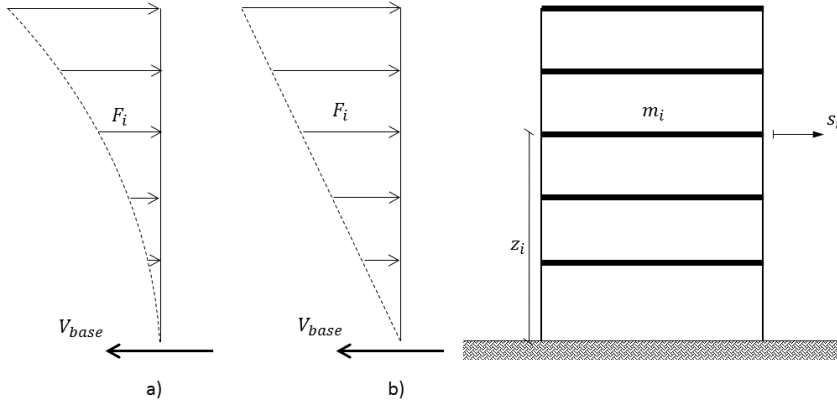
Figure 2.3: Force distribution over the height of the building: a) considering actual mode shape, b) considering semplified linear distribution

through horizontals displacements growing linearly along the height of the building, a distribution of horizontal forces proportional to the product of the height and mass at different levels is recommended:

$$F_i = V_{base} \cdot \frac{z_i m_i}{\sum z_j m_j} \qquad (2.11)$$

where z_i, z_j represent the height of the story diaphragms above the point of application of the seismic force. Fig. 2.3 represents the two possible distributions. In the American code, only the distribution of forces proportional to the product of the height and mass at different levels has been taken into account. The lateral force induced at any level is expressed through the equation:

$$F_i = C_{vx} V_{base} \qquad (2.12)$$

and:

$$C_{vx} = \frac{w_x h_x^k}{\sum_{i=1}^{n} w_i h_i^k} \qquad (2.13)$$

where C_{vx} is the vertical distribution factor depending on w_i, w_x (the portion of the total effective seismic weight of the structure located at level i or x) and h_i, h_x (the height from the base to level i or x), k is an exponent related to the structure period ($k = 1$ if $T = 0.5$ or less, $k = 2$ if $T = 2.5$ or more and for T between 0.5 and 2.5 k is the result of a linear interpolation between 1 and 2). The seismic design story forces shall be distributed at any level between the lateral force-resisting elements, such as frames and structural walls, after considerations based on the relative lateral stiffness of these elements and of the diaphragms.

7. The structure is then analyzed under lateral seismic design forces. The required moment capacity at the potential locations of plastic hinges is determined.

8. Once the values of the moments induced at the locations of plastic hinges are known, the structural design of the member sections at these locations can be performed.

9. Moreover, the displacements evaluation under the seismic action can be done. The deflection at Level x (δ_x), used to compute the story drift too, shall be determined in the American code in accordance to the following equation:

$$\delta_x = \frac{C_d \delta_{xe}}{I_e} \qquad (2.14)$$

where C_d is the deflector amplification factor defined for different seismic force-resisting systems, δ_{xe} is the deflection at the location required

determined with an elastic analysis. The designer must check that the calculated nonlinear displacements are lower than the code-specified limits in terms of displacements and drifts.

10. If the verification is not satisfied, redesign is required. The redesign normally consists in the increment of the member sizes in order to increase the members stiffness.

11. If, conversely, the displacements are satisfactory, the final step of the design is to determine the required capacity of members not subject to plastic hinging. The process known as capacity design ensures that the shear strength and the moment capacity of sections where plastic hinging must not occur should be bigger than the maximum possible value of the maximum feasible strength of the potential plastic hinges. Most codes also include a simplification of the capacity design approach.

The above description is a summary of the Force-Based Seismic Design method. In many cases the force levels are determined through modal response spectrum analysis instead of using the equivalent lateral seismic forces. These analyses are conducted to determine the natural modes of vibration for the structure and it shall include a sufficient number of modes in order to obtain a combined modal mass participation of at least 90 percent of the actual mass in each considered horizontal direction. Referring to the American code, the value for each parameter of interest shall be evaluated for the various modes using their properties and the response spectra divided by the quantity R/I_e (respectively force-reduction factor and importance factor). The value for displacement and drift quantities shall be multiplied by the quantity C_d/I_e, where C_d is the deflector amplification factor that is defined for different seismic force-resisting systems. The different modal values

shall be then combined using the *Square Root of the Sum of the Squares* (SRSS) method or the *Complete Quadratic Combination* (CQC) method. The second method has to be used if the closely spaced modes have significant cross-correlation of translational and torsional response. Later, the combined response for the modal base shear (V_t) has to be compared with the V_{base} computed with equivalent lateral force procedure (Eq. (2.9)). If V_t is less than 85% of V_{base}, the design base force shall be $0.85V_{base}$ and the drift has to the be multiplied by $0.85\,C_dW/V_t$. In this case, the determination of the distributed seismic forces shall be computed through a new modal analysis performed with a response spectra reduced by $0.85V_{base}/V_t$.

2.3   Problems with FBD

Priestley and other researchers decided to develop a new seismic design approach in order to fix problems detected in the force-based method that will be partially described in this section.

2.3.1   Stiffness Assumptions

At the beginning of the force-based procedure the geometry of the structure, including member sizes, must be assumed. This assumption is made before the calculation of the design seismic forces acting on the structure. Once the design forces are evaluated, they must be distributed over the height of the structure in proportion to the assumed stiffness. If member sizes turn out to be inappropriate and should be modified from the initial assumption, the computed design forces will no longer be true and recalculation is theoretically required. The problem with the assumption of member stiffness becomes more important with reinforced concrete and reinforced masonry. For

this kind of structures an important consideration has to be made about the way in which individual members stiffness are determined. The stiffness of an element can be calculated considering its elastic behavior, reflected by the gross-section stiffness, or considering the plastic behavior and the influence of cracking, so a reduced stiffness. In many codes, the stiffness of a component is generally assumed the 50 percent of the gross section stiffness to represent the influence of cracking. Some codes specify that it depends on the member type and the applied axial force. In New Zealand, for example, the concrete design code specifies effective sections as low as 35 percent of the gross section stiffness for beams. The design seismic forces will be significantly affected by the value of the assumed stiffness. In fact, the stiffness-based period implies a reduction in seismic design force with a reduction of the section stiffness.

2.3.2   Coupling Between Strength and Stiffness

The elastic strength is obtained from the elastic design spectrum, based on the period of the structure and so on the estimate lateral stiffness. This strength is then reduced through a force-reduction factor R to reach the design base shear. This approach implies that the original estimation of the stiffness will not change with the reduction of elastic strength. The behavior of a group of similar structures designed with different R values is shown in Fig. 2.4 in terms of force-displacement relationship. The picture on the left shows force-displacement relationships based on the assumption of constant member stiffness, which implies a yield curvature directly proportional to the flexural strength. Detailed analysis and experimental evidence showed that this assumption is illicit [17]. In fact, for reinforced concrete flexural walls it was demonstrated that for a given steel yield strain, the yield curvature of the wall was just a function of the wall length. This indicates that the yield
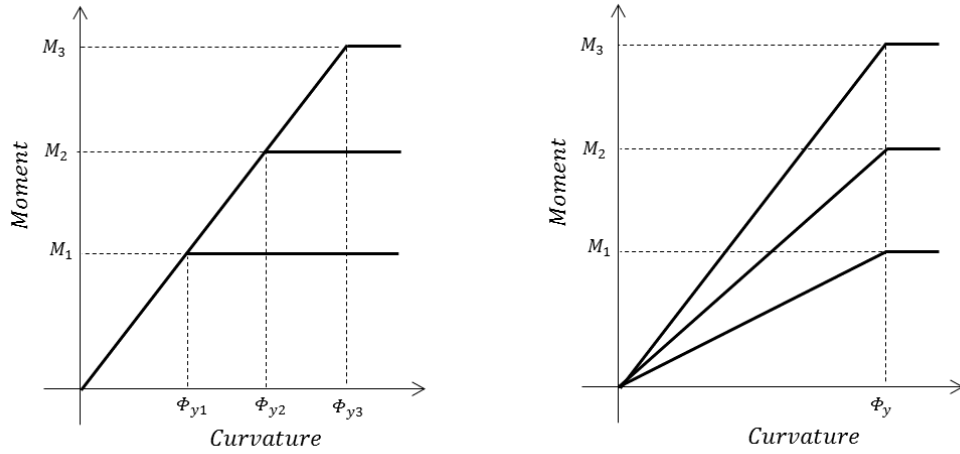
Figure 2.4: Force-displacement relationship

curvature is essentially independent from strength and the dependency is instead between stiffness and strength. Using elasto-plastic representation to describe the member behavior, on the right Fig. 2.4 shows the realistic force-displacement relationship of these members with the same overall dimensions but different amount of flexural reinforcement. Studies on flexural beams showed that also for moment resisting concrete frames the structural stiffness cannot be considered independent of the strength. As a consequence of these considerations, the stiffness as well as the period of this kind of structures depend on the definition of member strengths. This implies that successive iterations must be performed to reach an adequate elastic characterization of the structure, since the required members strengths are the final product of the force-based design procedure. The results of this iterative process are the overestimation of the overall ductility demand and the underestimation of the seismic displacement, as it is indicated in [22]. This can lead to design reinforced concrete structures that may not reach their ductility capacity before the codified drift limit is exceeded.

Moreover, for reinforced concrete and masonry structures the initial elastic stiffness will be no more valid after that yield occurs, because there is a degradation of stiffness after cracking and softening of the reinforcing steel. This behavior makes of doubtful validity the assumption that the elastic characteristics are the best indicator of inelastic performance, as assumed by the force-based method. It may be recommended that the structural characteristics at maximum displacement could be a more reasonable indicator of the structural behavior at maximum response than the initial values of stiffness and damping.

2.3.3 Period Calculation

Different assumptions on member stiffness can lead to different calculated periods, in particular the period increases when height-dependent equations are taken into account. In [15], the calculation and the comparison of fundamental periods of different structural wall buildings computed with different design assumptions are presented. These studies show that the fundamental period found with the height-dependent equation (presented in Table 2.1 in the column labeled *Eq.* (2.2)) as well as the one found with a modal analysis based on 50 percent of the gross section stiffness (the third column of the table) are very low compared with those resulting from a modal analysis in which the stiffness of the wall is evaluated from moment-curvature analysis (presented in Table 2.1 in the column labeled *Moment-Curvature*). The use of artificially low periods in seismic design is often considered conservative, but we can observe that if the displacement demand is based on low periods, it will be low and so non-conservative.

As presented in the FBD procedure, Eq. (2.4) (that has been incorporated in some building codes for frame structures) is an alternative to the

Table 2.1: Fundamental periods of wall buildings

Wall Stories	Eq. (2.2)	$I = 0.5I_{gross}$	Moment-Curvature	Eq. (2.15)
2	0.29	0.34	0.60	0.56
4	0.48	0.80	1.20	1.12
8	0.81	1.88	2.26	2.24
12	1.10	2.72	3.21	3.36
16	1.37	3.39	4.09	4.48
20	1.62	3.65	4.77	5.60

height-dependent equation. Other researches have recommended the use of a simplified expression:

$$T = 0.1\,H_n \tag{2.15}$$

with the building height H_n expressed in meters. In a similar way, if the building height is expressed in feet,

$$T = 0.033\,H_n \tag{2.16}$$

These last equations are referred to frame buildings with 3 meters story height. Table 2.1 in the right column shows their application to a structural wall buildings with 2.8 meters story height because it is interesting to compare these results with those resulting from modal analysis based on moment-curvature calculated stiffness. They turn out to be very similar for walls up to 12 stories and roughly comparable for walls up to 20 stories.

These results indicate that the first 2 approaches produce values that are very low, whereas the compatibility between the values in the last 2 columns can indicate that fundamental elastic periods of frame and wall buildings designed for similar drift limits will be slightly similar.

2.3.4   Ductility Capacity of Structural Systems

The research community finds it difficult to propose a unique definition of yield and ultimate displacements.. Referring to Fig. 2.5, the definition of the yield displacement is based mainly on: the intersection between the line with initial elastic stiffness and the nominal strength (point 1), the displacement at first yield (point 2) or the intersection between the line passing through point 2 and the nominal strength (point 3). The ultimate displacement is mainly defined as: displacement at peak strength (point 4), displacement at the 50 percent (or some other percentage) of the degradation from peak strength (point 5) or the displacement at initial fracture of the transverse reinforcement (point 6). It could be seen that the range of limit values is very wide, implying considerable variation in the estimation of the ductility capacity of structures, calculated as the ratio between the yield displacement and the ultimate displacement. This variation is expressed through the force-reduction factors defined by the different codes.

Moreover, a key aspect of force-based design is the uniqueness of the ductility capacities, and so the uniqueness of force-reduction factors associated to different structural systems. In [17], the influence of structural geometry on displacement capacity is illustrated for different structural systems.

To better understand the variability of ductility capacity, the example of a bridge column is presented. In this study point 3 of Fig. 2.5 represents the yield displacement and the ultimate displacement is the lower value between the displacement at point 5 and the one at point 6. Two bridge columns with different heights but same cross-section, reinforcement details and axial loads are considered. The two columns taken into account have the same curvature ductility factor $\mu_\phi = \phi_u/\phi_y$, since they have the same yield curvature ϕ_y and ultimate curvature ϕ_u. The yield displacement and the plastic displacement
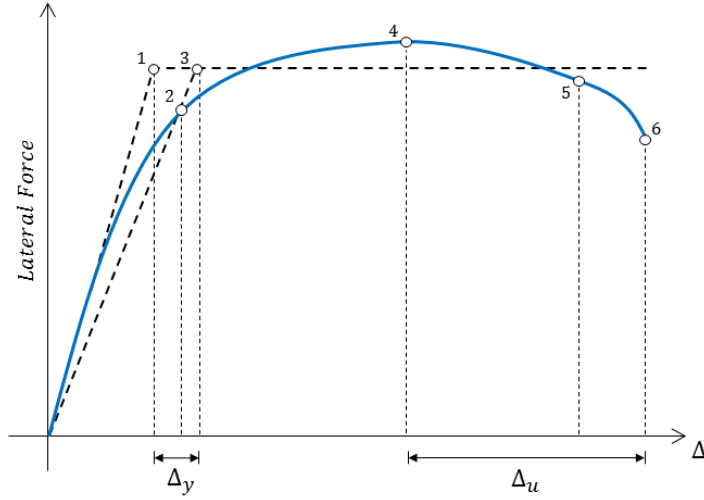
Figure 2.5: Possibles definition of yield and ultimate displacement

can be approximated respectively by:

$$\Delta_y = \frac{\phi_y H^2}{3} \tag{2.17}$$

and

$$\Delta_y = \phi_p L_p H \tag{2.18}$$

where H is the effective height, $\phi_p = \phi_u - \phi_y$ is the plastic curvature, and L_p is the plastic hinge length. In this way the displacement ductility capacity is given by:

$$\mu_\Delta = \frac{\Delta_u}{\Delta_y} = \frac{\Delta_y + \Delta_p}{\Delta_y} = 1 + 3\frac{\phi_p L_p}{\phi_y H} \tag{2.19}$$

The plastic hinge length L_p is weakly related to H, in fact it depends on the effective height, the extent of inclined shear cracking and the strain penetration of longitudinal reinforcement into the foundation. For this reason L_p is frequently assumed to be independent of H. Anyway, whether we consider L_p dependent on H or not the displacement capacity reduces as the height

increases, as we can see from Eq. (2.19). Using the approach that takes into account the height-dependency of L_p, we can find a ductility capacity equal to $\mu_\Delta = 9.4$ for a squat column with $H = 3$ m, while $\mu_\Delta = 5.1$ for a more slender column with $H = 8$ m. Clearly, the concept of unique displacement capacity is no more valid for this simple class of structure, and thus also the concept of unique force-reduction factor.

The other examples provided by the book show the variability of the displacement ductility capacity due to the consideration or not of the elastic flexibility of different components, as the capacity-protected members in portal frames or the foundations for cantilever walls. Moreover, the variation linked to the presence of unequal column heights for piers and bridges is take into account, where the different height of the columns implies different values of ductility capacity and so the consideration of different values of R in the same structure.

2.3.5   Summary of FBD problems

Here a summary of the problems associated with force-based design identified in the previous sections is presented.

- In the force-based design the distribution of forces between different structural elements is based on initial estimates of their initial stiffness. Since the strength of the elements is the end product of the design process and the stiffness depends on the strength, the stiffness remain unknown until the design process is complete.

- The distribution of seismic force between elements based on their initial stiffness is of doubtful validity, because it implies that different elements can be forced to yield at the same time.

- It is demonstrably invalid the assumption done by force-based design that unique force-reduction factor can be associated to a given structural type and material.

2.4 Direct Displacement-Based Design

An alternative design procedure known as *Direct Displacement-Based Design* (DDBD) has been developed by Priestley ([14], [15], [16], [17]) with the purpose to identify and moderate the lacks present in current force-based design methodology. The fundamental difference between the two methods is that the DDBD characterizes the structure by a single-degree-of-freedom (SDOF) representation of performance at peak displacement response. The design approach of this method is to design a structure that reaches a given performance in terms of displacement under a specific seismic event. This would result in uniform-risk structures. Direct Displacement-Based design characterizes the structure by equivalent secant stiffness K_e at maximum displacement Δ_d and by an equivalent viscous damping ξ_{eq} corresponding to the hysteretic energy absorbed during inelastic response, instead of defining the structure through its elastic properties related to first yield, as in the FBD. The design procedure determines the strength required at designed plastic hinge locations in order to achieve the design objectives in terms of displacements. Later, the strength design has to be combined with capacity design procedures to guarantee that plastic hinges take place only in the expected locations.

This section illustrates the fundamental aspects of the DDBD approach, common to all materials and structural systems. Later, the focus will be on the design procedure for structural reinforced concrete walls and for un-

bonded post-tensioned reinforced concrete shear walls. Only the basic aspects of the DDBD will be presented, focusing on its application to concrete shear wall and to unbonded post-tensioned concrete walls. An investigation of the method in its complexity and entirety can be carried out by studying in detail "Displacement Based Seismic Design of Structures", written by Priestley, Calvi and Kowalsky in 2007 [17].

2.4.1 Basic Aspects

Fig. 2.6 shows all the main aspects of the DDBD methodology, as proposed by Priestley in 2000, [14]. The seismic design method considers a SDOF representation of the structure, in the figure with reference to a frame building (Fig. 2.6 (a)). The bi-linear envelope of the lateral force-displacement response of the SDOF is shown in Fig. 2.6 (b) and it points out that the initial elastic stiffness K_i is followed by a post-yield stiffness rK_i. This graph also shows the secant stiffness K_e at maximum displacement Δ_d that together with the equivalent viscous damping ξ_{eq} characterizes the structure in the DDBD procedure. The equivalent viscous damping depends on the structural system (as shown in Fig. 2.6 (c)) and it is the combination of the elastic damping and the hysteretic energy absorbed during the inelastic response, provided for a given level of ductility demand. Once we know the displacement at maximum response Δ_d and the damping evaluated from the expected ductility demand, it is possible to define the effective period T_e at maximum displacement response and can be determined from a set of displacement spectra defined for different levels of damping (Fig. 2.6(d)).

The effective stiffness K_e of the equivalent SDOF structure at maximum displacement can be evaluated by inverting the definition of period for a
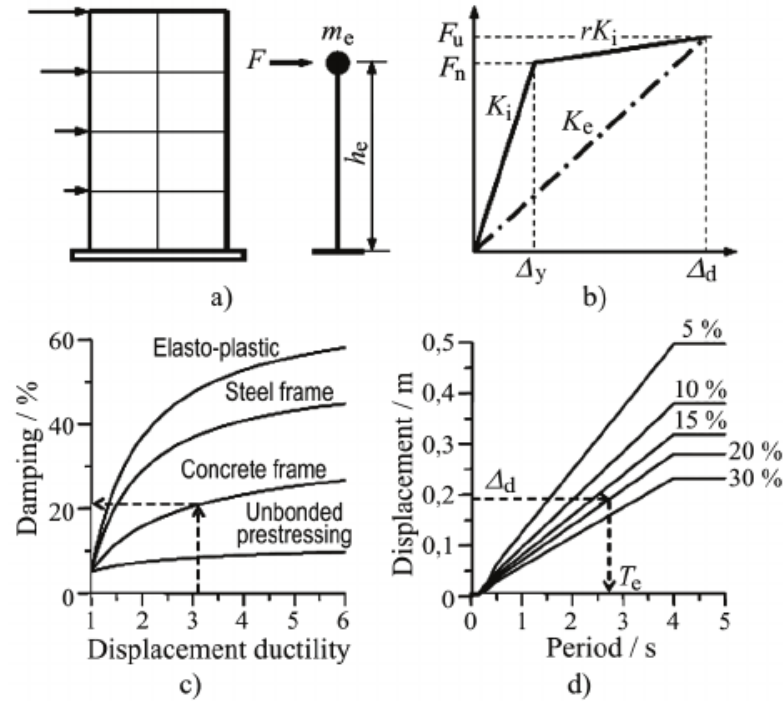
Figure 2.6: Fundamentals of DDBD, Priestley

SDOF structure. Thus:

$$K_e = \frac{4\pi^2 m_e}{T_e^2} \tag{2.20}$$

where m_e is the effective mass of the structure that participates in the fundamental vibration mode.

The design lateral force, which is the design base shear for the substitute structure, is thus:

$$F = V_{base} = K_e \Delta_d \tag{2.21}$$

Once the design base shear is known, it could be distributed over the mass elements of the real structure that should be analyzed under those forces in order to determine the design moments at locations of potential plastic hinges.

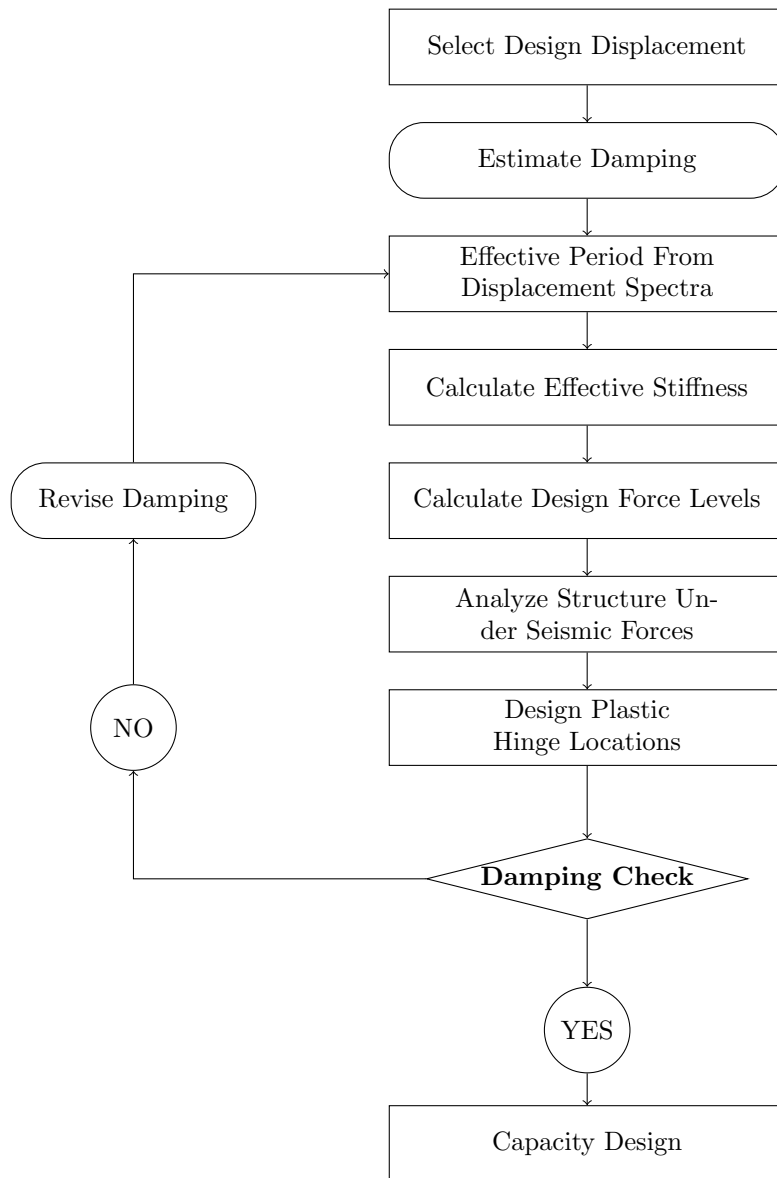The design procedure of the DDBD method is also summarized in Fig. 2.7.

Figure 2.7: Sequence of operations for DDBD methodology

The above design method is thus very simple and has the benefit that the relationship between damping and ductility is not generic, but it is specific and includes the characteristic of the structural resisting system under consideration. This is interesting for particular structures that are not present in current building code yet and for which the force-reduction factor is not defined. For example, ASCE 7-10 introduces in Table 12.2-1 the category *Special reinforced concrete shear walls* and assigns a unique value of the force-reduction factor $R = 5$ for this category of structures (which includes also the enhanced shear walls proposed in the present research), without considering the behavior of the particular system under seismic loads.

In the following pages the terms that compose the DDBD procedures are taken into consideration individually. The complexity of the method consists in the characterization of the *substitute structure*, the determination of the displacement design, and the development of design displacement spectra. The inelastic displacement spectra has to be generated for different ductility demand starting from the damping/ductility relationship, the displacement reduction factor, and the elastic displacement spectrum. The effective period is then determined through the inelastic displacement spectra, depending on the design displacement for the design level of ductility.

2.4.2   Design Displacement

There is a number of different limit states or performance levels that could be considered in the design process. Generally, only one of them is taken into account and the structural performance is governed by limiting the material strains since damage is related to the deformations of the structural elements. Instead, the damage of non structural elements is considered to be controlled by the drift.

The limit state taken into consideration is the starting point for the definition of the design displacement of the substitute structure. In fact, it depends on the limit state displacement or drift of the most critical member of the real structure. Moreover, this displacement is connected with an assumed displacement shape for the structure, corresponding to the inelastic first-mode at the design level ground motion. In this manner the design considers the inelastic behavior of the structure from the very beginning and it is coherent with the definition of the structure by the secant stiffness at maximum response, instead of the initial one. From a practical standpoint, the inelastic first mode-shape is often very similar to the elastic one, so the design displacement is given by:

$$\Delta_d = \frac{\sum_{i=1}^{n}(m_i\Delta_i^2)}{\sum_{i=1}^{n}(m_i\Delta_i)} \tag{2.22}$$

where n is the number of lumped masses m_i subject to a displacement Δ_i. For multi-stories buildings n corresponds to the number of stories.

As previously said, the structural performance is governed by strain limits and the design displacement can be computed from the curvature corresponding on the limit state. However, in many cases the common practice is to design the structure for a code specific drift and then define the size of the structural members in order to achieve this limit. For example, for frame building the design displacement is governed by drift limits in the lower story of the building. Thus the individual mass displacement can be calculated as:

$$\Delta_i = \delta_i \frac{\Delta_c}{\delta_c} \tag{2.23}$$

where Δ_c is the design displacement, referred to the critical mass, δ_c is the inelastic mode shape on it and δ_i is the inelastic mode shape at the generic mass i. For a multi-story building, the critical mass is usually the one representing the roof level.

2.4.3 Effective Mass

The effective mass of the substitute structure is evaluated considering the mass participating in the first inelastic vibration mode, thus:

$$m_e = \sum_{i=1}^{n} \frac{m_i \Delta_i}{\Delta_d} \tag{2.24}$$

where Δ_d is the design displacement.

The effective mass for multi-stories cantilever walls is generally around 70 percent of the total mass. The remaining fraction of the mass is related to the higher modes, that are inadequately represented in elastic analysis. Priestley assures that it is better to consider higher modes in the capacity design phase rather than in the preliminary phase of design.

2.4.4 Structure Ductile Demand

The total design displacement is the sum of two contributions: the yield displacement Δ_y and the inelastic displacement Δ_p. In order to calculate the ductility demand and thus the equivalent viscous damping, the yield displacement is necessary, as it will be discussed later. Analytical results showed that for reinforced concrete and masonry members, the yield curvature is a function of the yield strain and the section depth only but not of the amount of reinforcement. The general equation that define its value is:

$$\phi_y = C_1 \varepsilon_y / h \tag{2.25}$$

where C_1 is a constant depending on the type of element considered, $\varepsilon_y = f_y/E_s$ is the yield strain of the flexural reinforcement and h is the section depth.

For concrete and steel frame, the yield drift can be expressed as:

$$\theta_y = C_2 \, \varepsilon_y \, \frac{L_b}{h_b} \tag{2.26}$$

where L_b is the beam span, h_b is the beam depth, $C_2 = 0.5$ for concrete frame and $C_2 = 0.65$ for steel frame.

The effective yield displacement Δ_y has to be interpolated from the displacements at yield but before it is necessary to define the effective height, that is given by:

$$H_e = \frac{\sum_{i=1}^{n}(m_i \Delta_i H_i)}{\sum_{i=1}^{n}(m_i \Delta_i)} \tag{2.27}$$

From frames it is reasonable to assume the yield drift constant over the height, in this way the yield displacement is:

$$\Delta_y = \theta_y H_e \tag{2.28}$$

For walls, the yield displacement is defined by:

$$\Delta_y = \frac{\varepsilon_y}{l_w} H_e^2 \left(1 - \frac{H_e}{3H_n}\right) \tag{2.29}$$

For low rise cantilever wall, the value of the yield displacement can be approximated with the one of the SDOF vertical cantilever:

$$\Delta_y = \phi_y (H + L_{sp})^{2/3} \tag{2.30}$$

where L_{sp} is the penetration on the plastic strains inside the foundation.

The ductility displacement demand can be thus computed at the beginning of the design even if the strength is not defined yet. So:

$$\mu = \frac{\Delta_d}{\Delta_y} \tag{2.31}$$

2.4.5 Equivalent Viscous Damping

A key aspect of the DDBD is the definition of the equivalent viscous damping (EVD) that reproduces the hysteretic damping. The EVD is the sum of the elastic damping ξ_{el} and the hysteretic one ξ_{hyst}:

$$\xi_{\text{eq}} = \xi_{\text{el}} + \xi_{\text{hyst}} \tag{2.32}$$

where the hysteretic damping depends on the hysteretic rule that appropriately describes the behavior of the designed structure. Usually the elastic damping ratio is taken equal to 0.05 for concrete structures. Anyway, both components needs additional explanation.

Hysteretic Damping

The approach proposed by Priestley calibrates the EVD for different hysteresis rules in order to have the same peak displacements as the hysteretic response, which are computed using inelastic time-history analysis. The level of equivalent viscous damping has been derived with two different studies based on different methodologies. The former considers a large number of real earthquake accelerograms and computes for each of them the EVD for different ductility levels, effective periods and hysteresis rules. An average over the records was then conducted in order to define a relationship for a given ductility, rule and period. The latter considers a wider range of hysteresis rules with a smaller number of accelerograms and the elastic and inelastic results were then averaged and compared. The equivalent viscous damping defined was the one that achieved the match between the elastic results of the equivalent substitute structure and that of the real hysteretic model. The results found in the two approaches showed similar relationship for equivalent viscous damping for all hysteretic rules, except for the elasto-perfectly plastic one that is sensitive to duration effects.

Elastic Damping

The definition of a hysteretic rule is based on the assumption that its elastic response is perfectly linear in the elastic range, without processing any energy dissipation. Moreover, it does not consider the additional damping provided

by the foundation and the interaction between structural and non-structural elements. So the elastic damping is added in time-history analysis in order to compute the amount of damping which is not taken into account yet.

The damping coefficient depends on the value of stiffness considered. In DDBD the initial elastic damping is based on the secant stiffness at maximum displacement, that is in contrast with the conventional inelastic time-history analysis in which the elastic damping is linked to the initial stiffness. It is possible to consider the secant stiffness in the common practice too, but in this case the elastic damping is reduced with the softening of the structural stiffness. In the DDBD procedure, the reduction of stiffness in the substitute structure, in which $k_{\text{eff}} = k_i/\mu$, required a modification of the elastic damping to ensure compatibility between the *real* and the *substitute* structure. The value of the correction factor depends on the assumption of stiffness and on the results of the inelastic time-history analysis. In this way Eq. (2.32) becomes:

$$\xi_{\text{eq}} = \kappa \xi_{\text{el}} + \xi_{\text{hyst}} \tag{2.33}$$

where κ is based on the time-history analysis. Calling μ the displacement ductility factor and defining a factor λ that depends on the hysteretic rule and the elastic damping assumption, the parameter κ can be written as:

$$\kappa = \mu^\lambda \tag{2.34}$$

In many cases it is possible to simplify the process and consider an elastic damping ratio of 0.05, because the period-dependency is insignificant for $T > 1\,\text{sec}$ for most rules. The equivalent damping-ductility relationship results thus expressed in the following way:

$$\xi_{\text{eq}} = 0.05 + C_3 \left(\frac{\mu - 1}{\mu \pi} \right) \tag{2.35}$$

where C_3 varies from 0.1 to 0.7 for the assumption of $\xi_{\text{eq}} = 0.05$ and it depends on the hysteresis rule of the structure.

When the lateral resistance of a building is provided by multiple walls, the ductility demand of each of them differs because the yield displacement is inversely proportional to the wall lengths. In general, when the seismic resistance is produced by different structural elements with different damping and strength, the global damping can be calculated as the average of each contribution weighted on the basis of the energy dissipation of each structural elements. The global damping results to be:

$$\xi_{\text{eq}} = \frac{\sum_{j=1}^{m}(V_j \Delta_j \, \xi_j)}{\sum_{j=1}^{m}(V_j \Delta_j)} \tag{2.36}$$

where j refers to the jth structural element and V_j is his design strength at design displacement, Δ_j is its displacement at the height of the seismic force, while ξ_j is the relative damping.

Being the displacements of the different walls the same and the wall strength proportional to the square of the length, the global damping results to be:

$$\xi_{\text{eq}} = \frac{\sum_{j=1}^{m}(l_{wj}^2 \xi_j)}{\sum_{j=1}^{m}(l_{wj}^2)} \tag{2.37}$$

2.4.6 Inelastic Displacement Spectra and Effective Period

Direct displacement-based seismic design considers a secant stiffness representation of the structural response and thus a modification to the elastic displacement response spectrum is required to take into account the ductile response. The influence of ductility can be represented through inelastic displacement spectra, which can be developed from the elastic one for different ductility levels.

Assuming that the force-displacement relationship is bilinear elasto-plastic with post-yield stiffness equal to rk_i, the secant period T_e relative to the design displacement response is linked to the elastic period T_i in the following way:

$$T_e = T_i \left[\frac{\mu}{1 + r(\mu - 1)} \right]^{0.5} \tag{2.38}$$

In order to have the inelastic displacement at T_e equal to the elastic one at T_i, a modification factor R_μ must be applied to the elastic spectrum. Inelastic spectra sets can be generated from the parameters used to determine the damping-ductility relationships. In fact, the use of spectra modified by different level of damping requires relationships between ductility and damping, so that they can be defined for different hysteretic rules. Spectral displacement reduction factors can be defined by a common expression presented in the 1998 edition of Eurocode EC8 [31]:

$$R_\mu = \left(\frac{0.07}{0.02 + \xi} \right)^\alpha \tag{2.39}$$

The parameter α is set to 0.5 for normal conditions and 0.25 for velocity-pulse conditions. By replacing in the above equation the expression of the hysteretic damping of Eq. (2.35), R then results as:

$$R_\mu = \left[\frac{0.07}{0.07 + C_3 \left(\frac{\mu-1}{\mu\pi} \right)} \right]^\alpha \tag{2.40}$$

This factor depends on α, C_3 and the value of the assumed elastic damping.

As we saw in Fig. 2.6(d), the displacement spectra remain essentially linear with period up to the corner period T_c (usually equal to 4 sec). It has been demonstrated that for earthquakes with moment magnitude greater than $M_w = 5.7$, the corner period increases almost linearly with magnitude:

$$T_c = 1.0 + 2.5(M_w - 5.7) \quad \text{seconds} \tag{2.41}$$

with a corresponding displacement amplitude relative to 5% damping that is:

$$\delta_{max} = C_s \frac{10^{M_W-3.2}}{r} \quad \text{mm} \tag{2.42}$$

where r is the distance from the earthquake epicenter expressed in km and C_s depends on the ground typology.

For a corner period equal to 4 seconds, the effective period found with for interpolation from Fig. 2.6(d) results:

$$T_e = T_c \cdot \frac{\Delta_d}{\Delta_{c,5}} \cdot \left(\frac{0.02+\xi}{0.07}\right)^\alpha \tag{2.43}$$

where $\Delta_{c,5}$ is the displacement at the corner period for the displacement spectra with 0.05 damping, Δ_d is the design displacement, ξ is the design damping.

Once the design displacement, the effective mass and the effective period are known, the effective stiffness, and thus the base shear force, can be computed with Eq. (2.20) and Eq. (2.21) respectively.

2.4.7   Distribution of Design Base Shear Force

The evaluated base shear must be distributed as design force to the different lumped masses of the structure in proportion to their value and displacement. This is based on the assumption of essentially sinusoidal response at peak response. In this way the design moments at plastic hinges location can be established. The design force at mass i results to be:

$$F_i = V_{base} \cdot \frac{m_i \Delta_i}{\sum_{j=1}^{n}(m_j \Delta_j)} \tag{2.44}$$

This equation shows similarities with force-based design with the difference that here the design inelastic displacement profile is used and the relative distribution can be generalized to all structures.

2.4.8   Analysis of Structure

In order to determine the design moments at the potential plastic hinge locations, it is necessary to analyze the structure under the lateral design forces determined with Eq 2.44. During the analysis, in order to be compatible with DDBD basis, members stiffness should represent the effective secant stiffness at design displacement response.

2.4.9   Damping Validation

The estimated hysteretic damping has to be compared with the energy dissipated by the structure per load cycle. The energy dissipation can be determined with a cyclic pushover analysis, and it is represented by the area A_h of Fig. 2.8. The equivalent elastic strain energy A_e represents the energy that would be stored in an equivalent purely elastic system without dissipation under static conditions. Hence, the equivalent viscous damping ratio is given by:

$$\xi_{\text{eq}} = \frac{A_h}{4\pi A_e} \tag{2.45}$$

The elastic damping of 5 percent has then to be added to the value computed above in order to have the total value of the equivalent viscous damping coefficient.

If the current value markedly differs from the one initially estimated, the previous steps should be performed again using the results of Eq. (2.45). Once convergence is reached, capacity design can be performed.
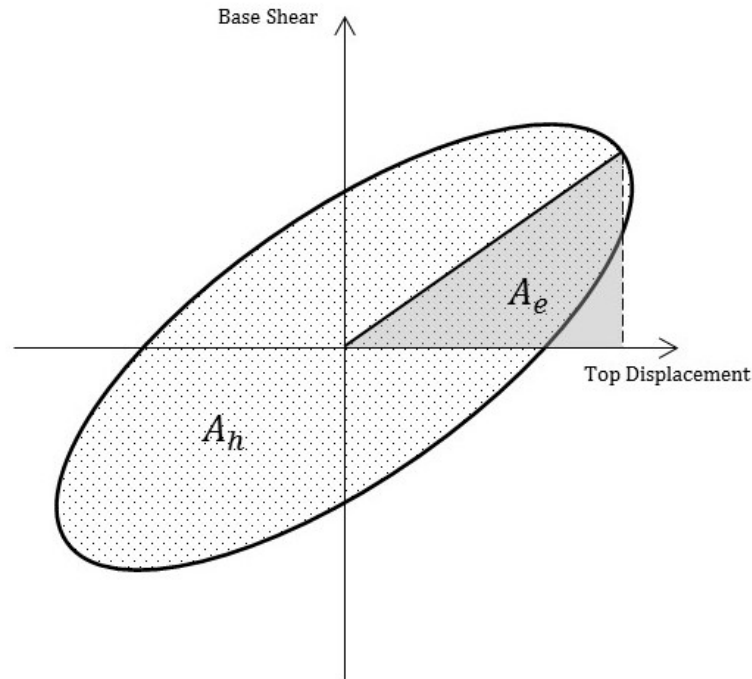
Figure 2.8: Schematic representation for computing equivalent viscous damping coefficient

2.4.10 Capacity Design

The direct displacement-based design procedure determines the structural strength in order to achieve a given performance state, in terms of flexural strain or drift limits, under a specified seismic intensity level. The design process requires the definition of the locations of potential plastic hinges and it wants to ensure that inelastic actions occur only there and only in the desired inelastic mode. Specified measurement must be performed to avoid the formation of plastic hinges in undesired locations and to ensure that inelastic shear displacement does not occur.

The values of moments and shears computed from the distribution of the

base shear take into account only the first inelastic mode of vibration. This is adequate to determine the strength at plastic hinge locations, whereas the structural response will include also the effects of higher modes. This implies a modification of the values of moment and shear in other locations.

Moreover, the material strength normally considered in the computations represents a conservative estimate. In the case that the strength exceeds the design values, the resisting moment developed at the plastic hinge will be greater than the design value since the actual strength, rather than the theoretical one, will be developed under a seismic design event, due to the inelastic response.

The general requirement for capacity protection can be expressed by:

$$\phi_s\, S_D {\geq} S_R = \phi^0\, \omega\, S_E \qquad (2.46)$$

where:

S_E is the basic strength of the location considered, corresponding to the design lateral force distribution defined by DDBD;

ϕ^0 is the overstrength factor;

ω is the dynamic amplification factor;

S_D is the design strength;

S_R is the required dependable strength of the design action;

ϕ_s is the corresponding strength reduction factor.

A value of $\phi_s = 1$ is appropriated for the flexural design of plastic hinge locations, whereas value of $\phi_s < 1$ should be adopted for other locations and actions. The amplification factor ϕ^0 accounts the maximum possible

flexural overcapacity at the plastic hinges, and hence it is the ratio between the capacity of the overstrength moment and the required capacity of these locations. Finally, the dynamic amplification factor ω represents the possible increment of the design actions due to the effects of higher modes.

In many cases, instead of dealing with the additional efforts required to perform modal analysis of the designed structure, a simpler approach to determine the capacity design distribution of moments and shears may be preferred. Simplified rules, similar to existing capacity design rules, have been elaborated for walls, wall/frames, frames, and bridges. The example of cantilever wall structures will be showed in the following section. The validation of the procedure has been determined with the comparison between the results found with time-history analysis for different elastic periods and ductility levels.

When the final level of design forces is evaluated, and thus the necessary level of strength, it is possible to finalize the design of the structure. This approach has been developed for a wide range of different structural types, including walls, frames, bridges, dual systems, etc., and for different materials, such as reinforced, prestressed, precast concrete, steel, masonry and timber.

2.5 DDBD for Cantilever Wall Buildings

In this section the DDBD procedure is applied to cantilever wall buildings.

2.5.1 Design Displacement

In order to determine the design displacement, that is the sum of the yielding and the plastic one, it is necessary to compute the displacement profile of the building, and thus the displacement at each floor-level.

Each building code defines for every structural typology a drift limit θ_c which must be compared with the maximum drift of the structure, that corresponds to the roof drift. If the roof drift is lower than the code drift limit, the design displacement profile is defined by:

$$\Delta_i = \Delta_{y_i} + \Delta_{p_i} = \frac{\varepsilon_y}{l_w} H_i^2 \left(1 - \frac{H_i}{3H_n}\right) + \left(\phi_m - \frac{2\varepsilon_y}{l_w}\right) L_p H_i \qquad (2.47)$$

where ϕ_m is the base curvature corresponding to the design limit state, L_p is the plastic hinge length.

The curvature distribution over the wall height is computed thanks to the assumption that the moment-curvature response is bi-linear: the elastic curvature is linear all along the wall, starting from zero at the top, while the plastic curvature is assumed lumped at the plastic hinge location. The latter is constant and its value corresponds to the actual maximum curvature at the wall base, as shown in Fig. 2.9. The elastic branch is based on the secant stiffness that connects the origin and the first yield. The latter is defined as the point on the moment-curvature response where the tension reinforcement farthest from the neutral axis reaches the yield strain, or where the concrete compression fiber at the same location reaches a strain of 0.002.

The plastic hinge length is defined as:

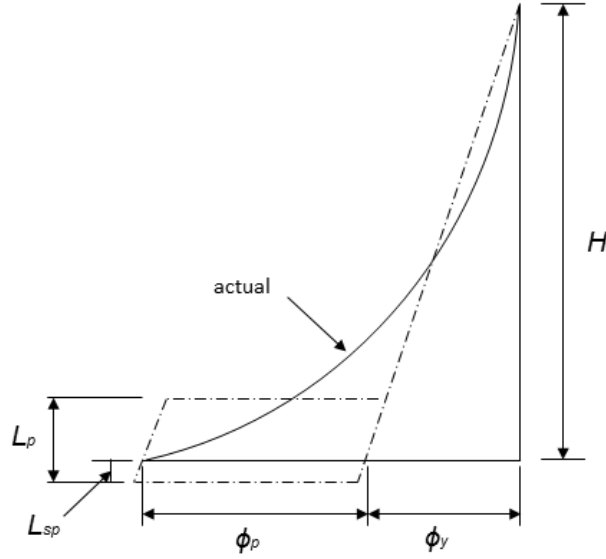$$L_p = k H_e + 0.1 l_W + L_{sp} \qquad (2.48)$$

Figure 2.9: Bilinear approximation of curvature distribution

where $k = 0.2(f_u/f_y - 1) \leq 0.08$. The plastic hinge length incorporates the strain penetration length L_{sp}, which corresponds to the penetration of the plastic strains inside the foundation. It can be computed as:

$$L_{sp} = 0.022 f_{ye} \, d_{bl} \qquad (2.49)$$

where f_{ye} (expressed in MPa) and d_{bl} are yield strength and diameter of the longitudinal reinforcement.

In the case in which the code drift limit governs the roof drift, the design displacement profile is:

$$\Delta_i = \Delta_{y_i} + (\theta_c - \theta_{yn})H_i = \frac{\varepsilon_y}{l_w} H_i^2 \left(1 - \frac{H_i}{3H_n}\right) + \left(\theta_c - \frac{\varepsilon_y H_n}{l_w}\right) H_i \quad (2.50)$$

where θ_{yn} is the yield drift at the top of the wall and depends on the yield curvature of rectangular concrete wall $\phi_y = 2\varepsilon_y/l_w$.

Once the displacement profile is known, the design displacement of the

substitute structure can be computed, so:

$$\Delta_d = \frac{\sum_{i=1}^{n}(m_i \Delta_i^2)}{\sum_{i=1}^{n}(m_i \Delta_i)} \tag{2.51}$$

2.5.2 Yield Displacement

The effective height of the SDOF substitute structure can be determined as:

$$H_e = \frac{\sum_{i=1}^{n}(m_i \Delta_i H_i)}{\sum_{i=1}^{n}(m_i \Delta_i)} \tag{2.52}$$

The yield displacement results from:

$$\Delta_y = \frac{\varepsilon_y}{l_w} H_e^2 \left(1 - \frac{H_e}{3H_n}\right) \tag{2.53}$$

2.5.3 Wall Displacement Ductility Factor

The displacement ductility factor is:

$$\mu = \frac{\Delta_d}{\Delta_y} \tag{2.54}$$

2.5.4 Wall Equivalent Viscous Damping Coefficient

The equivalent viscous damping coefficient ξ_{eq} can be defined through:

$$\xi_{\mathrm{eq}} = 0.05 + 0.444 \left(\frac{\mu - 1}{\mu \pi}\right) \tag{2.55}$$

2.5.5 Effective Period

The elastic displacement spectra may be developed from the design acceleration spectrum for 5 percent damping as follows:

$$\Delta_{(T,5)} = S_{(T,5)} \frac{T^2}{4\pi^2} g \tag{2.56}$$

where $S_{(T,5)}$ is spectral response acceleration at period T relative to 5 percent viscous damping, expressed in terms of gravity acceleration g.

The inelastic displacement spectrum can be determined from the elastic displacement spectrum for the corresponding viscous damping level using the modification factor R_μ defined in Eq. (2.39).

$$\Delta_{(T,\xi)} = \Delta_{(T,5)} \cdot \left(\frac{0.07}{0.02 + \xi} \right)^{0.5} \tag{2.57}$$

The effective period is found through interpolation:

$$T_e = T_c \cdot \frac{\Delta_d}{\Delta_{(c,\xi)}} \tag{2.58}$$

where $\Delta_{c,\xi}$ is the displacement value of the inelastic displacement spectrum with damping ξ corresponding to the corner period T_c.

2.5.6 Effective Mass

The effective mass of the SDOF structure can be defined with:

$$m_e = \sum_{i=1}^{n} \frac{m_i \Delta_i}{\Delta_d} \tag{2.59}$$

2.5.7 Effective Stiffness

The effective stiffness of the SDOF is:

$$K_e = \frac{4\pi^2 m_e}{T_e^2} \tag{2.60}$$

2.5.8 Base Shear

The base shear design force is:

$$F = V_{base} = K_e \Delta_d \tag{2.61}$$

The design base shear V_{base} can be distributed over the height of the wall according with Eq. (2.44), .
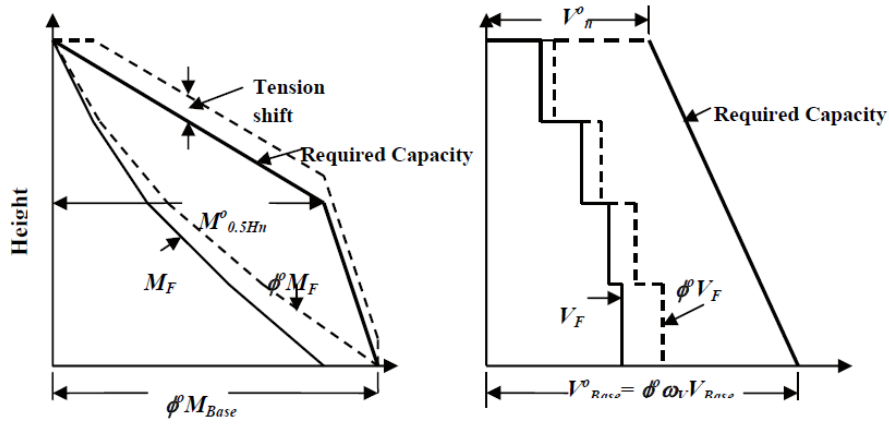
Figure 2.10: Simplified capacity design moment and shear envelopes for cantilever walls, Priestley

2.5.9 Capacity Design for Cantilever Walls

The moment capacity envelope and the shear capacity envelopes are individually studied in case of cantilever walls, following the features proposed by Priestley.

Moment Capacity Envelopes

The envelope of the overstrength moment is bi-linear, with zero moment at the top of the wall as shown in Fig. 2.10 on the left for a four-stories wall.

The overstregth moment at mid-height $M^0_{0.5Hn}$ is found from the overstrength base moment, $\phi^0 M_{base}$, by the relationship:

$$M^0_{0.5Hn} = C_{1,T}\, \phi^0\, M_{base} \tag{2.62}$$

where

$$C_{1,T} = 0.4 + 0.075\, T_i \left(\frac{\mu}{\phi^0} - 1 \right) \geq 0.4 \tag{2.63}$$

In the previous equation the overstrength factor ϕ^0 is determined from section and reinforcement properties using moment curvature analysis, or with

simplified prescription, and T_i represents the initial (elastic) cracked-section period of the structure.

Shear Capacity Envelopes

The envelope of the shear force capacity-design, as Fig. 2.10 shows on the right, is defined by a straight line that goes from the base to the top of the wall. The design base shear is evaluated thought the following equation:

$$V_{base}^0 = \phi^0 \, \omega_V \, V_{base} \tag{2.64}$$

where ω_V is the dynamic amplification factor that is defined by:

$$\omega_V = 1 + \frac{\mu}{\phi^0} \, C_{2,T} \tag{2.65}$$

and $C_{2,T} = 0.067 + 0.4(T_i - 0.5) \leq 1.15$

Once the design base shear is found, the design shear force at the top of the wall can be defined with:

$$V_n^0 = C_3 \, V_{base}^0 \tag{2.66}$$

where $C_3 = 0.9 - 0.3 \, T_i \geq 0.3$

2.6 DDBD for Post-Tensioned Precast Wall Buildings

The DDBD approach could be developed for enhanced structures that are not present in the building code yet. In particular, its application to the unbonded post-tensioned precast wall will be presented. As it will be described in more detail in the following Chapters, the lateral resisting system is composed by two vertical precast wall panels stacked one above the other and it is vertically post-tensioned from the roof level to the foundation. The walls are unrestrained at the base allowing gap openings at the base, while the post-tensioning strands provide a clamping force that pulls the systems back to the undisplaced position. The additional damping system is required since the energy absorbed by the system is very low, and hence it doesn't assure enough hysteretic damping. Ductility could be provided for example by mild reinforcement at the base of the wall or by shear connectors spread over the vertical joints between the wall panels, if multiple panels are placed side by side. On the other hand, unbonded post-tensioned precast jointed walls have higher re-centering capacity than conventional walls, exhibiting low or zero residual displacement under the design seismic forces. Therefore those systems present minor cracks at the connections compared with monolithic systems, thanks to the gap opening at the base that allows the wall panels to remain essentially elastic during the seismic event, as it can be seen in Fig 2.11.

In this section the intent is to highlight their main characteristics in order to show the differences of the design procedure in comparison with monolithic cantilever walls. The unique characteristics of those systems are reflected in the DDBD procedure, since this method takes into account the typical dis-
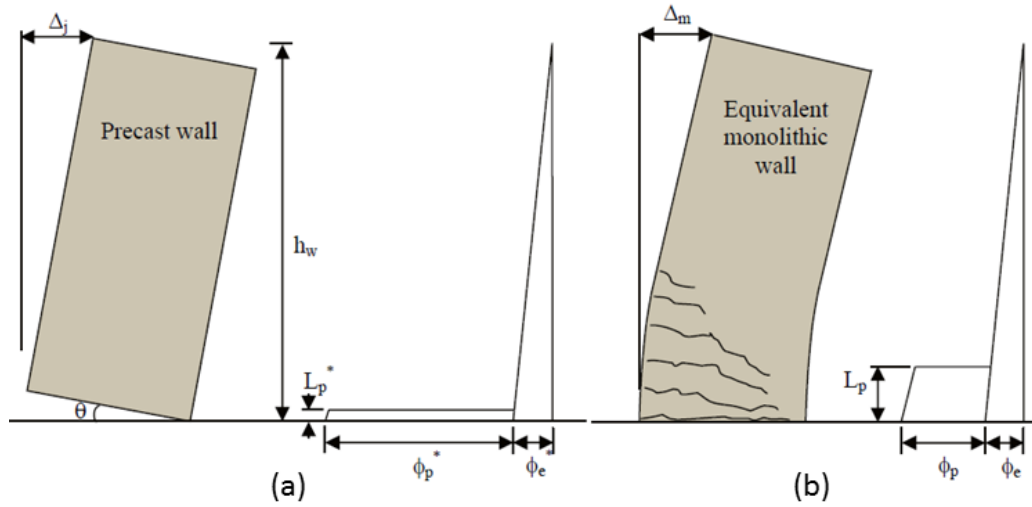
Figure 2.11: Flexural response and associative curvature for precast jointed wall (a) and equivalent monolithic wall (b)

placement profile and hysteresis rule of the structure from the very beginning.

The considered structure is an unbonded pressed wall, without any additional damping provided by mild reinforcement or other means. The design procedure is similar to the one presented in the previous section for cantilever wall building, except for the displacement profile and the hysteretic damping.

2.6.1 Design Displacement

Since the design deformation is dominated by cracks only at the base of the wall, the design displacement profile at the limit state can be assumed to be linear. Design will always be governed by the code drift limit θ_c.

The design displacement profile results to be:

$$\Delta_i = \theta_c H_i \tag{2.67}$$

The design displacement is then computed in the usual way with Eq. (2.51).

2.6.2 Equivalent Viscous Damping

The effective damping level for these kind of walls without supplemental damping can be assumed to be 5 percent related to the effective stiffness.

In this way:

$$\xi_{\text{eq}} = \xi_{\text{el}} = 0.05 \tag{2.68}$$

2.6.3 Effective Period

The effective period can be evaluated directly from the elastic displacement spectrum, and thus:

$$T_e = T_c \frac{\Delta_d}{\Delta_{(c,5)}} \tag{2.69}$$

Chapter 3

Unbonded Post-Tensioned Concrete Shear Wall

3.1 Introduction

In this chapter we describe all the steps that led to the investigation of lateral load resisting system that differ from the conventional solution in region with low to high seismicity. In fact, in the seismic engineering philosophy it is becoming more and more important to realize structures that not only prevent the collapse but that can be cost-efficient as well, in terms of structural and non-structural repair and in terms of loss of business operation after the earthquake. The self-centering system is an earthquake resisting system that could achieve the aforementioned enhancement, proving a restoring force that pulls the structure back in its undisplaced configuration. This alternative fits well with precast concrete, since it is necessary that the single structural members are not tied and a gap could occur between them.

Therefore we start taking into account the precast concrete structures and their behavior during a ground motion, then we talk about self-centering

structures and their unique properties before focusing on a particular lay-out, called unbonded post-tensioned precast concrete wall. This lateral load resisting system is studied in detail, considering its global behavior and different possibles design options already present in literature. At the end, a preliminary design methodology is described.

3.2   Precast Concrete Benefits and Limitations

The use of precast concrete in the structural design provides many advantages over cast-in-place concrete systems, primarily attributed to the factory-like setting. We can summarize them as follows [19]:

High quality The quality of construction is higher in precast concrete than cast-in-place one, since precast members are produced in a controlled environment, where curing conditions like humidity and temperature are constantly monitored. The manufacturing plant also implies more production inspection in relation to design specifications, because workers can be easily supervised. Moreover, the prestressing and the placement of post-tensioning ducts can be easier performed than in the construction site.

Reduced construction time The reduction of the amount of formwork and temporary supports increases the speed of on-site construction. Furthermore, bad weather conditions no more limit the construction site organization and the time wasting.

Reduced costs Faster erection time lead to reduced labor and construction costs. It can be a huge part of the total building costs, for example in the cities.

Advanced technology Advanced technology including computer-aided man-
ufacturing and robotics increase the efficiency of the construction pro-
duction.

Despite all these advantages, poor performance of precast concrete struc-
ture in past earthquakes led designers and contractors to prefer cast-in-place
concrete for constructions in seismic regions and thus to discard the precast
concrete as a possible design option. The brittle structural behavior was
due to the insufficient connection details between precast members. Large
gap openings in the horizontal joints between the wall panels cause high
compressive stresses near the wall ends and large deformations on the floors.

For this reason nowadays the U.S. building code ACI 318 severely con-
strains the use of precast concrete seismic systems, permitting their design
only if they emulate the behavior of monolithic cast-in-place concrete struc-
tures. Otherwise, specific experimental investigations are needed. Specifi-
cally, Chapter 21 of ACI 318 (2011) states that "a reinforced concrete struc-
tural system not satisfying the requirements of this chapter shall be per-
mitted if it is demonstrated by experimental evidence and analysis that the
proposed system will have strength and toughness equal to or exceeding those
provided by a comparable monolithic reinforced concrete structure satisfying
this chapter". The "emulative" behavior is provided through cast-in-place
concrete connections between the precast members. The resulting structure
is intended to be continuous, thus emulating a cast-in-place structure. How-
ever, these systems lose all the unique properties of precast structures, like
the economic one, requiring steel or cast-in-place concrete components in
their joints.

Poor behavior of conventional lateral resisting systems in recent earth-
quakes shows that new opportunities for precast concrete buildings exist and

innovative systems could be developed. After the 6.3 magnitude earthquake that occurred in Christchurch, New Zealand in February 2011, approximately 50% of the buildings in the financial district were declared unusable because they suffered critical structural damages or because they were adjacent to unsafe buildings [2]. The estimated cost only for rebuilding after this earthquake is $40 billion (New Zealand Dollars), to which must be added the economic losses due to business inactivity. It is just an example that buildings with more resilient lateral resisting systems are needed to create a structure that is cost-efficient. Seismic base isolation is one of the most popular means to reduce seismic effects in a building, decoupling the substructure from the ground motion in the horizontal direction with specific devices. But the cost of isolation systems confines such options to building of significant importance and to bridge structures. Self-centering lateral load resisting system could be a cheaper solution, that uses more conventional construction technologies.

3.3   Self-Centering Structures

Conventional seismic lateral force resisting systems resist collapse through inelastic behavior of structural elements. For example a reinforced concrete wall should withstand earthquakes actions with the formation of a flexural plastic hinge at the base of the wall. However, it induces cracking and crushing of the concrete in this region, as well as yielding of the longitudinal reinforcing steel, resulting in significant and often irreparable damages. In general, structural damages may also include permanent horizontal displacement of the structure and buckling, yielding or fracture of single members, both structural and non-structural. Repairing them is expensive and

time-consuming, and the building could remain out of service for a long period. If the residual drift is too severe or if the structural damage is significant, the structure may have to be demolished. Since the 1990's researchers started studying high-performance structures which can resist design earthquake with little structural damages and residual drift, in order to reduce the economic disruption after a seismic event. This new kind of seismic resisting systems prevent yielding in structural components through gap opening mechanism between different elements, in order to soften the structural response. Post-tensioning strands are used to return the structure to the upright position after the earthquake, minimizing the residual lateral displacement. The re-center property confers to these new systems the name of *self-centering systems*. An additional energy dissipation system is needed to reduce drift during the earthquake and to provide ductility to the structure.

3.3.1 Review of Literature

The PREcast Seismic Structural Systems (PRESSS) research program coordinated the efforts of many researchers across the United States and started to understand and improve the performance of precast concrete buildings in seismic regions. Starting in 1990, the PRESSS program and its developments were described for the first time by Priestley in the PCI Journal (Precast/Prestressed Concrete Institute) in 1991. In particular, considering frames and walls as lateral resisting system, he showed that the use of unbonded post-tensioning to connect precast concrete members has beneficial effects on the response of precast subassemblages. So Priestley and Tao (1993) proposed the use of precast concrete moment resisting frame systems prestressed with partially unbonded tendons as earthquake resisting system. Their studies were carried out by MacRae and Priestley (1994) with experi-

mental investigations of single components. Stanton et al. (1993) proposed a frame system with ordinary reinforcement and unbonded tendons in the critical connections in order to dissipate the seismic energy.

Additionally, a research team at Lehigh University tried to apply the self-centering concepts to concrete shear walls developing unbonded post-tensioned precast concrete single walls with no yielding components [5] [6], and subsequently they were tested under simulated lateral seismic loading by Perez et al. (2004). Experimental investigations show how the small energy dissipated by these structures limits their application under strong earthquake, resulting in larger lateral displacement than a conventional cast-in-place shear wall. Therefore, a number of researchers have investigated the use of different supplemental dissipation systems. Part of the PRESSS program began focusing on the unbonded post-tensioned precast jointed wall system, where multiple wall panels are placed side by side and connected with yielding shear plates. This program culminated with the testing of a 60% scale five-story test building that used precast jointed walls and prestressed concrete frames as lateral force resisting systems.

Relevant studies were carried out for unbonded post-tensioned hybrid walls, that dissipate energy through yielding steel bars inside the concrete. Rahman and Restrepo (2000) and Holden et al. (2001) conducted experimental researches on this type of wall. A research group, born in 2007 in Notre Dame University (USA) and led by Smith and Kurama, focused on hybrid walls producing a large amount of works and summarized in analytical design guidelines for solid and perforated walls [23], [24].
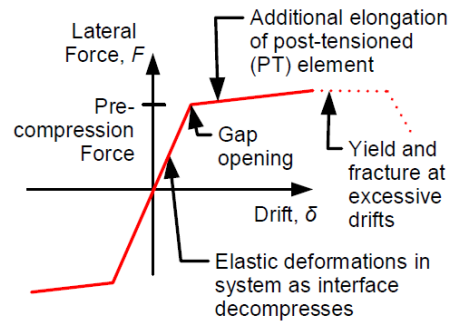
Figure 3.1: Restoring behavior due to gap opening

3.3.2   Hysteretic Behavior

The hysteretic response of a self-centering seismic lateral resisting system can be tuned by the proportion of restoring force and energy dissipation components. The most common approach for creating a restoring force results in gap formation between two surfaces that are initially precompressed together. The expected load-deformation behavior is bilinear elastic, where the gap opening creates the non-linearity.

Two examples of structures that use PT steel to provide self-centering are the hybrid moment resisting frame and the unbonded post-tensioned precast wall. The former allows gap opening in the joints between beams and columns and the unbonded post-tensioning steel running along the beams closes it when the lateral force is removed. The latter forms the gap at the joint between wall and foundation when the lateral load applies an overturning moment on it. Vertical unbonded post-tensioned tendons pull the structure back to its undisplaced configuration. Gap opening mechanism allows the self-centering behavior, but does not provide energy dissipation to the structure, so damping devices are required. They can be divided into 3 families:

<div align="center">(a)   (b)</div>
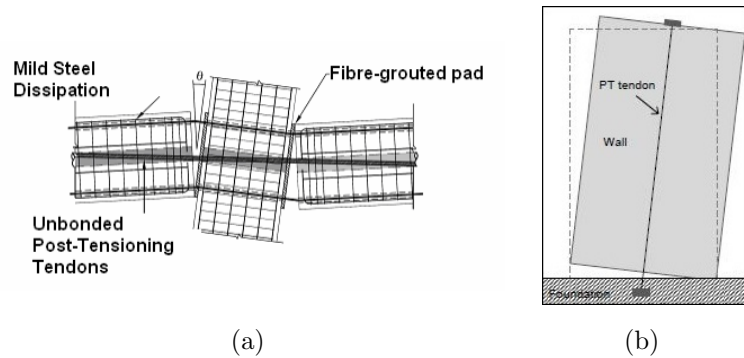
Figure 3.2: Examples of Self-Centering System: **(a)** Hybrid moment frame, **(b)** Unbonded post-tensioned precast wall
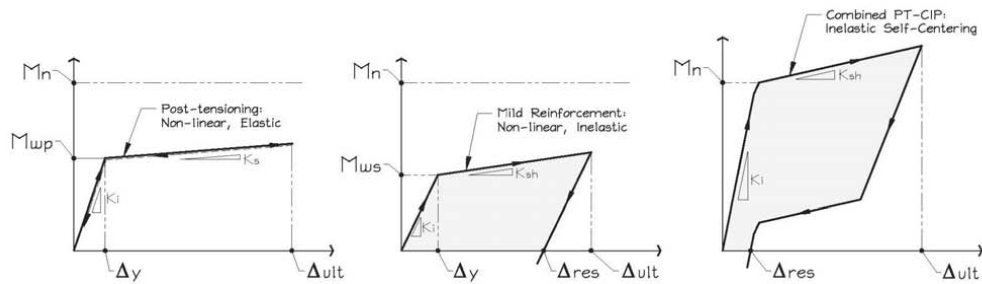

Figure 3.3: Expected flag-shaped behavior of a generic self-centering system, [12]

- Hysteretic damping elements;

- Viscous damping devices;

- Friction damping devices.

For example unbounded mild steel reinforcement at joints between different members can be used as hysteretic damping element. When the gap opens, the steel yields and dissipates energy. Its response can be modeled with an elasto-plastic hardening constitutive law. The behavior of the full structure under lateral loads is the sum of its contributions and the one of the restoring system and the result is called flag-shaped hysteresis loop.

Figure 3.3 represents the moment-displacement relationship in the lateral load-unload conditions, where the gray area is the dissipated energy. We can observe that the main parameter to consider in the design phase in order to minimize the residual displacement and design a structure which perform efficiently is the proportion between the restoring force and the damping system. Furthermore, the ability of these systems to return in the undisplaced configuration is guaranteed only if the post-tensioning tendons remain elastic. For now on we will focus on the unbonded post-tensioned precast concrete wall, deepening its behavior and how to design it.

3.4 Unbonded Post-Tensioned Precast Concrete Wall

Self-centering precast concrete walls use all the advantages of structural concrete walls by adopting both prestressing and precast technology to accomplish enhanced seismic performance. This research investigates a lateral resisting system constructed by piling rectangular precast panels along horizontal joints above the foundation. Dry-pack grout is used at these joints to permit inaccuracies during construction. The self-centering ability is provided by the gravity loads acting on the wall and by multi-strand tendons running inside ungrouted ducts through the wall panels and the foundation. The post-tensioned strands are anchored at the foundation and at the top of the wall.

As gap opening occurs at the horizontal joint between wall and foundation during the earthquakes, the unbonded prestressing tendons are elongated, with the strain evenly distributed along the length of the tendons. If the tendons are designed to remain in their elastic state, they provide a restoring
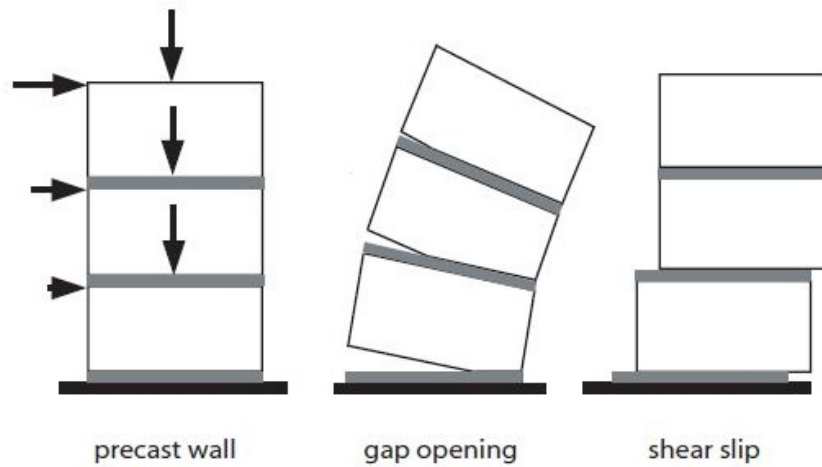
precast wall   gap opening   shear slip

Figure 3.4: Possibles behaviors along the horizontal joints of a precast wall

force that can re-center the wall back to its undisplaced position when the seismic action is removed. As a result, minimal structural damage occurs during an earthquake, compared to the extensive damage that would be expected for a monolithic reinforced concrete wall.

No energy dissipation system is taken into account at the moment. We will discuss later different dissipating options, how to design them and how they interact with the full structure.

3.4.1   Expected Lateral Behavior

The behavior of this system under lateral load is governed by how it works along the joints. The possibles behaviors are called gap opening and shear slip, that could be seen as flexural response and shear response respectively. Studies conducted by Oliva et al.(1989,1990) on precast wall without pre-compression show that gap opening is more desirable that shear slip, since shear slip develops unrestrained motion and gravity loads can't provide the necessary restoring force to reverse it. On the contrary, in the case of flexural

response dead loads tend to close the gaps upon unloading. This behavior is emphasized in post-tensioned walls where the tendons increase the restoring force. Therefore proper joints design and detailing are necessary to prevent shear slip and ease gap opening. We don't take it into account in the seismic response of the structure, since shear deformations of the wall panels should be negligible compared to the axial-flexural deformations.

Kurama et al. in [6] specified 4 states in the base-shear-roof-drift relationship of an unbonded post-tensioned precast wall under lateral and gravity loads, in order to identify its seismic performance. The base shear V is the sum of the lateral loads applied at each level, while the roof drift Δ is the ratio between the wall displacement at the roof level and the wall height. The seismic actions are distributed over the height of the wall as the inertial forces corresponding to the first mode of the structure that come from a linear-elastic modal analysis.

1. **Decompression State** identifies when a gap begins to open at the base horizontal joint. It indicates the starting point of the nonlinear behavior of the wall, but it is negligible until the gap opening affects a significant portion of the length of the wall.

2. **Softening State** designates the notable reduction in the lateral stiffness of the wall due to gap opening along the horizontal joints and non-linear behavior of the concrete in compression. It represents a sort of effective linear limit, governed by gap opening or by concrete non-linearity depending on the concrete extent: if the concrete stress is large, the effective linear limit is governed by non-linear behavior of the concrete, otherwise it is governed by gap opening.

3. **Yielding State** is the point when the strain in the post-tensioning

steel reaches the yielding value. From here on, extensive damage to the wall occurs.

4. **Failure State** is the final state where the wall fails as a result of crushing of concrete at the wall toe. Sufficient confinement should be provided such that the failure state is far from the yielding state in terms of roof displacements.

Kurama also examines the base-shear-roof-drift relationship under gravity load and cyclic lateral load. It shows that the behavior of the wall with no energy dissipation system is nearly nonlinear-elastic, where the loading and unloading paths are very close. Moreover we can observe that upon unloading from a large nonlinear drift, the wall returns back towards its original position with no residual drift.

The global lateral behavior of a self-centering wall is highlighted in Fig. 3.7, which shows the differences in the roof-drift time-histories of an unbounded post-tensioning precast concrete wall and a comparable monolithic cast-in-place reinforced concrete wall. The two walls have comparable strength, initial stiffness, viscous damping and linear-elastic fundamental period. The lateral hysteretic behavior is the only difference. The evolution in time of the roof drift is determined through a nonlinear dynamic analysis under the Hollister ground motion (recorded during the 1989 Loma Prieta earthquake) scaled to a peak acceleration of 0.52 g. As shown by the chart, the maximum roof-drift of an unbounded post-tensioning precast wall is larger than the one of a conventional wall. Furthermore the response of a self-centering wall oscillates around zero drift values, indicating its re-centering ability, but it decays less rapidly, resulting in a large number of large drift cycles. This means that it doesn't dissipate enough energy.
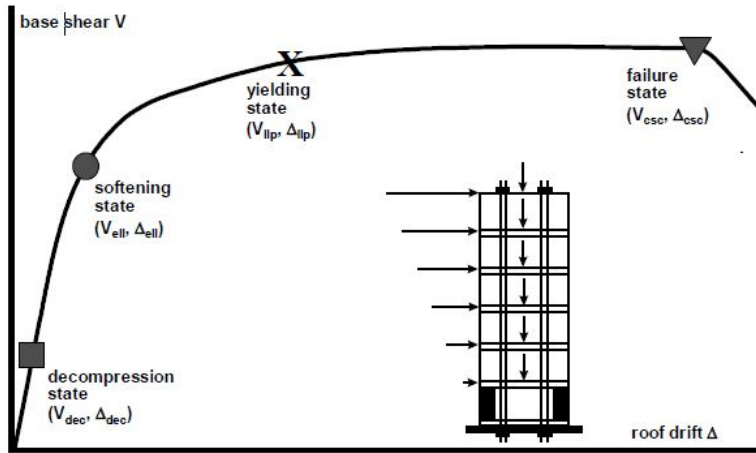
Figure 3.5: Base-Shear-Roof-Drift relationship of an unbonded post-tensioned precast wall, Kurama
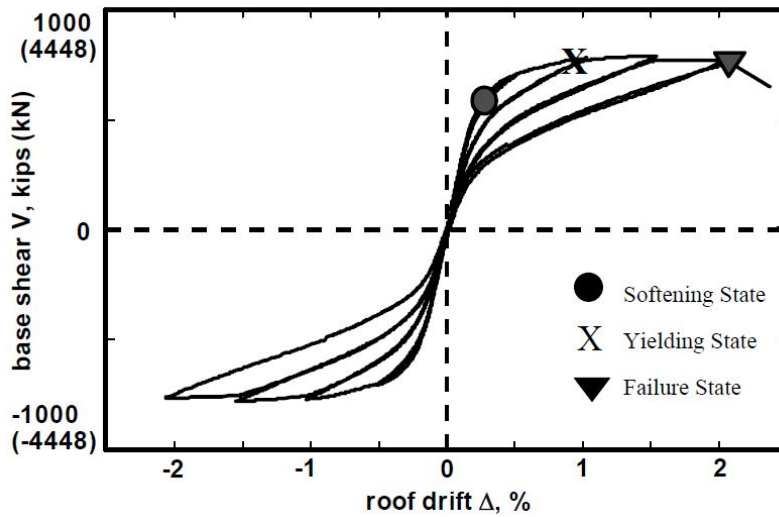

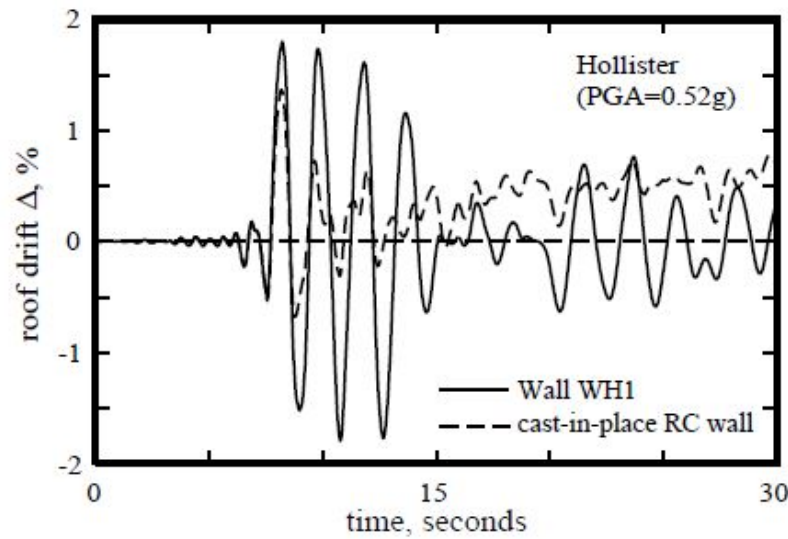**Figure 3.6:** Hysteretic loop under cyclic load, Kurama

Figure 3.7: Roof-drift time-history, Kurama

3.4.2   Energy Dissipation System: Design Options

In the previous section we saw that the unbonded post-tensioning precast concrete wall is an interesting design option as lateral resisting system under seismic loads. The system exhibits the re-centering capacity, reducing residual drift and permanent damages. It affects the repairing costs of the structural and non-structural components, and all the economic losses related to building non usability after the earthquake. But the wall requires a supplemental energy dissipation system. This section describes the most studied unbonded post-tensioning precast wall with passive energy dissipation systems. Then other possible configurations will be proposed.

Unbonded Post-Tensioned Precast Jointed Wall

The unbonded post-tensioned precast jointed wall is the most studied configuration, because it was part of the PRESSS (PREcast Seismic Structural System) research program, initiated in the United States in the early 1990's.
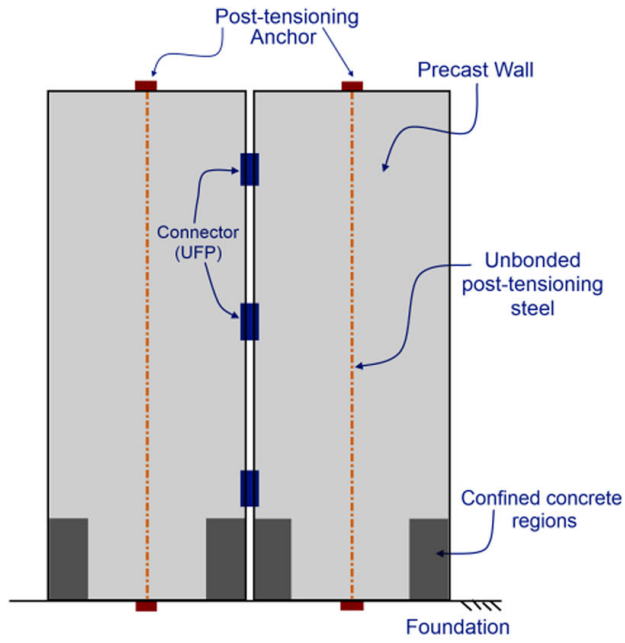
Figure 3.8: Unbonded post-tensioned precast jointed wall

Figure 3.9: U-shaped flexural plate (UFPs)

One of the objective of this program was the design, modeling and testing of an unbonded post-tensioned precast jointed wall. The lateral resisting system is composed of two vertical precast wall panels placed side by side. Shear sliding occurs at the vertical joint between them. Each wall may be composed by several elements stacked one above the other or by a single element and it is vertically post-tensioned from the roof level to the foundation. The tendons may be placed at the edge or at the middle of the wall. The second option is preferable because it induces the least average tendon elongation. The tendons are designed to remain elastic for the design drift, and therefore for the design gap opening. The vertical joint presents several shear connectors that dissipate energy by yielding. PRESSS building test contains the U-shaped Flexural Plates, initially proposed by Kelly et al. (1972), even if other connector types may be considered. A relative vertical displacement occurs between adjoining panels, as the walls rotate and the base crack causes uplift. When the ends of the UFP are subjected to a relative displacement, the semi-circular section rolls along the plate and dissipate energy where the radius of curvature changes from straight to curved and vice versa [1].

Unbonded Post-Tensioned Hybrid Wall

The term "hybrid" reflects that a combination of unbonded post-tensioning steel and traditional mild steel reinforcing bars is used for lateral resistance across the wall base joint. The hybrid wall behaves as a single unbonded PT precast concrete wall: the base joint opens up and the tendons elongate between their anchors. The mild steel reinforcement undergoes tension and compression yielding, providing a source for energy dissipation during seismic event. For these reasons it is called energy dissipation steel, or just ED steel. The bars are normally debonded over a short length of the base wall panel
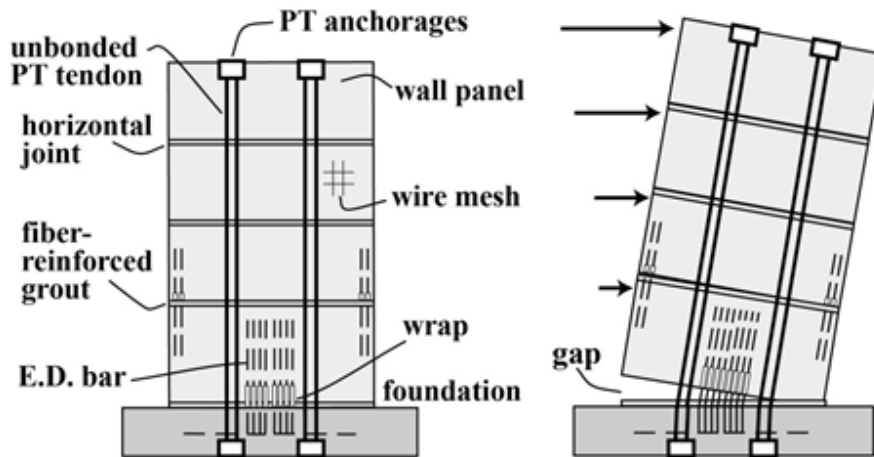
Figure 3.10: Unbonded Post-Tensioned Hybrid Wall: general layout and displaced configuration

in order to reduce the strain demand and prevent fracture of concrete while the steel elongate. On the other side the ED steel is cast into the foundation. The main advantage of this system is that while the seismic response of a hybrid wall is fundamentally different than a traditional reinforced concrete wall, its construction components are conventional and standardized, not requiring special manufacture or expensive devices like viscous dampers. On the other hand, the ED steel inside the precast concrete panels can not be so easily repaired or replaced in case of fracture as external devices such as the U-shape flexural plates.

Unbonded Post-Tensioned Precast Concrete Walls With Supplemental Damping Devices

Another way to dissipate energy could be using additional damping devices, that could be viscous dampers or friction dampers. A viscous damper is a mechanical device which softens the imposed displacement, turning it into a
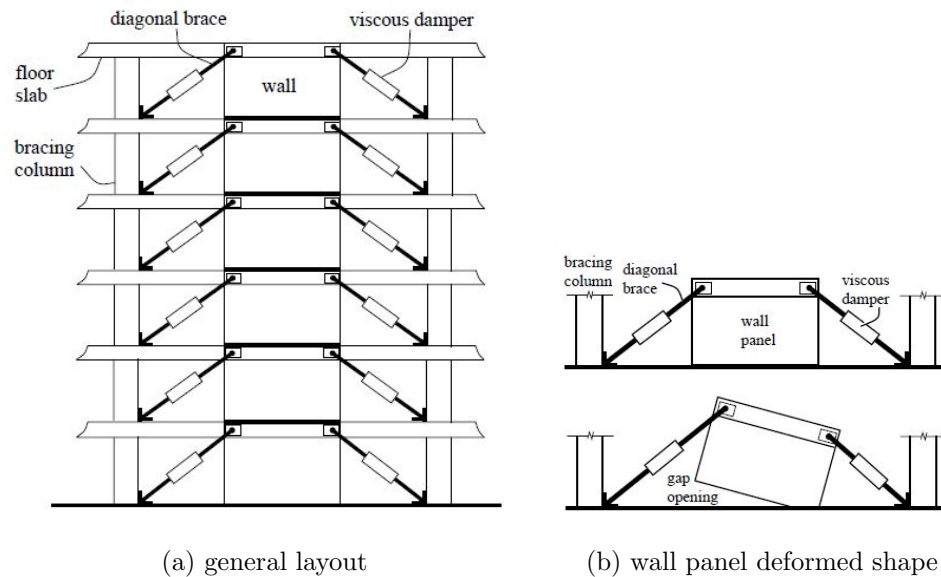
(a) general layout   (b) wall panel deformed shape

Figure 3.11: Unbonded post-tensioned precast walls with spread viscous dampers

viscous friction. The resulting viscous force is proportional to the velocity, and it has opposite sign to the applied force. The resultant force will be smaller than the force applied to the device, and consequently the motion decreases. In particular a fluid viscous damper device dissipates energy by pushing fluid through an orifice, producing a damping pressure, therefore a damping force.

Friction dampers are designed to have moving parts that slide over each other during a strong earthquake. When the parts slide over each other, they create friction which dissipates some of the energy from the earthquake that goes into the building. For example the pall friction dampers consist of a series of steel plates which are clamped together with high strength steel bolts and allowed to slip at a predetermined load. These plates are treated in a particular way to develop friction. Usually friction dampers are simpler and less cheap than viscous dampers.

Kurama in [7] proposed unbonded post-tensioned precast concrete walls

in which the supplemental energy dissipation system is made with linear fluid viscous dampers placed inside diagonal braces anchored to the precast wall at one end and to a column on the other end. The unusual characteristic of this system is that it uses not only the panel-to-foundation joint, but also the panel-to-panel joint. Each gap opening in the wall creates a relative displacement between the two ends of the braces and therefore velocity in the dampers. Interesting from the engineering point of view, this solution could not fit architectural requirements.

The use of friction and viscous damping devices improve the performance of self-centering systems providing the necessary energy dissipation. In an hybrid wall the presence of mild reinforcement and PT tendons at the base wall create congestion problems between all the components. Therefore in some cases construction issues imposed the use of external damping devices instead of bars inside the concrete. On the other hand, these systems represent a specialized, relatively unfamiliar and therefore expensive technology. Another possible configuration of self-centering wall with viscous damping devices will be presented in Chapter 6.

Propped Rocking Wall

In the San francisco Bay Area several buildings underwent seismic retrofitting using propped shear wall systems, monolithic cantilever walls propped with friction dampers (Wolfe et al. 2001). Fathali (2009) proposes an enhancement of the existing propped shear wall, called propped rocking wall (PRW), which consists of a post-tensioned concrete wall which is propped near its top by multistory diagonal braces. These long braces can incorporate hysteretic dampers and they are supported by the floor slabs of the building to reduce buckling instability. Unbounded PT bars are installed at the cen-
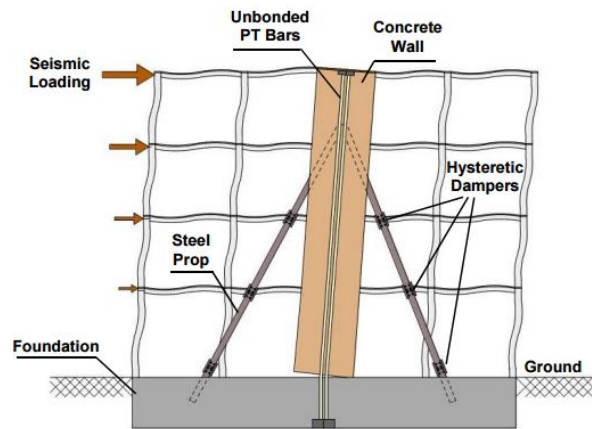
Figure 3.12: Propped rocking wall: general layout and deformed shape, [11]

ter of the wall section to minimize axial strains and prevent steel yielding
resulting from large lateral drifts. Nicknam at al. [11] developed a direct
displacement-based design (DDBD) methodology for PRWs.

3.5   Unbonded Post-Tensioned Hybrid Wall

After looking at all the possible configurations of unbonded post-tensioned
precast concrete walls with different energy dissipation systems, we focused
on the hybrid solution. Fig. 3.10 shows the elevation and of a typical un-
bonded post-tensioned hybrid wall. It consists of vertical panels stacked one
over the other. The desired nonlinear behavior under lateral load is governed
by the opening of gaps along the horizontal joints, in particular the one
between the wall and the foundation. High strength post-tensioning (PT)
steel and mild steel reinforcement cross the base joints and provide enhanced
seismic characteristic to the wall system. A restoring force that closes the
uplift upon unloading is given by the PT steel, resulting in the ability of the
structure to return toward its original undisplaced position after the seismic

event. For this reason the strands should remain elastic during the ground motion and don't lose their re-centering peculiarity. To protect the tendons from yielding as the gap opening at the base joint occurs, the initial pre-stress of the strands f_{pi} usually ranges from 55 to 65 percent of the ultimate strength of the post-tensioning steel, f_{pu}.

The tendons are covered with corrosion inhibiting coating and encased in a plastic sheathing and the bond between them and the concrete is intention-ally prevented. Therefore the strains and stresses of the tendon depend on the overall deformation of the wall over the unbonded length rather than the sectional deformations. The use of unbonded tendons allows the wall to suffer significant lateral displacements without yielding of the high strength steel. Moreover the PT steel does not transfer tensile stresses into the concrete and the wall panels remain undamaged without cracking. For this reason the unbonded post-tensioned solution is preferable to the bonded one.

The mild steel reinforcement is designed to yield in tension and compres-sion providing inelastic energy dissipation (so it is called energy dissipating (ED) steel). In order to prevent fracturing of the ED steel and cracking of concrete while the steel yields, the reinforcement can be isolated from the concrete by wrapping it with plastic sleeves over a predetermined height near the horizontal base-panel-to-foundation joint. The amount of mild reinforce-ment is reduced thanks to the addition of post-tensioning which provides a significant increase in flexural strength. This results in more compact wall dimensions with respect to a conventional cast-in-place reinforced concrete wall. A small amount of mild reinforcement is placed at the upper joints and avoids gap openings.

The gap opening behavior of the hybrid wall leads to minimal concrete cracking but localized compression damage should be expected at the toes

of the base panel, around which the wall rotates at the base. Under a strong earthquake, the cover concrete at the wall toes will be damaged and possibly spalls, but it is acceptable and could be easily repaired if necessary. However, extended damages of the concrete are unwanted and confinement reinforcement in the form of closed hoops should be placed at the ends of the base panel to prevent compression failure of the boundary regions. From a practical standpoint, these regions could be very congestioned and it is necessary to have the ED steel and PT steel outside them.

The horizontal joints must ensure shear slip capacity, especially the one between the wall and the foundation. The prestress, together with the gravity loads, provide a clamping force which resists shear slip along the horizontal joints. Usually the joints present plain dry-packed connections with surface contact and their shear slip capacity is given by the product of the shear friction coefficient and the compression force acting on them due to gravity loads and PT force. Previous researches (Foerster 1989) show that a reasonable value of shear friction coefficient for horizontal connections of unbonded post-tensioned precast walls could be 0.5. Gap opening due to seismic force reduces the contact area and the shear slip capacity decreases. In a properly designed and proportioned hybrid wall, shear slip displacements along the horizontal connections can be neglected as a result of unbonded post-tensioning.

Basing on the technologies developed for unbonded post-tensioned precast hybrid wall, recent studies tried to apply it to cast-in-place concrete walls. Panian et al.([12], [13]) design the retrofit of buildings that use unbonded post-tensioned cast-in place hybrid walls as lateral resisting system in Berkeley and in general in the San Francisco Bay Area. This technology tries to blend the self-centering capability provided by the vertical post-tensioning

with the intrinsic advantages of cast-in-place construction to provide a more effective and efficient seismic resistance system. There are specific construction details that differ precast and cast-in-place constructions, but the lateral behavior of the two systems under seismic loads is analogous.
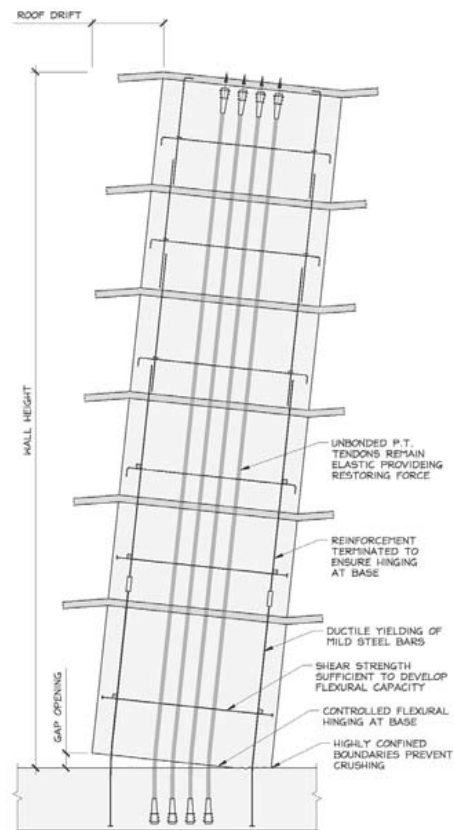

Figure 3.13: Hybrid PT-CIP wall behavior, [12]

3.5.1   Design Assumption

The study of the hybrid wall described above is conducted with two-dimensional analysis of simple isolated walls, neglecting the three-dimensional seismic effect. The following assumptions and considerations are made for two-dimensional analysis and modeling:

1. Seismic forces are in the direction of the wall;

2. Torsional, shear or out-of-plane displacements are ignored and the wall is subject only to in-plane flexural displacement;

3. The wall itself resists to the entire seismic force in the wall direction;

4. The foundation and the supporting ground are rigid;

5. Out-of-plane instability of the wall is not modeled;

6. Anchorages of the tendons remain fully effective during the seismic response of the wall;

7. The interaction between the wall and the floor diaphragms is limited to the lateral forces that each level transfers to the wall;

8. In case of precast wall, there is no panel-to-panel gap opening.

3.5.2   Seismic Design Approach

The best way to design a lateral resisting system under seismic loading is a performance-based design approach, where the designer specify the expected performance of the structure under a specified earthquake magnitude. For this reason we need to establish seismic performance levels, and therefore seismic input levels and building limit states.

Seismic Performance Levels

ASCE 41, Seismic Rehabilitation of Existing Buildings (2007), recommends four levels of performance, which are the Collapse Prevention, the Life Safety, the Immediate Occupancy and the Operational Building. The performance levels are selected based on the level of post-earthquake service that needs to be provided.

- The **Operational Building performance level** assumes that the building sustains minimal or no damage to their structural and non-structural components and it is able to continue its normal operations after the seismic phenomenon.

- The **Immediate Occupancy performance level** requires that the structure would be in operation right after a major earthquake without loss of lives. It is usually assigned to essential facilities like control buildings, hospitals or police centers. Buildings that meet this building performance level are expected to support limited structural damage and only minor damage to their nonstructural elements. Although immediate occupancy is possible, some repair of utility services may be necessary before the building full functionality is restored.

- The **Life Safety performance level** reduces the risk to life loss or serious injury to the plant personnel or public during the design earthquake. This performance level includes extensive damage to both structural and nonstructural components of the structures but some margin against total or partial collapse still remains. Repairs may be required before re-occupancy, though in some cases they are so widespread that it may not be cost effective.

- The **Collapse Prevention performance level** describes a post-earthquake condition in which the entire building is tending toward total collapse but it already has safety margin in order to avoid significant loss of lives. However, many buildings designed to meet this performance level may lead to complete economic losses and should be demolished.

Seismic Input Levels

Earthquake records for a specific site where the building will rise are scaled to two different seismic input levels. These levels are related to the seismic hazard of that geographic area, so to the probability that an earthquake of the same magnitude will occur during the life of the structure. The Design Basis Earthquake (DBE) is defined to have a 10% probability of being exceeded in 50 years, corresponding to 475 years return period. Instead the Maximum Considered Earthquake (MCE) is defined to have a 10% chance of exceeding in 250 years and it is usually defined in the common practice as 3/2 of the DBE. The Life Safety performance level and the Immediate Occupancy performance level are the target level for the DBE, while the Collapse Prevention performance level is the target level for the MCE.

During the design phase these input levels can be taken into account in terms of response spectra or ground motion time histories, depending on the type of analysis the designers are conducting. If they are performing a static equivalent lateral force procedure, the distribution of the lateral loads over the height of the building is determined through the well-known Force-Based Design method (FBD) or through the Direct-Displacement-Based Design method (DDBD). It is important to notice that these two methodologies lead to lateral forces that could be very different in some kind of structures, as we saw in the previous chapter. For this reason it is interesting to un-

derstand which static-equivalent method brings to more realistic values, in order to find a solution that minimize the size of structural components and the material quantities for reaching the same performance goal.

Building Limit States

The building limit states should consider the entire construction, including limit states for the unbonded post-tensioned hybrid wall, the moment resisting frame (if present), the gravity load resisting system, and also the non-structural components. As regards the hybrid walls, the most important limits states could be:

1. Gap opening at the base;

2. Spalling of cover concrete at the base;

3. Yielding of the post-tensioning steel;

4. Crushing of the confined concrete;

5. Shear slip along the horizontal joints.

The wall design capacities should therefore satisfy these limit states, which are associated to different performance levels. The wall demands are summarized by two parameters: the base shear demand and the roof drift demand. For the DBE we define the design base shear demand V_{wd} and the design roof drift demand Δ_d, while the maximum base shear demand V_{max} and the maximum roof drift demand Δ_{max} correspond to the MCE.

3.5.3 Design Objectives

Before developing an analytical procedure to design an unbonded post-tensioned hybrid wall, we need to define the expected behavior of the structure in the

different performance levels considered. The enhanced properties of the self-centering structures, described above, allow to design structures that achieve the Immediate Occupancy performance level under the design basis earthquake and the Collapse Prevention performance level under the maximum expected earthquake. The goals of this research is to understand which analysis methodology between common FBD and DDBD is suitable for design unbonded post-tensioned hybrid walls and to study the response of different possible configurations. We are not interested in a full-detailed design procedure, which is already present in literature. For this reason we develop just a preliminary design of the structure in order to assess the re-centering capacity and the energy dissipation of the wall subject to the design level ground motion. So we will focus on the Immediate Occupancy performance level, that is reached if:

1. The wall behavior is approximately elastic, but nonlinear;

2. Non-linearity is primarily due to gap opening at the base;

3. Shear slip at the base horizontal joint does not occur;

4. No residual displacement of the wall after the ground motion occurs;

5. PT steel remains in the linear-elastic range;

6. ED steel yields during the seismic event;

7. Wall panels remain linear-elastic, behaving as a rigid body, except for the wall toes;

8. The non-linearity of concrete in compression occurs only at the wall toes, where the cover concrete is on the verge of spalling;

9. Lateral load strength and gravity load strength of the wall are not reduced after the earthquake.

3.5.4 Base Cross-Section Design

These considerations provide us all the required tools for developing an analytical procedure for the design of an unbonded post-tensioned hybrid wall. The amount of PT steel and ED steel, their location at the cross-section and the wall dimensions are calculated to satisfy the wall design base forces (calculated with the FBD or the DDBD). The wall section should have a symmetric layout and the ED and PT steel should be placed outside the confined regions at the wall toes.

Sectional behavior

The sectional behavior will be determined through the basic concepts of prestressed concrete mechanics, with only one main difference: steel behavior doesn't follow compatibility, but kinematic. In fact a gap opens at the base and neither the PT steel nor the ED steel are bonded to the concrete and therefore the hypothesis of perfect adherence between steel and concrete is no more valid. We have to use kinematic considerations due to base section rotation, that creates a relative displacement between the two ends of the debonded mild reinforcement and the two anchorages of the PT steel. Since the wall panel behaves approximately as a rigid body, the base section rotation is equal to the roof drift θ_d, calculated as the ratio between the design roof displacement Δ_d and the wall height h_w. Fig. 3.14 shows the base horizontal joint and the displaced configuration of an hybrid wall with PT tendons less eccentric than the ED bars, but the following design procedure is still valid if the section has a different layout. The steel areas are consid-
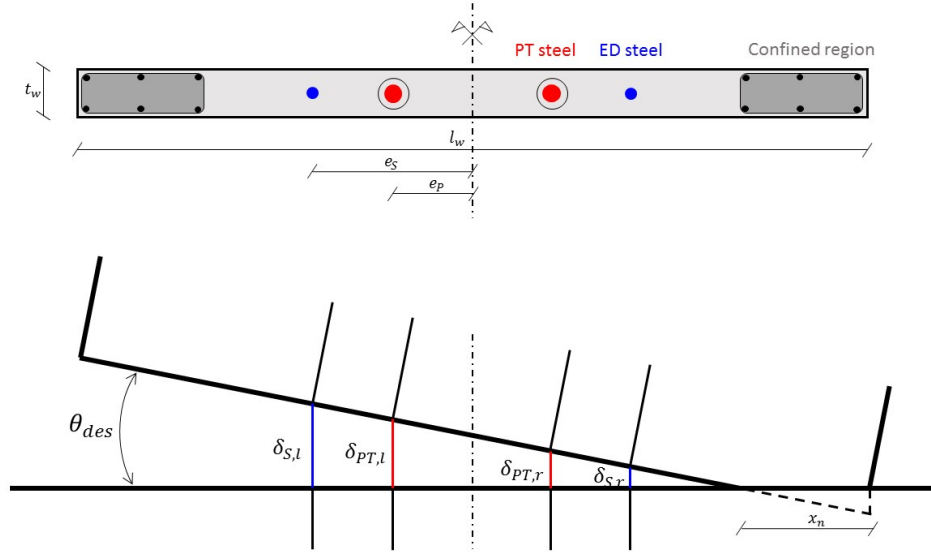
Figure 3.14: Base joint: exaggerated deformed shape at Δ_d

ered lumped, respectively, in two areas placed symmetrically respect to the centerline. We can determine the elongation of the ED bars $\delta_{s,l}$ and $\delta_{s,r}$ and the elongation of the PT steel $\delta_{pt,l}$ and $\delta_{pt,r}$, where l and r define respectively the displacement on the left and on the right of the centerline.

$$\delta_{s,l} = \theta_d \left(\frac{l_w}{2} - x_n + e_s \right) \tag{3.1a}$$

$$\delta_{s,r} = \theta_d \left(\frac{l_w}{2} - x_n - e_s \right) \tag{3.1b}$$

$$\delta_{pt,l} = \theta_d \left(\frac{l_w}{2} - x_n + e_p \right) \tag{3.1c}$$

$$\delta_{pt,r} = \theta_d \left(\frac{l_w}{2} - x_n - e_p \right) \tag{3.1d}$$

where:

l_w is the wall length;

x_n is the neutral axis length, i.e the contact length between wall and foundation;

e_s is the eccentricity of the ED bars from the wall centerline;

e_p is the eccentricity of the PT tendons from the wall centerline.

In literature the relative location of ED and PT steel is a very discussed topic. Panian et al. in [13] say that it is advantageous to keep the tendons grouped closely in the middle of the wall to minimize strains resulting from large lateral drifts and prevent yielding. On the other hand, Smith et al. in [23] assert that placing the mild reinforcement close to the centerline assures that all the bars yield minimizing the steel area required to achieve the expected energy dissipation. The value of e_s and e_p should be carefully selected in the design phase and could substantially modify the final amount of steel. The relative strains can be calculated with the uniaxial strain equation. The total strand strains are the sum of the gap opening strains and the initial strains due to prestress. So:

$$\varepsilon_{s,l} = \frac{\delta_{s,l}}{l_s} \tag{3.2a}$$

$$\varepsilon_{s,r} = \frac{\delta_{s,r}}{l_s} \tag{3.2b}$$

$$\varepsilon_{pt,l} = \frac{\delta_{pt,l}}{l_{pt}} + \frac{f_{pi}}{E_p} \tag{3.2c}$$

$$\varepsilon_{pt,r} = \frac{\delta_{pt,r}}{l_{pt}} + \frac{f_{pi}}{E_p} \tag{3.2d}$$

where:

l_s is the debonded length of the mild reinforcement;

l_{pt} is the unbonded length of the post-tensioned tendons, equal to the wall height h_w;
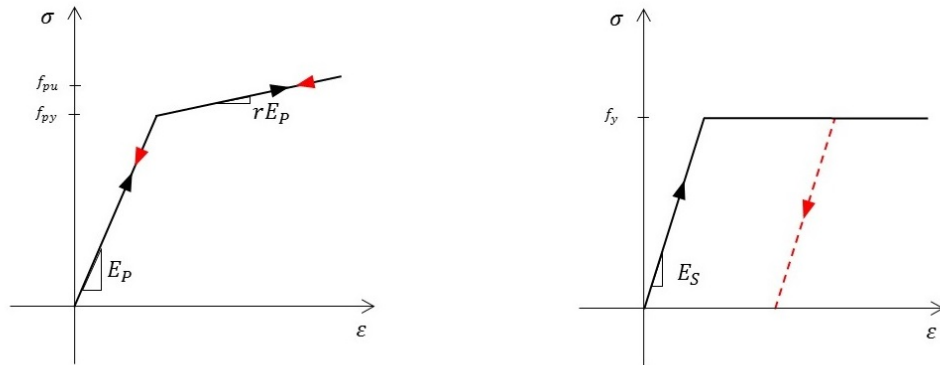
Figure 3.15: Stress-strain relationship for PT strands (on the left) and ED bars (on the right)

f_{pi} is the initial prestress, that ranges from 55 to 65 percent of the ultimate
strength of the post-tensioning steel, f_{pu};

E_p is the elastic modulus of the strand.

The calculated strains can be used to determine the stresses from an assumed stress-strain relationship for the steel. They are called $\sigma_{s,l}$, $\sigma_{s,r}$, $\sigma_{pt,l}$ and $\sigma_{pt,r}$. In this project the perfect elastoplastic behavior is used for the ED bars, while the PT strands are assumed bilinear elastic, but more accurate constitutive laws could be used without modifying the method. Since the only reason why the reinforcement has been positioned within the section is to dissipate energy, at least one of the two lumped areas should yield. The relative wrapped length is selected in the design in such a way that the ED bars reach the yield strength f_y. Note that these equations are based on the approximation of neglecting the flexural and shear deformation of the wall panels over the height of the structure. In this way the process tends to overestimate the steel strains and thus the stresses.

Figure 3.16: Base joint: free body diagram at Δ_d

Equilibrium Equations

In order to determine the ED and PT steel areas needed, to satisfy the design base moment demand M_{wd} and the design axial load N_{wd} due to gravity loads, simple equilibrium equations of the free body diagram (see Fig. 3.16) at the wall base are needed. M_{wd} is calculated from the distribution over the height of the wall of the design shear force V_{wd} due to lateral forces.

$$C_d = 0.85\, f'_c\, t_w\, \beta_1\, x_n \tag{3.3}$$

$$C_d = N_{wd} + A_s\left(\sigma_{s,l} + \sigma_{s,r}\right) + A_{pt}\left(\sigma_{pt,l} + \sigma_{pt,r}\right) \tag{3.4}$$

$$\frac{M_{wd}}{\phi_f} = C_d\left(\frac{l_w}{2} - \beta_1\frac{x_n}{2}\right) + A_s\left(\sigma_{s,l} - \sigma_{s,r}\right)e_s + A_{pt}\left(\sigma_{pt,l} - \sigma_{pt,r}\right)e_p \tag{3.5}$$

where:

C_d is the total concrete compressive stress resultant;

f'_c is the compressive strength of the unconfined concrete;

t_w is the wall thickness;

β_1 is the parameter that relates the neutral axis length x_n and the relative rectangular concrete compression stress block;

A_s is the lumped ED steel area;

A_{pt} is the lumped PT steel area;

ϕ_f is an reduction factor that ACI 318 recommend equal to 0.9.

The formulas imply that the steel areas are placed symmetrically respect to the wall centerline. They could be further simplified considering a mean value of the steel stresses:

$$\sigma_{s,m} = \frac{\sigma_{s,l} + \sigma_{s,r}}{2} \tag{3.6}$$

$$\sigma_{pt,m} = \frac{\sigma_{pt,l} + \sigma_{pt,r}}{2} \tag{3.7}$$

The equilibrium equations can be written as:

$$C_d = 0.85\, f_c'\, t_w\, \beta_1\, x_n \tag{3.8}$$

$$C_d = N_{wd} + 2A_s \sigma_{s,m} + 2A_{pt}\sigma_{pt,m} \tag{3.9}$$

$$\frac{M_{wd}}{\phi_f} = C_d \left(\frac{l_w}{2} - \beta_1 \frac{x_n}{2} \right) \tag{3.10}$$

Note that the compressive strength of the unconfined concrete is considered, even if boundary regions are confined. This limitation protects the concrete from possibles premature cracking, that should be avoided for the selected performance requirements.

Proportioning ratio

One of the key aspect for an efficient design of an hybrid wall is the proportioning between the yielding contribution, which is responsible for the energy dissipation of the system, and the self-centering contribution. In fact unbonded post-tensioned precast walls are excellent self-centering systems, able to resist to an earthquake with minimal structural damage. However, the walls don't have the ability to dissipate energy which is subject to the structure during a ground motion, because the response is nearly elastic. Supplemental energy dissipation elements are therefore needed but they should not compromise the favorable rocking response and the re-centering tendency of the system. This design criteria could be summarized as the ratio between the yielding components and the elastic restoring components. In terms of base flexural resistance, it means:

$$\kappa_d = \frac{M_{\text{yielding}}}{M_{\text{restoring}}} \tag{3.11}$$

The influence of κ_d on the overall response of the generic self-centering system is well described in figure, representing the idealized flag-shaped hysteretic loop describes in Section 3.3.2. The value of the ratio determines the amount of dissipated energy and the re-centering ability of the system. The nominal base moment strength of an unbonded post-tensioned hybrid wall can be seen as the sum of three components, M_{wn}, M_s and M_{pt}, representing respectively the contributions of applied axial loads, the wall mild steel reinforcement and PT tendons. Thus the parameter κ_d, proposed by Kurama and called "ED steel moment ratio" is defined as:

$$\kappa_d = \frac{M_s}{M_{pt} + M_{wn}} \tag{3.12}$$

Referring to Fig. 3.16, the moment equilibrium around the center of compression allows us to rewrite Eq. (3.13). If both the ED steel areas yield, it
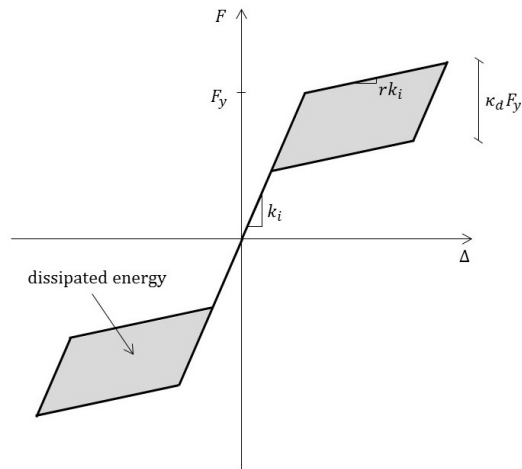
Figure 3.17: Idealized flag-shaped hysteretic loop

become:

$$\kappa_d = \frac{2A_s f_y}{2A_{pt}\sigma_{pt,m} + N_{wd}} \tag{3.13}$$

Design steps

An appropriate value for κ_d should be selected for design. If the yielding contribution is too small (i.e., κ_d ratio is too small), then the system doesn't provide adequate energy dissipation. Conversely the self-centering capability of the wall may be too small and thus it may not be sufficient to close the gap opening at the base joints after the seismic event, if the κ_d ratio is too large. Kurama suggested to use values of the ED steel moment ratio that ranged from 0.50 to 0.80 to satisfy the required performances and the code requirements of the ACI ITG.

An iterative process is needed to estimate the flexural steel areas required at Δ_d. An initial value of the neutral axis length can be used to determine the ED steel and PT steel elongations using the displaced configuration and the selected location of the bars (e_s) and tendons (e_p) from the wall centerline.

Then the stresses $\sigma_{s,l}$, $\sigma_{s,r}$ and $\sigma_{pt,m}$ are calculated with the selected unbonded length (l_s and l_{pt}) and the selected stress-strain relationship. l_s must be selected in such a way that at least one of the lumped areas yield. The required A_{pt} and A_s can be found by solving Eqs. (3.4) and (3.13) for an assigned value of κ_d. Finally if Eq. (3.5) is satisfied, the trial value of x_n is correct, otherwise it must be changed and the process starts over until convergence.

For lumped steel areas, the design is made without iterations and x_n is solved directly from Eqs. (3.8) and (3.10). The steel areas are computed using Eqs. (3.9) and (3.13), after the definition of their relative strains and stresses.

Chapter 4

Model Validation

4.1 Introduction

The objectives of this chapter are to develop an analytical model to validate
the design strength and to see if the wall reproduces the expected behavior.
Another purpose of this research is to understand which seismic methodology
between FBD and DDBD results to be more efficient in terms of strength in
order to reach the target performance of the structure. Since there was no
possibility to verify our results with a test building, in the present research
some models already present in literature have been studied in details with
the attempt to reproduce their results. Most of them use finite element
softwares that are not usually present in structural firms and therefore their
results are not so easily applicable to real case study, and result to be relevant
only in the research field. On the other hand, unbonded post-tensioned
precast shear-walls already built do not have a well detailed analytical design
procedure and their structures were designed using high-performance finite
elements softwares. It appears clear that the use of high-performance analysis
is not convenient in terms of time for the preliminary design of structures.

The most important research in the analysis of unbonded post-tensioned precast shear wall is the phase III of the PRESSS research program and it is the culminating part of the entire project (already mentioned in Chapter 3). In this phase a five-story precast concrete building has been designed, erected and tested under simulated seismic loading. The structure presented unbonded post-tensioned jointed precast concrete walls in one direction, and a frame system in the other one. Focusing on the wall system, it has been designed with both the Force-Based and the Direct-Displacement-Based methodologies to define the required strength at each level. Later, the post-tensioned tendons and the energy dissipation devices have been designed. The intent of the work was to create an analytical model whose results could match the experimental one found with a 60 percent scaled building.

After a brief summary of previous work, in this chapter the PRESSS research is studied in detail as a prototype in order to fully understand how an unbonded post-tensioned jointed precast concrete wall has been modeled. Later the same wall system is modeled using a well-known and commercially available finite element software like ETABS 2015, highlighting the problem encountered during the implementation and the advantages derived by its utilization. Understood how to model it, the methodology can be applied to different configurations of walls. This will be part of the next chapter, where different configurations of enhanced lateral load resisting systems with unbonded post-tensioned walls will be modeled in order to verify that the design procedure developed in previous chapters is able to provide well designed structures.

4.2   Literature Review

Over the past few years, research teams and engineering firms tried to model self-centering walls with unbonded post-tensioned tendons with different energy dissipation devices. Principally fiber element models have been created, because in this manner a reasonably accurate model can be developed using only uni-axial stress-strain models for the various components of the lateral resisting system. All the fiber element models present in literature are similar to the one proposed by Kurama et al. at University of Notre Dame whose main features will be summarize later.

The computer program PERFORM-3D (CSI) is specific for performance-based seismic analysis and has been used for unbonded post-tensioned walls. This software gives the possibility to model the structural system in all its details with minor simplifications. For this reason the relative analysis are very time-consuming, so it becomes very difficult and inefficient to implement the model considering the whole structure.

For example the David Brower Center, situated in Berkeley, CA, has been designed by the engineering firm Tipping Mar with nonlinear time-response analysis conducted using Perform-3D [28]. The inelastic flexural behavior of the post-tensioned walls and frames was modeled with inelastic fiber element sections applied on three-dimensional finite elements. The behavior of the unbonded tendons is achieved by connecting them only to the wall elements at the location of the actual anchorages, so the top and bottom of the wall. The engineers used the model not just as a verification tool, but they also designed the structure with it.

<div align="center">(a)   (b)</div>
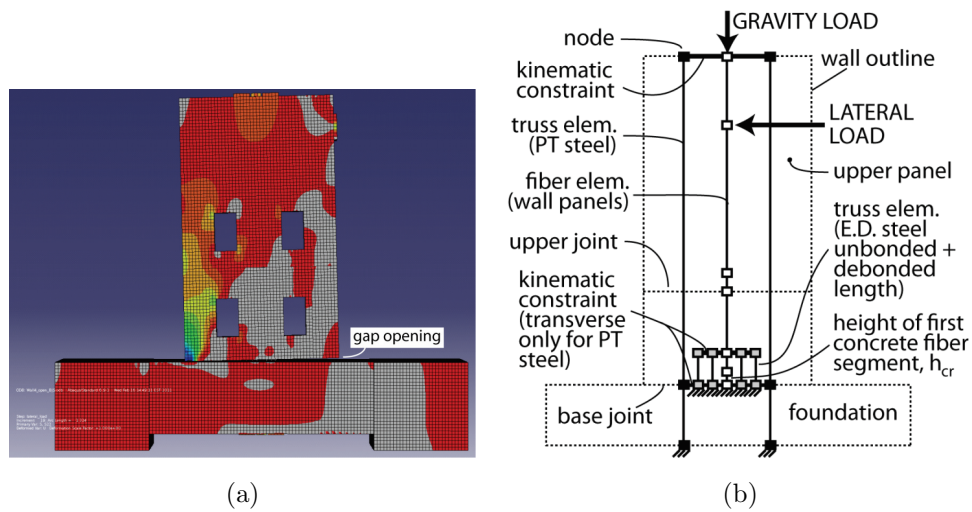
Figure 4.1: Examples of models developed by University of Notre Dame: (a) is the finite element model, (b) is the fiber element model

4.2.1 Models developed by University of Notre Dame

A research team leaded by Kurama and Smith in University of Notre Dame, Indiana, is developing many studies on hybrid precast wall systems in seismic regions. During the investigations the group proposed 2 different analytical models that can be used for the analysis of precast concrete shear walls with unbonded post-tensioning tendons and mild steel that dissipates energy [24] [23]. Both of them have interesting features, but the main drawback is that their way of modeling makes it difficult to develop an analytical model to look at the whole structure and not only at the lateral resisting system. A brief description of the two models is provided below.

Finite Element Model

A simplified finite element model was created using ABAQUS (Hibbitt et al. 2009) and can be used for pushover analysis and to analyze the local stresses in case of perforations in the wall panels. 3D eight-node stress/displacement

solid elements are used for the concrete of the wall panels and the foundations and their behavior is linear elastic in tension, so that the steel reinforcement inside each wall is considered. It assumes that the amount of ordinary reinforcement is enough to guarantee the limitation of cracks inside the concrete. Regarding the wall toes, the confinement reinforcement is not explicitly modeled but rather represented by incorporating the effect of the confinement on the stress-strain relationship of the concrete in compression, following the Mander theory.

The PT steel as well as the ED steel across the base joints and the panel-to-panel joints are modeled with 3D eight-node stress/displacement truss elements. The ED steel trusses are partitioned into bonded regions, where they are constrained with the wall solid elements, and unbonded regions that are not embedded instead. An initial tension force in the PT trusses simulates the initial prestress.

The gap opening is allowed thanks to "Hard contact" surfaces at the horizontal joint and the shear slip depends on the properties of these surfaces.

Detailed Fiber Element Model

The fiber element model using DRAIN-2DX (Prakash et al. 1993) was created for nonlinear reversed-cyclic and dynamic analysis. The axial-flexural behavior of the wall panels is reproduced using fiber beam-column elements, while the foundation is assumed to be fixed. The effect of gap opening at the base joint is modeled setting to zero the tension strength of the concrete fibers over the height of the confined concrete at the wall toes. The remaining height of the wall panels is linear-elastic in tension and the cracks in the concrete are considered negligible.

The PT steel and the ED bars are modeled with truss elements. The ends

of the truss elements are kinematically constrained to the corresponding fiber element nodes for the wall panels at the same elevation. An initial tension force in the truss elements simulates the initial prestress in the PT tendons. The stiffness of the PT strands should be reduced compared to the actual material properties, to take into account the concrete deformations at the anchorage regions. So the researchers proposed to reduce the elastic stiffness of the PT trusses by a factor of 0.75.

Similar to the finite element model, the confinement reinforcement is not explicitly modeled, but only in its effects on the stress-strain relationship of the concrete in compression.

4.3   The PRESSS Research Project

The Precast Seismic Structural Systems (PRESSS) research program started in 1991 and was sponsored by the National Science Foundation, the Precast/Prestressed Concrete Institute and the Precast/Prestressed Concrete Manufacturers Association of California with two main purposes [27]:

- to define design recommendations for better performances of precast concrete structures in seismic region;

- to discover new material, design concepts and technology for precast concrete during an earthquake to stand out its peculiarity;

The project could be divided in 3 different phases. Phase I focused on the identification of the precast building system, among the existing ones, which has better response under a ground motion. Later, phase II studied different ductile connections and developed design procedures for precast concrete buildings; finally the third phase executed the design, erection and testing of a

five-story precast concrete building providing the definition of detailed design recommendations for the implementation of the present building codes. The precast wall panels was evaluated as a part of the first phase, its results and developments were then tested during Phase II.

The project culminated in 1999 with a five-story precast concrete building that was erected and tested under simulated seismic loading at the UCSD Charles Lee Powell Structural Laboratory (San Diego, California). For practical purposes, the test building was a 60% scaled version of the designed one. The design of the structure was performed comparing the direct-displacement based procedure and the force-based one, with the aim to sustain a target drift of 2% under a design level ground motion. The PRESSS test building presented two different seismic resisting systems in the two directions of the structures: a moment resisting frame in one direction and unbonded post-tensioned jointed precast concrete walls in the other direction. An analytical model was then developed in order to predict the results found by tests, using Ruaumoko software, developed at the University of Canterbury (New Zealand) and specialized on time history non-linear analysis of structures under seismic loading.

In this research a well-detailed description of the test building, including structural dimensions, material properties and applied load (both vertical and horizontal), is present, as well as the definition of the analytical model in all its part. All these data are fundamental in order to have the assurance that the created model will be correct and accurate compared to the real problem. These studies are useful also to validate the design procedures in order to define the seismic forces acting on the wall.

Figure 4.2: Global view of the test building

Table 4.1: PRESSS test building scale factors, [3]

Quantity	Scale Factor
Length	0.6
Mass	0.6^3
Time/Period	0.6
Stress	1.0
Acceleration	1/0.6
Force	0.6^2
Moment	0.6^3
Damping	0.6^2

4.3.1 Building Description

The present Section is not meant to be a detailed design report of the PRESSS test building, that could be easily found in literature ([3] [10] [26] [27]) , but just an overview of the structural features relevant for the present research. In reports written by the PRESSS research program, all the quantities are present according to the United States customary units, so for a more precise study, they will be shown both in International System of Units (SI) and in United States Customary System (USCS). The prototype building is $100\,\text{ft} \times 200\,\text{ft}$ in plan ($30.48\,\text{m} \times 60.96\,\text{m}$) with equal story heights of $12\,\text{ft}$ $6\,\text{in}$ ($3.81\,\text{m}$) and $25\,\text{ft}$ ($7.62\,\text{m}$) bay length, as shown in Fig. 4.3. The lateral load resistance is developed by moment-resisting frames in one direction of response and shear walls in the other direction.

Since there was not enough space at the UCSD Powell Lab, a 60% scaled version of the building was erected. The quantities were therefore scaled themselves according to Table 4.1. Therefore the test building consists of 2 bays x 2 bays in plan of $15\,\text{ft}$ ($4.57\,\text{m}$) span each and it has pretopped double tee planks as flooring system for the first three floors, while in the upper two floors topped hollow-core panels are used, as shown in Figure 4.4.

Figure 4.3: Floor plan of the prototype building
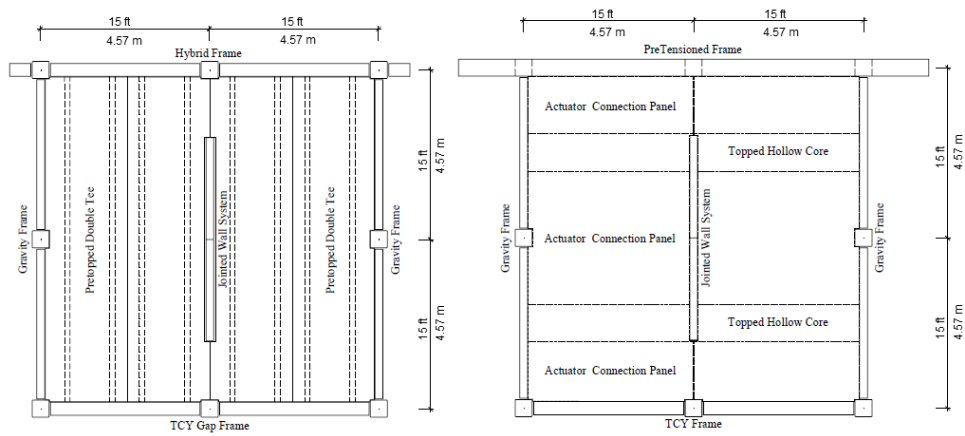
Figure 4.4: Flooring system at different levels

Two different precast frames are present in the longitudinal direction: one with unbonded post-tensioned beams, one with mild reinforcing steel connections. They also have four different connection details between beams and columns, based on the previous phases of the PRESSS research program, and they are modeled at different levels. In the transverse direction there are an unbonded post-tensioned jointed precast concrete wall, that provides the earthquake resistance of the structure, and gravity frames that run parallel to the structural wall. Each wall is composed of two vertical precast wall panels placed side by side and shear sliding occurs at the vertical joint between them. Each one is composed by 2 elements with a height of two-and-a-half stories stacked one above the other. The connection across horizontal joint between panels at mid-height of the structure is developed by vertical rebar debonded for a specific length across the joint with specific sleeves. Unbonded post-tensioned high strength steel runs from the roof level to the foundation and is placed in the middle of each wall panel, providing the self-centering capacity of the system as well as the horizontal connection. U-shaped flexural plates are welded to plates installed in the adjacent panels, providing the vertical

connection between them, and thus increasing the lateral resistance. They also dissipate energy thanks to the relative displacement of the two ends of the device. The wall panels are 9 ft (2.74 m) wide and 8 in (20.3 cm) thick.

4.3.2   Wall Lateral Resisting System

The wall should remain elastic during tests, so it is significantly reinforced and it presents spiral confinement at the base toes in order to sustain the high compressive stresses at maximum drift. The foundation is considered rigid, with high strength bars that run horizontally on it. High strength fiber reinforced grout are used at the base-panel-to-foundation joints, to avoid shear slip. The centerline of each panel collects 4 unbonded tendons (Dywidag coupled thread bars) of 1 in (25.4 mm) diameter. Bolted to anchor plates which are imbedded into the foundation, these bars should remain elastic up to the 2% drift design limit. Therefore each bar is post-tensioned to a force of 41 kips (182.4 kN). In this way the wall has re-centering capacities after the design ground motion. In order to limit the deformations of the flooring system when the wall rocks during the seismic event, specific connections are needed to transfer the horizontal loads, but not the vertical ones. The weight of the wall, the weight of its tributary area at each floor and the post-tensioning force are considered as concentrated loads at the base of the wall. In this manner it is possible to model the restoring force that pulls the structure back to the initial configuration. Adjacent panels are then coupled with U-shaped flexural plates (UFPs) placed along the vertical joints between them. Moreover these devices assures energy dissipation capacity to the system, as they yield thanks to the relative vertical displacement of the ends of the plates. Welded to imbedded plates in the panels, the semicircular section of the device rolls along the plate and dissipate energy where

the radius of curvature changes from straight to curved and vice versa.
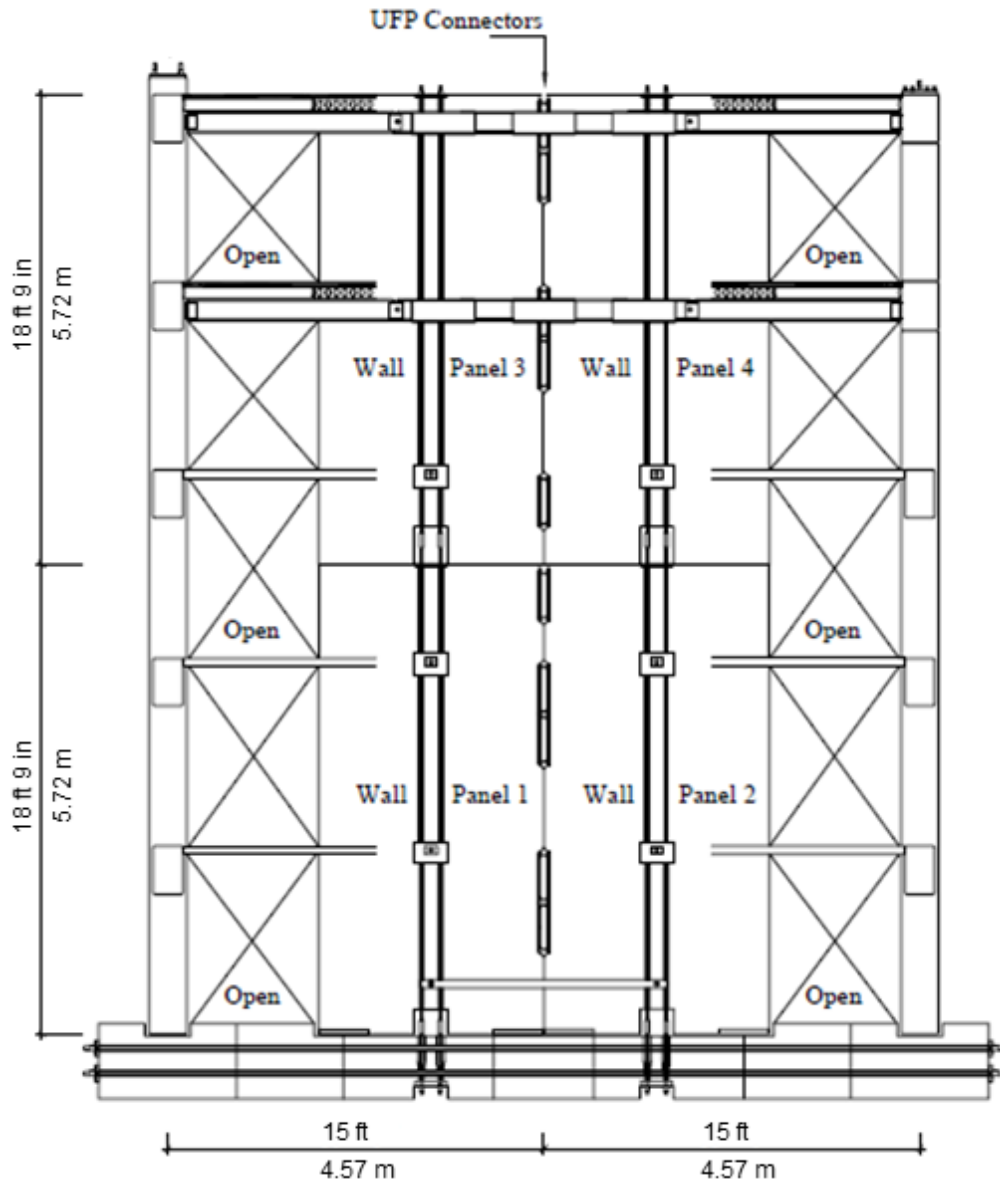
Figure 4.5: Elevation of the unbonded post-tensioned jointed precast wall, [10]

Figure 4.6: Erection of the unbonded post-tensioned jointed precast wall

4.3.3   Design Procedure

The required strength of the wall under seismic loads was computed with both the DDBD method and the FBD method. The value found with the DDBD resulted to be the optimal one, and thus it leaded the design of the wall. The FBD reduces the elastic forces generated on the structure by an R factor in order to take into account the non-linear behavior of the structure. The R factor used is related to the ductility of the system assuming an emulation of monolithic concrete behavior. In this way, this procedure does not capture the specific behavior of the jointed precast system because its energy dissipation characteristics and its yield displacement profile are different from the one of a conventional monolithic wall.

The PRESSS building was designed to carry a maximum drift of 2% under a design level earthquake that follows the 1997 UBC acceleration spectrum provisions, considering seismic hazard Zone 4 and intermediate soil type S_c, which corresponds a PGA equal to 0.4 g. The displacement spectra of Appendix G of the SEAOC Bluebook (PBSE-SEAOC, 1998) were used.

In the DDBD an equivalent viscous damping of 20% was estimated by the designers. The displacement profile was assumed to be linear along the height, due to essentially elastic behavior of the wall during the seismic event as illustrated in Chapter 2. The values resulting from the DDBD procedure to compute the design base shear are listed in Tab. 4.2. These results consider the 4 walls composing the lateral resisting system of the prototype building.

In the test building a 60% scale version of only one of the 4 wall system in the prototype building was modeled. Hence, the design base shear of one wall is:

$$2167 \cdot \frac{1}{4} = 541.75 \, \text{kips} \, (\, 2409.8 \, \text{kN} \,) \tag{4.1}$$

Table 4.3 shows the values of base shear force found with DDBD and

Table 4.2: Results from the DDBD procedure

Properties	Parameters			
	USCS		SI	
Δ_d	11	in	0.28	m
M_e	41.32	kips/in.s²	7164.66	ton
T_e	2.88	sec	2.88	sec
K_e	197	kips/in	34500	kN/m
V_b	2167	kips	9639.30	kN

FBD. This table allows to make a comparison between the forces obtained with the two methods in the wall direction. The force based design was applied in accordance with different codes (UBC 94, UBC 97 and NEHRP 97) and in all cases the values provided by this method was higher than the one estimated by the DDBD method. It is of interest to see that the FBD method produces a force that was 80-100 % higher than the one produced by the DDBD method. Reduction of base shear indicates cost saving in the realization.

Table 4.3: Comparison of the design base shear obtained from DDBD and FBD, [26]

Design Method	Code	Base Shear			
		USCS		SI	
DDBD	PBE-SEAOC	2167	kips	9639	kN
FBD	UBC 94	3900	kips	17348	kN
	UBC 97	4333	kips	19274	kN
	NEHRP 97	3900	kips	17348	kN

In the analysis with FBD different values of C_t and R_w were considered. For UBC 94 they were $C_t = 0.02$ and $R_w = 6$, for UBC 97 $C_t = 0.02$ and $R_w = 4.5$, for NEHRP 97 $C_t = 0.02$ and $R_w = 5$.

The prototype building was then tested with a 60% scale building test. The quantities found with DDBD method were scaled according to Table 4.1. The values of interest are the design base shear and the floor weight. These values are interesting for the creation of a validation model that tries to reproduce the values found with the PRESSS program. The design base shear of the test building in the wall direction resulted to be:

$$2167 \cdot \frac{1}{4} \cdot 0.6^2 = 195.0 \, \text{kips} \, (\, 867.4 \, \text{kN} \,) \tag{4.2}$$

The weight associated to each floor of the test building was calculated from the total building weight of 19500 kips:

$$19500 \cdot \frac{1}{5} \cdot \frac{1}{4} \cdot 0.6^2 = 351 \, \text{kips} \, (\, 1561.3 \, \text{kN} \,) \tag{4.3}$$

The test executed on the wall designed with the DDBD provided also a validation of this method, as it will be shown in the following sections.

4.3.4 Modeling Assumption

The model of the wall system developed in this work is based on previous attempts to model this kind of structures, first of all the studies leaded by Kurama on unbounded post-tensioned precast concrete walls and described in Sec. 4.2. The model, obtained using the Ruaumoko Software, adopts only frame elements and spring elements, with different section properties and different elasto-plastic behavior, to represent the various structural components. The wall is represented also with a column on its right side, representing the potential unbonded post-tensioning frame, which gives additional lateral resistance to the structures. This column is not modeled in the present

research, so it will not be described in the following part. The floors are modeled as lumped masses located at the same elevation, suggesting the hypothesis that each level behaves as rigid diaphragm. These represent the seismic masses used for the definition of the horizontal forces due to the earthquake. The vertical loads, computed as the sum of the wall self-weight, the weight of the floors sustained by the wall and the initial prestress, are applied as concentrated loads at the base of the panels. As it will be described later, this procedure assure that the system develops the necessary restoring force at the base during the seismic event. Finally, the Rayleigh damping used for the time history analysis is equal to 2.5% for the first mode, and 5% for the second mode.

Below it is present a full description of the single elements that model the different components present in the wall seismic resisting system, according to [3].

Wall Members

The wall member is modeled with 5 frame elements that start from the base and their length is equal to the story height. The panels are designed to remain elastic during the earthquake, so the gross section properties are considered, without taking into account the reduced moment of inertia due to cracks inside the concrete. As other conclusion of the design assumptions, the hysteretic characteristic of the wall components are the ones of a simply linear-elastic element, without energy dissipation nor stiffness degradation. During the PRESSS research program, experimental tests on materials used in the test building were conducted and the relative results are present in different reports. In this manner they could estimate the elastic modulus and the shear modulus of the precast concrete panels. The global properties
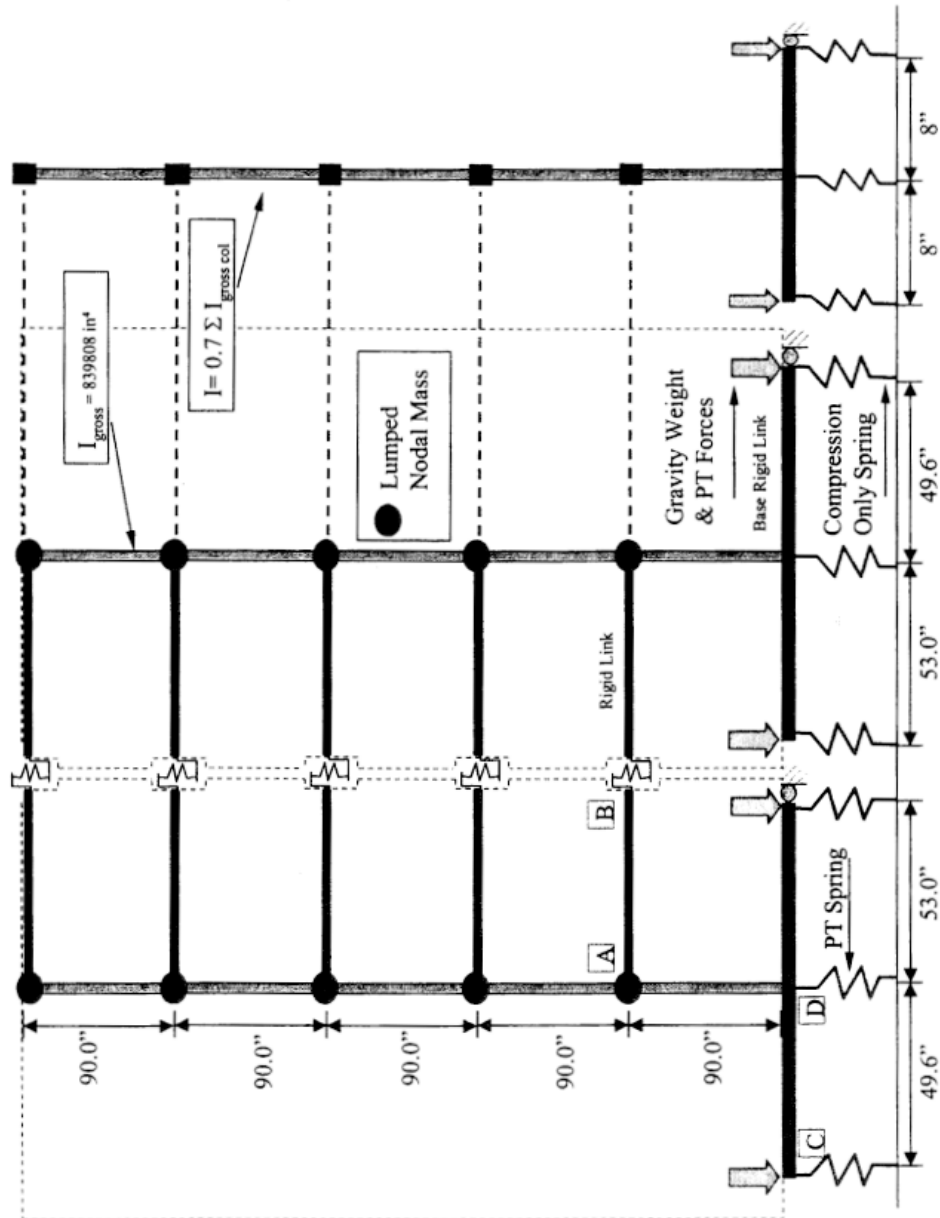
Figure 4.7: Ruaumoko model, PRESSS report

can be summarized as below:

Table 4.4: PRESSS test building, wall member parameters

Properties	Parameters			
	USCS		SI	
Elastic Modulus E	5200	ksi	35853	MPa
Shear Modulus G	2200	ksi	15168.5	MPa
Cross Section Area	864	in^2	5574	cm^2
Shear Area	736	ksi	4748	cm^2
Moment of Inertia	839808	in^4	34955448	cm^4

Rigid Links

As shown in Fig. 4.7, the nodes at the base of the wall component have 2 rigid-links that are horizontal and have different length: the outer link is 49.6 in (126 cm) long, while the length of the inner one is 53 in (134.6 cm) from the centerline of the wall panel. These nodes do not represent the real size of the wall panels, but they are the centers of compressions of the wall section calculated with a sectional analysis at a total drift of 2% and assuming a concrete compressive stress block distribution at the toe of the wall panels.

The other wall nodes also have rigid links that extends inward, to the center of the wall. Their modeling as rigid is consistent with the assumption of rigid diaphragm behavior of the flooring system, because in this manner the horizontal displacements of the walls are constrained. Between the extremities of these links there are the UFPs, modeled as springs. To simplify the model, the energy dissipation devices are not placed in the real location of the test building, but they are placed one at each floor. So, instead of having 4 U-shaped flexural plates spread along the vertical joint between the wall panels for each level, they are only 5. Later it will be described how to

model them.

The researchers found some problems in the definition of these elements. High values of their properties change significantly the stiffness matrix, moreover the model used to fail and crash during the analysis due by the fact that Ruaumoko doesn't have any stability checks of the solution. They fixed the problem applying to the rigid-link the properties of the stiffest element (the wall frame) multiplied by 100, putting at zero the shear area, in order to neglect the shear deformations.

Foundation Springs

As described in Chapter 3, a self-centering wall system allows the formation of a gap at the joint between wall and foundation when the lateral load applies an overturning moment on it in order to prevent yielding in the concrete components. Therefore the foundation must be modeled so that the wall panel could be able to uplift avoiding the compenetration between the two concrete elements. This is obtained through the modeling of compression-only elements that have no resistance when the gap opening occurs but that provide the concrete resistance when the wall and the foundation are in contact. Hence, the researchers used springs with bi-linear elastic hysteretic characteristics with different behavior in tension and compression, as shown in Fig. 4.8. The foundation springs are zero weight elements acting only in the vertical direction, placed at the external and internal nodes of the base rigid links. For the moment the focus is on the force reaction that the foundation apply to the wall panels and not on the displacements, so the springs extend conventionally for 3 in (7.62 cm) below the base.

Initially the elements have a linear-elastic behavior, with stiffness k equal for positive and negative forces, after that they deform with zero stiffness.
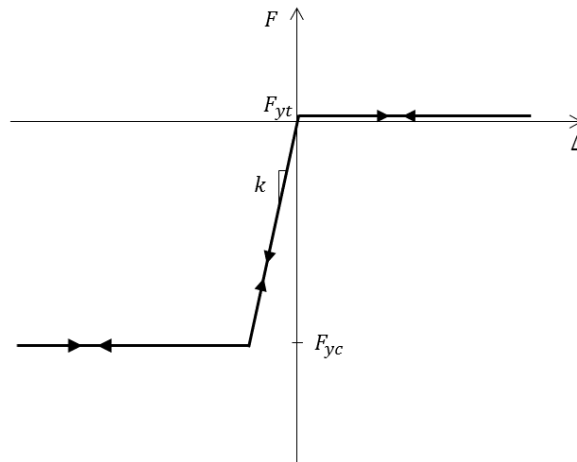
Figure 4.8: Foundation spring hysteretic behavior

The point of discontinuity is almost null in tension (0.1 kips, i.e. 0.45 kN) and a high value in compression, equal to 800 kips (3558.6 kN) in order to ensure elastic response. The stiffness instead is the one corresponding to a deflection of the foundation of 0.02 in (0.05 cm) for a force of 200 kips (890 kN), so 10 000 kip/in (88 512 kN/m).

PT Springs

In the test building post-tensioned tendons run from the foundation up to the top of the wall. As gap opening occurs at the base-panel-to-foundation joint during the design earthquake, the strands elongate and provide a clamping force that can re-center the wall back to its undisplaced position when the seismic action is removed. The modeling of the PT tendons, fundamental for a true representation of the advantages related to these kind of structures, can be done with springs located at the base of the wall panels. These springs start at the centerline base node of the wall member and are fixed 3 in (7.62 cm) below. In each wall panel 4 tendons prestressed up to a force

of 41 kips (182.38 kN) are present, for a resultant force of 164 kips (729.5 kN). This force, is modeled as a concentrated load applied not in the PT spring locations, but on the base foundation springs and it provides, with the other gravity loads, the re-centering effect. Since Ruaumoko gives the possibility to apply an internal force to an element affecting only its initial deformation and not the global response, the initial condition of the strands in terms of stress-deformation due to the prestess was taken into account pre-loading the PT springs in the vertical direction by 164 kips (729.5 kN). In this manner the PT springs capture only the increase in the elongation of the post-tensioning tendons at the center of the walls and not the re-centering behavior.

The researchers chose bi-linear isotropic hardening hysteretic characteristics for the PT springs, with yield value of 375 kips (1668 kN) both in tension and compression. The properties are summarized in Table 4.5, where the bi-linear factor is the ratio between the elastic stiffness and the slope of the hardening segment. They are based also on experimental investigations on Dywidag bars used in the test building. Tensile tests resulted in an average yield stress of 153 ksi (1055 MPa) and an average elastic modulus of 29 000 ksi (199 948 MPa). The elastic stiffness k_{PT} is therefore calculated as:

$$k_{PT} = \frac{E_p \cdot A_{pt}}{l_{pt}} \tag{4.4}$$

where l_{pt} is the unbonded length of the PT bars, equal to the height of the test building, A_{pt} is the total area of the strands and E_p is their elastic modulus.

UFP Springs

The U-shaped flexural plates are modeled with spring elements that connect among them the horizontal rigid links that start from the wall frame inward the panels. They are rigid in the horizontal direction in order to show only

Table 4.5: PRESSS test building, PT springs parameters

Properties	Parameters			
	USCS		SI	
Elastic Stiffness	197	kip/in	35052	kN/m
Yield force	375	kips	1668	kN
Bilinear factor	0.02		0.02	
Pre-load force	164	kips	729.5	kN

the effects of vertical displacements on the devices. This is consistent with the assumption of rigid diaphragm behavior of the floor. During the PRESSS report experimental tests on UFPs were carried out in UCSD to understand their hysteretic behavior and then how to model it in the analytical model. The force-displacement relationship that was found is the solid line in Fig. 4.9, representative of the characteristics of the dissipating devices actually present in the PRESSS test building. It is possible to see that the yielding of the UFP results in a gradual change in stiffness. Moreover, plastic deformations in one direction affect subsequent plastic response in another direction and when the UFPs is pulled in tension, for example, it shows a reduction in compressive strength. This is called Bauschinger effect.

The hysteretic rule that was used in the PRESSS report is the Al-Bermani Bounding Surface Hysteresis, which is able to model the kinematic hardening behavior due to Bauschinger effects. As shown in Fig. 4.10, after an initial constant stiffness k_1, the curve has a variable slope till it reaches a line with stiffness k_2 where the curve follows this line. So the hysteretic model define 2 boundary surfaces, both with slope k_2: one called F_1 that intersects the elastic straight line in P_2, equal to the yielding force P_y, and one called F_2 that intersects it at a certain fraction of P_2. Hence, these two values result
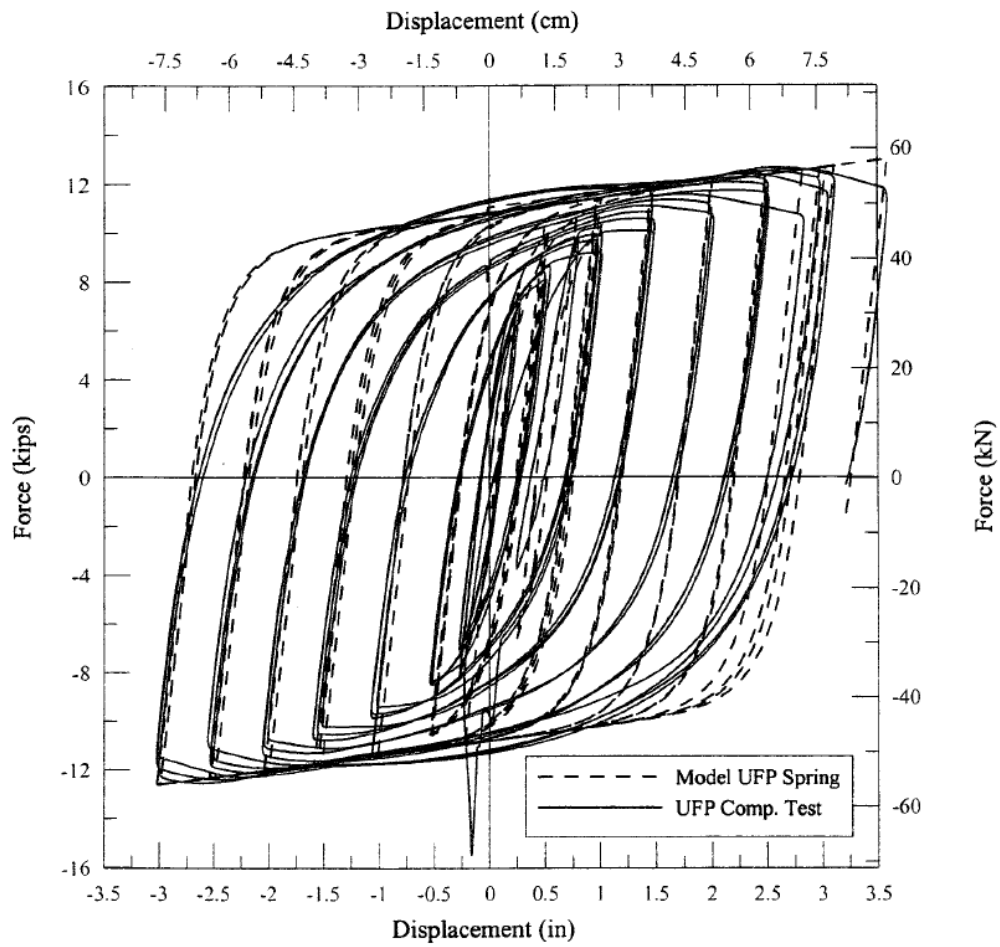
Figure 4.9: Force-Displacement relationship of the UFPs, PRESSS report
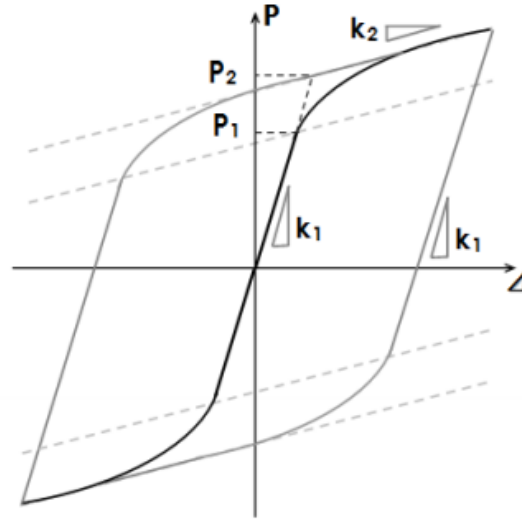
Figure 4.10: Al-Bermani Hysteretic Rule

to be:

$$P_2 = P_y \tag{4.5}$$

$$P_1 = \alpha P_y \tag{4.6}$$

Between these lines the stiffness is variable and its law is:

$$k_T = k_1 \left[1 - \left(\frac{P - F_2}{F_1 - F_2} \right) (1 - p) \right] \tag{4.7}$$

where p is the ratio between the hardening stiffness and the elastic stiffness, and thus:

$$k_2 = pk_1 \tag{4.8}$$

The unloading path has the initial slope equal to k_1 till it passes through the first boundary line in the opposite direction, then it works as before.

The test results were then used for the definition of the Al-Bermani, the

following values were used:

$$k_1 = 40 \, \text{kip/in} = 7117 \, \text{kN/m} \tag{4.9}$$

$$k_2 = 0.6 \, \text{kip/in} = 106.75 \, \text{kN/m} \tag{4.10}$$

$$F_y = 11 \, \text{kips} = 49 \, \text{kN} \tag{4.11}$$

The result of this is the dashed line in Fig. 4.9, that correlates fairly well with the curve obtained by experimental investigations.

The dimensions of the test specimen were different than the one of a UFP really present in the test building. Therefore, the previous quantities had to be scaled by a factor equal to 14/3, obtained as the ratio between the cross sectional areas of the UFPs of the test building per floor level and those of the test setup. Finally, the UFP springs are zero weight elements with no strength degradation.

Now it is possible to summarize the properties of the UFP springs used in the PRESSS model using the Al-Bermani hysteretic rule. As it will be discussed later, the definition of the UFP springs as defined by the PRESSS researchers introduces some misunderstanding and inaccuracies. One of them is that the value of α factor proposed is equal to 0.001, that seems not coherent with the comparison that suggested by them in Fig. 4.9. For consistency with PRESSS model, in Table 4.6 the α value listed is the one that they proposed.

Loads and Constraints

The model is vertically constrained thanks to the springs situated at the base rigid-links, both the UFP springs and the PT springs, that are fixed at the base. In the horizontal direction instead the right nodes of the rigid links at the base corresponding to the right extremity of the wall frames are fixed

Table 4.6: PRESSS test building, UFP springs parameters

Properties	Parameters			
	USCS		SI	
k_1	186.6	kip/in	33201.5	kN/m
k_2	2.8	kips	498	kN
p	0.015		0.015	
P_y	51.3	kips	228.2	kN
α	0.001		0.001	

from moving in that direction. As the base links are rigid, this assures the horizontal constrains of the all base and is consistent with the hypothesis that shear slip is prevented by the design.

The sum of the self-weight of the wall panels, the weight of each floor level sustained by them, and the initial prestress of the PT tendons, is applied to the structure as concentrated static loads. The application point of these forces is at the extreme nodes of the base rigid links in a proportional manner. Hence, the resulting forces are 120.88 kips (537.70 kN) at the exterior nodes and 113.12 kips (503.18 kN) at the interior ones.

The seismic masses supported by each floor level have been taken into account in the PRESSS analytical model as lumped at the wall frame node locations. These masses act only in the horizontal direction and each one is equal to 175.50 kips (780.66 kN). They were applied in form of weight because Ruaumoko subsequently converted them into mass units. It should be noted that, since length and time are scaled at 60% in the model building, the acceleration of gravity had to be scaled by a factor 1/0.6, as shown in Table 4.1.

4.3.5   Seismic testing

The PRESSS building is designed by the researchers using the direct-displacement based approach (DDBD) to carry a maximum drift of 2% under a design level earthquake that follows the 1997 UBC acceleration spectrum provisions, considering seismic hazard Zone 4 and intermediate soil type S_c, which corresponds a PGA equal to $0.4\,g$. As starting point of the DDBD procedure, a trial value of the equivalent viscous damping coefficient ξ equal to 20% is used.

The building test was subject to seismic testing in the two main directions independently. Three different test schemes were used, called:

Flexibility test: a quasi-static loading test in order to compute the stiffness matrix of the test.

Pseudo-dynamic test: the dynamic loads due to earthquake ground motions are applied quasi-statically thanks to ten on-line controlled hydraulic actuator.

IT test: a cyclic loading test using an inverse triangular force distribution is performed till the maximum displacement achieved in the previous pseudo-dynamic tests. This analysis in useful to evaluate the equivalent viscous damping of the structure. Moreover, it gives the possibility to immediately compare the experimental results with the design procedure, where an inverse triangular acceleration pattern is approximately used.

The PRESSS reports show the procedure adopted for obtaining suitable input motions. They derived a design level input motion from the El Centro record obtained from the 1940 Imperial Valley earthquake [25].

4.3.6   Experimental and Analytical Comparison

The PRESSS reports show that the response of the test building during tests was satisfactory. The wall panels presented no damage after the application of the design level earthquake to the structure. Minimal cracks in the cover concrete occurred due to the high compressive strains at the wall toes, but spalling of the concrete was prevented. Aside from the base, no other damage to the precast wall panels was noticed. The U-shaped flexural plates present no fractures and significant yields occurred as assumed during the design phase. Finally, the post-tensioned tendons provided the self-centering capability to the lateral resisting system and remained elastic during the design level ground motion. Among the several results presented by the PRESSS reports, the present research shows only few of these and the respective pictures presented below have been taken directly from [3].

Fig. 4.11 shows the envelopes of the maximum lateral displacement of the roof level of the wall under simulated earthquake records, where EQ1, EQ2 and EQ3 correspond respectively to 33, 50 and 100 and 150 percent of the design level earthquake. The displacement profiles are very close to linear, according with the profile used in the design procedure of the DDBD method. The measured peak roof displacement at EQ3 was 8.28 in, equal to 92% of the design target displacement corresponding to the 2% drift assumed during the design.

A good indicator of the lateral resistance of the test building in the wall direction is the relationship between the base moment and the horizontal displacement of the top floor. The predicted results were obtained through a pushover analysis, which is usually applied to verify the structural performance of a building and estimate the expected plastic mechanisms. Pushover is a static-nonlinear analysis method where a structure is subjected to gravity
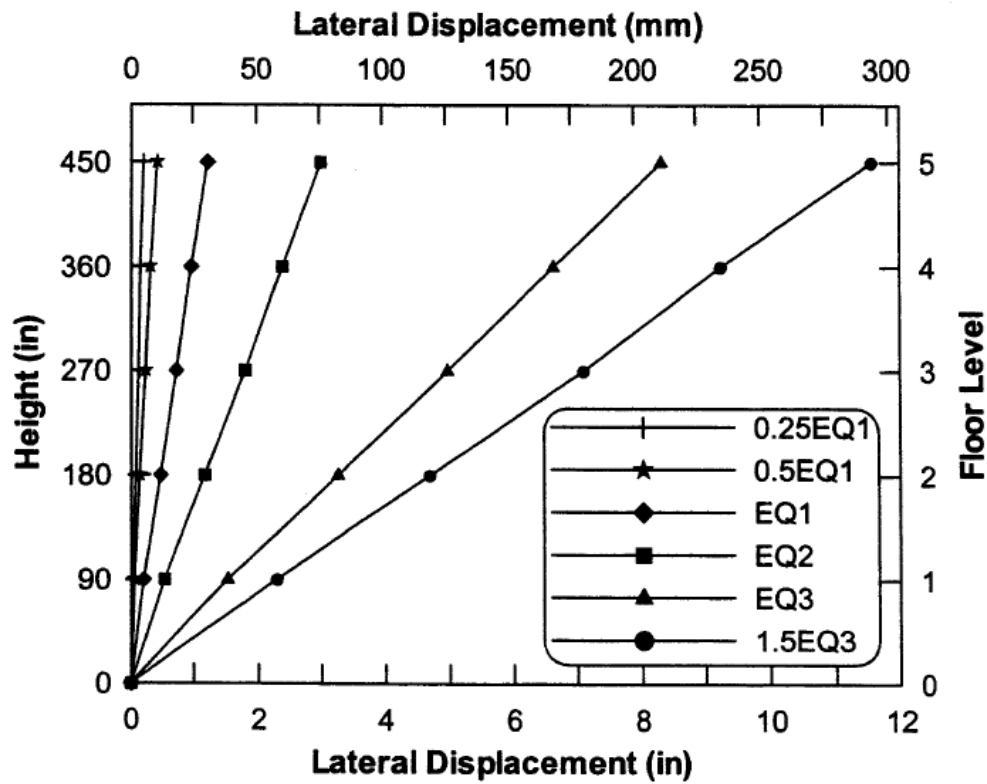
Figure 4.11: PRESSS results, test maximum displacement profiles

loading and a monotonic displacement-controlled lateral load pattern which continuously increases through elastic and inelastic behavior until an ultimate condition is reached. Lateral load may represent the range of base shear induced by earthquake loading, and its configuration may be proportional to the distribution of mass along building height, mode shapes, or another practical means. The load pattern applied by the PRESSS researches to the wall model was based on the displacement profile used during the DDBD procedure, normalized to the top displacement. Fig. 4.12 shows the comparison between the predicted results and the experimental ones in terms of base moment-top displacement relationship. It has been preferred with respect of the base shear-top displacement relationship because the higher mode effects

present in the base shear and floor force time histories do not heavily impact the base moment. Initially, it was used an analytical model composed
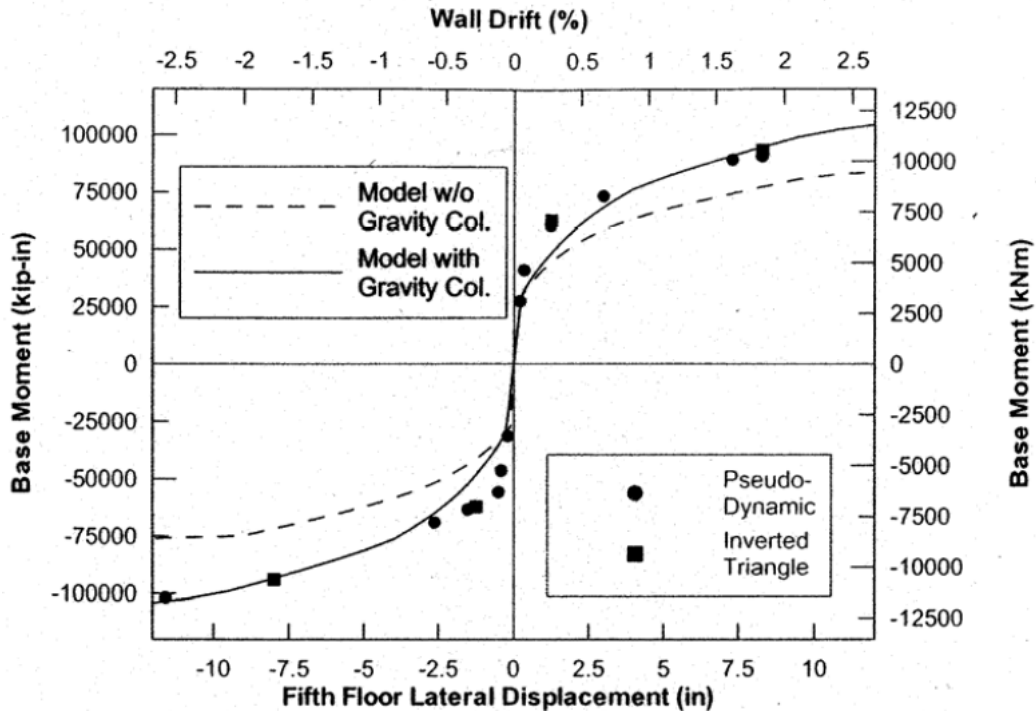
Figure 4.12: PRESSS results, pushover curve

only by the wall system but after running the analysis they discovered that it accounted for about 80% of the response at the maximum displacement in the wall direction, as shown in Fig. 4.12. The remaining moment resistance was suspected to be due to the moment resistance at the base of the eight columns in the test building and thus was added to the model. The result was an increase of about 23% in base overturning moment resistance, that matches extremely well the experimental evidence expressed by dots in Fig. 4.12.

Finally, it will be presented the viscous damping calculation performed in order to verify the equivalent viscous damping coefficient for the wall system

assumed in the DDBD procedure. If the computed value markedly differs from the one initially estimated, the design procedure should be performed again. As already discussed in Chapter 2, the hysteretic viscous damping coefficient could be calculated thanks to the base shear-top displacement relationship of a full hysteretic loop, as:

$$\xi_{\text{hyst}} = \frac{A_h}{4\pi A_e} \tag{4.12}$$

where A_e is the equivalent elastic strain energy and A_h is the energy loss per cycle by the structure.

IT tests were used to have the experimental results of one complete hysteretic loop. The values of the hysteretic viscous damping coefficient were 15.78%. Their sum with the assumed elastic damping coefficient equal to 5% is coherent with the global 20% equivalent viscous damping assumed in the design procedure.

4.4 Proposed Model For Unbonded Post Tensioned Concrete Walls

In the present research a finite element model of unbonded post-tensioned concrete walls in different configuration will be developed, in order to understand which one is the most suitable as lateral load resisting system. The main objectives are:

- to accurately reproduce the nonlinear behavior of the structure including gap opening/closing at the base joint and the hysteretic stress-strain behaviors of the materials;

- to develop modeling guidelines in order to create a model that should be easily reproduced by a structural engineering firm in the prelim-

inary design phase. In this manner the engineers should be able to compare this solution to a conventional one and understand which one is the most suitable for the specific case study in terms of building performance.

For this reasons ETABS 2015 has been used. It is a software package for structural analysis and design of buildings and it is very common in the structural engineering field. For example, it is widely used at Skidmore, Owings and Merrill LLP (SOM), one of the leading civil engineering firm in the world, that collaborates in this research. Below the individual components of the proposed model are analyzed separately and the effectiveness of different modeling assumptions will be discussed, based on the comparison with the results of the PRESSS research project. The ETABS Analysis Reference Manual [29] has been studied to develop the analytical model here proposed.

4.4.1   Wall Members

Modeling the wall panels as frame elements, the PRESSS researchers faced the problem of how to model the rigid links. In fact, the use of frame elements gives rise the necessity of understand how to connect the adjacent wall panels in order to work in a coupled manner preserving the rigid diaphragm behavior of the floor levels. So they used rigid links starting from the frame nodes that go inward the wall panels. The same consideration can be made for the nodes at the base of the frame elements, where rigid elements are required to link them with the foundation springs placed at the center of compressions. Researchers admitted that the modeling of those rigid links was initially a problem, as discussed above. Moreover, the section properties are not automatically computed by the software but must be calculated by the user and imposed to the element, creating inconveniences.
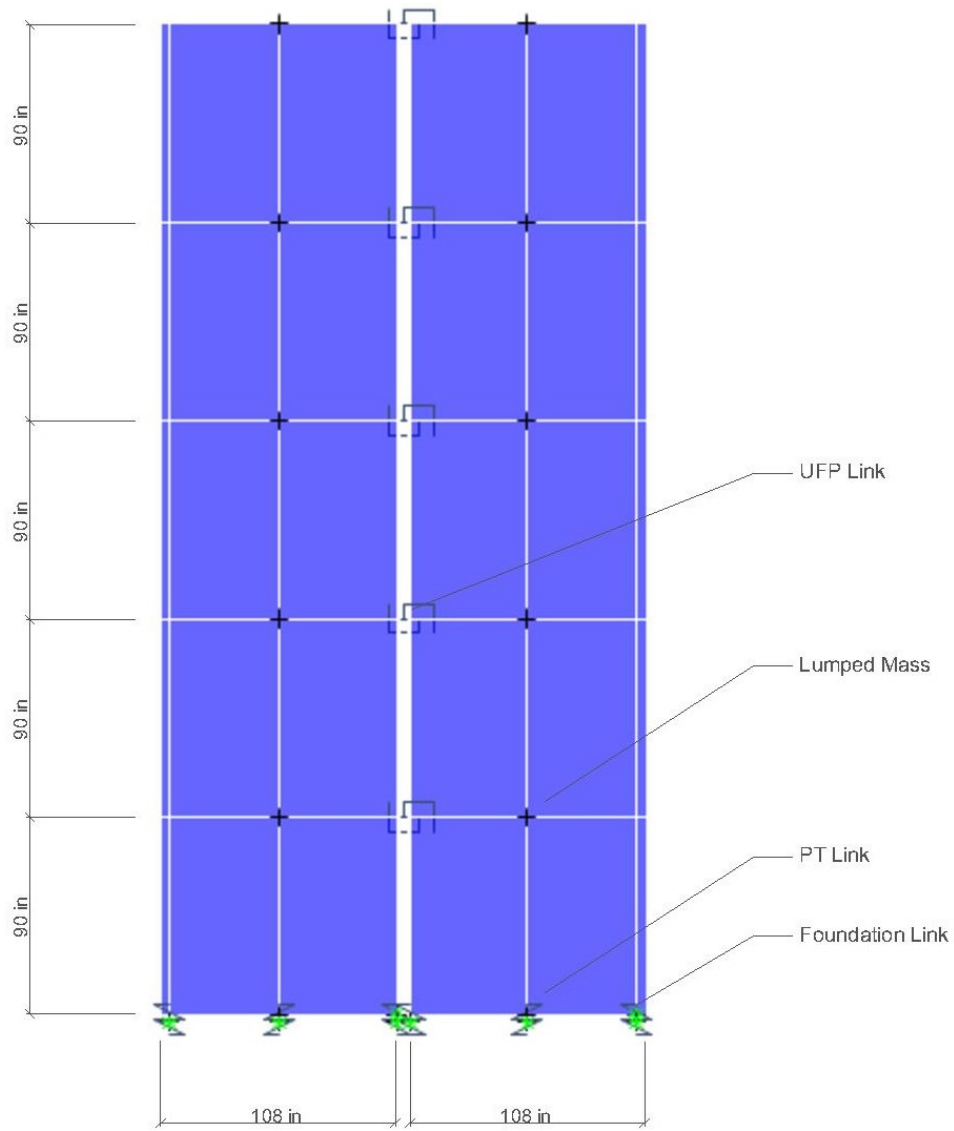
Figure 4.13: Elevation of the proposed model
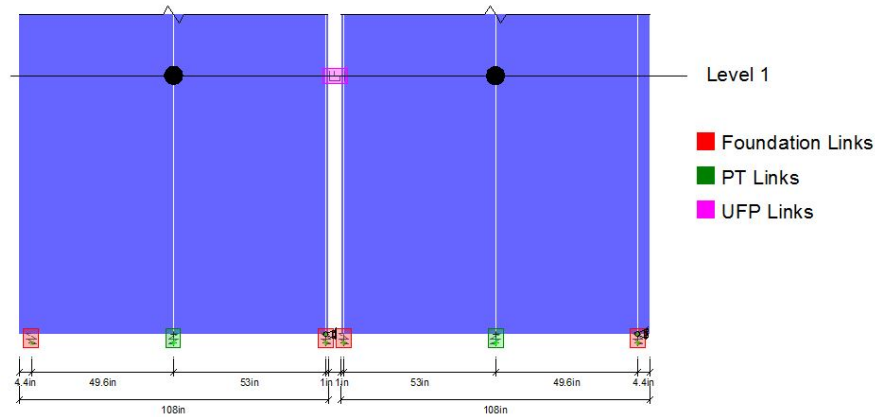
Figure 4.14: Base of the proposed model

In order to solve these complications it was made an attempt of modeling the wall panels using 2D shell elements that connect two consecutive floor levels. As before, the wall panels are designed to remain elastic during the design earthquake, thus a perfect linear-elastic hysteretic behavior is used. As ETABS 2015 considers this hysteretic rule by default, the assignment of the correct characteristic of the material that makes up the wall panels is sufficient for a correct linear-elastic response. The main characteristics of the material are presented in Table. 4.7. The software gives also the possibility to restraint the points of a floor level so that it behaves like a rigid diaphragm assigning the *Diaphragm* option to these points. Each wall panel is vertically discretized into 4 shell elements in line with the centerline and the centers of compressions, in order to have the nodes of the shells at the locations of the springs. In this way computational errors made by the software are avoided.

Table 4.7: Proposed Model, wall member parameters

Properties	Parameters			
	USCS		SI	
Elastic Modulus E	5200	ksi	35853	MPa
Shear Modulus G	2200	ksi	15168.5	MPa
Section Thickness	8	in	20.3	cm

4.4.2   Modeling of Gap Opening at the Base

The rocking behavior during seismic events of this system is allowed by the
creation of a gap opening at the base of the wall realized with a horizontal
joint between wall and foundation. The correct modeling of this behavior
was one of the first issues that have been observed in the model creation.

Initially the modeling of the rocking behavior was faced through fiber
elements. The foundation was assumed to be fixed, the wall panel constrained
at the base and the gap opening was modeled using concrete fibers at the
wall toes with zero tension strength. Since the non-linear behavior of the
wall is concentrated at the base, the upper part was modeled as linear-elastic
with negligible cracks in the concrete. It has been found that this model
produces non-linear deformations in the wall panels till the first floor level.
It is not in agreement with the real behavior of the system, in which the wall
remains a rigid block. Moreover, the use of fiber elements in ETABS 2015
introduces computational problems if the discretisation of the shell elements
is not almost squared. This limit constrains the positions of the nodes of the
wall panel and does not allow the match between these nodes and the ones
of the PT elements which are placed into design positions.

For these reasons, it has been decided to go towards a model in which
the elements at the base of the wall allow its uplift and maintain the wall
as a rigid block. The direction taken was the one for the creation of specific

additional elements that simulate this behavior, and thus it has been decided to use links elements defined in ETABS 2015. With these elements, the wall panel is constrained to the foundation through these links, which elongation could simulate the uplift without causing wall deformations. Moreover, this choice is in line with the modeling way used in the PRESSS model and allows the comparison with its results. The characteristics of the link elements are showed in the following part.

Foundation Links

As it as been said previously, the foundation is modeled in a similar fashion with respect to the model proposed by the PRESSS researchers since compression-only elements are used in order to model the wall uplift when the gap opening occurs and the vertical reaction that is present when the wall is in contact with the foundation. ETABS 2015 gives the possibility to define Gap elements, that should have the desired characteristics, but the use of these kind of elements give problems during the analysis and they don't work as expected. For this reason it has been decided to model them as multilinear elastic links as in the PRESSS model and their properties could be summarized as:

Table 4.8: Proposed Model, foundation link parameters

Properties	Parameters			
	USCS		SI	
Stiffness k	10000	kip/in	88512	kN/m
Compression Yield Force	800	kips	3558.6	kN
Tension Yield Force	0.1	kips	0.45	kN
Link Length	3	in	7.6	cm

4.4.3 Modeling of PT Tendons and the Self-Centering Behavior

The self-centering capacity of the system is provided by the gravity loads acting on the wall and by multi-strand tendons running through the wall panels and the foundation. In order to model this behavior it is essential that the PT steel and the prestressing force are modeled in the correct way.

According to the initial idea the PT tendons were modeled through frame elements placed at the centerline of each wall with the application of the pre-stress by means of thermal deformations. The gravity loads were represented through the self-weight of the elements composing the wall and with a surface load applied at each level corresponding to its tributary weight. This option allows to represent the initial stress in the frame elements but do not take into account the restoring forces. It was understood that in order to have the re-centering behavior it is necessary to apply the corresponding quantity in the way of external forces. Thus, two forces representing the restoring capacity of the system were applied at the top of the each frame element but this solution showed other complications. In fact, the concentrated forces do not follow the deformed shape of the wall in terms of inclination, but only in term of application point, as it can be seen in Fig. 4.15. The force remains in the initial direction, i.e in the straight configuration, and thus it does not reproduce the expected behavior as it becomes a destabilizing force. Its ap-plication line results to be more external than the centroid of the wall. In order to solve this disadvantage it was supposed to define a lateral spring that produces the re-centering effect pulling back the wall. The law governing the stiffness of the spring should be able to follow the changes of inclination of the wall thus changing the value of the reacting force.

Another possibility is to model the PT tendons with springs element.

(a)   (b)
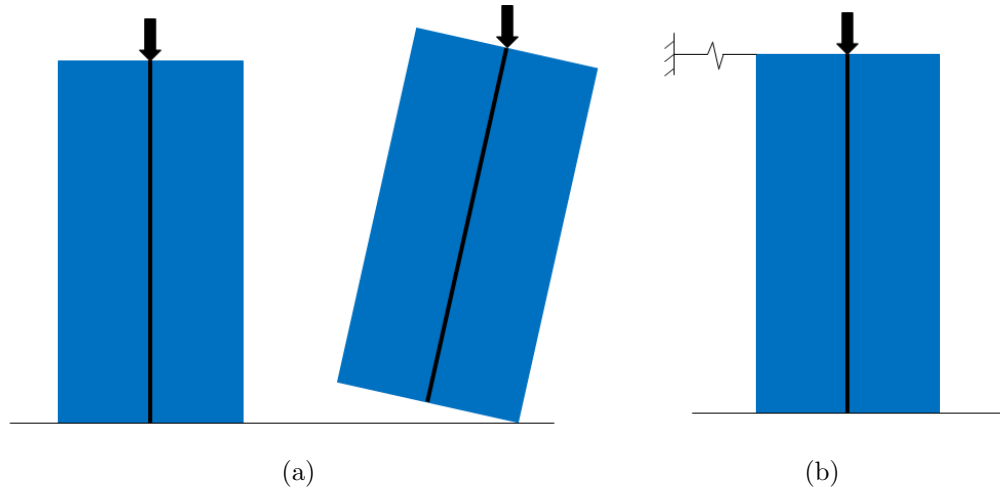
Figure 4.15: Differents model of the re-centering behavior

Spring elements that go from the base to the top of the wall can be used, substituting in this manner the frame elements previously adopted. The limitation of this employment is that the springs do not follow the deformed shape of the wall and remain straight not reproducing the real elongation of the PT steel. In order to solve this problem a discretisation of the springs along the height was performed but also this solution did not reproduced the expected results. Thus, springs with concentrated length at the base were adopted and the restoring forces were applied at their locations at the base of the wall panel. This solution is consistent with what carried out by the PRESSS research program and this solution avoids the transformation of the vertical forces in destabilizing forces. It was found that such a representation of the PT strands well reproduce the real elongation of the PT and the self-centering behavior. The characteristics of these elements representing the PT steel are summarized in the following part.

4.4.4 PT Links

The post-tensioning steel is modeled as links at the base of the wall panels and placed at their centerline. They develop reaction forces due to the elongation of the unbonded strands at the center of the walls. The hysteretic behavior of these components is bilinear elasto-plastic. The main difference with respect to the PRESSS model is that with ETABS 2015 it is not possible to apply a load to the links that affects only their behavior and not the global response of the structure. Therefore, it is necessary to find an other way to represent the initial prestress. Thus, it has been decided to shift the origin of the hysteretic
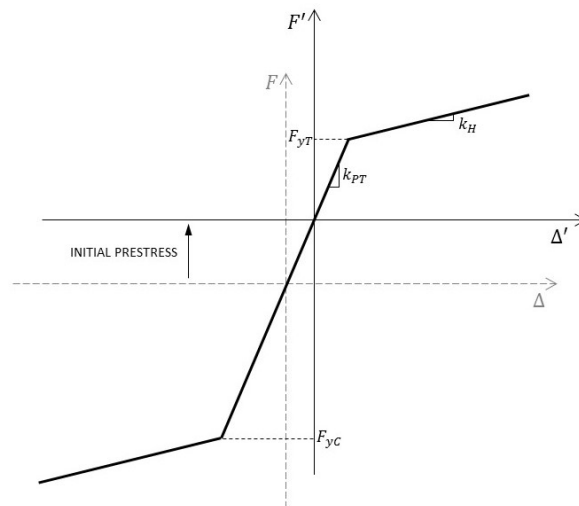
Figure 4.16: Hysteretic rule of the PT springs

force-displacement relationship up to the initial prestress force acting on the tendons. In Fig. 4.16 it is possible to see this change, where F_{PT} and Δ_{PT} are respectively the initial prestress force and the correspondent elongation acting on the tendons of the test building. Therefore the yield forces of the

new hysteretic rule will be:

$$F_{yT} = F_y - F_{PT} \tag{4.13}$$

$$F_{yC} = F_y + F_{PT} \tag{4.14}$$

where F_y is the material yielding force, equal to the yielding stress $f_{pt\,y}$ multiplied by the gross area of the tendons.

Table 4.9: Proposed model, PT links parameters

Properties	Parameters			
	USCS		SI	
k_{PT}	197	kip/in	35052	kN/m
k_H	4	kip/in	701	kN/m
F_{yT}	211	kips	938.6	kN
F_{yC}	539	kips	2397.6	kN

4.4.5   UFP Links

The most tricky part of the entire model is the definition of the properties of the U-shaped flexural plates that could be consistent with the comparison model because the PRESSS reports lack information for their correct determination. ETABS 2015 do not give the possibility to define a link that follows the Al-Bermani hysteretic rule, this rises the issues to manually compute the relative force-displacement relationship for UFP links. It has been seen that the definition of the tangent stiffness between the two bounding surfaces is not accurate, in particular the relation between P, F_1 and F_2. Moreover, the proposed value of the α factor, equal to 0.001, seems to be too small and not coherent with Fig. 4.9.

It has been found that the type of nonlinear behavior defined by ETABS 2015 that better reproduces the Al-Bermani one is called *Wen Plastic* and its curve is shown in Fig. 4.17.
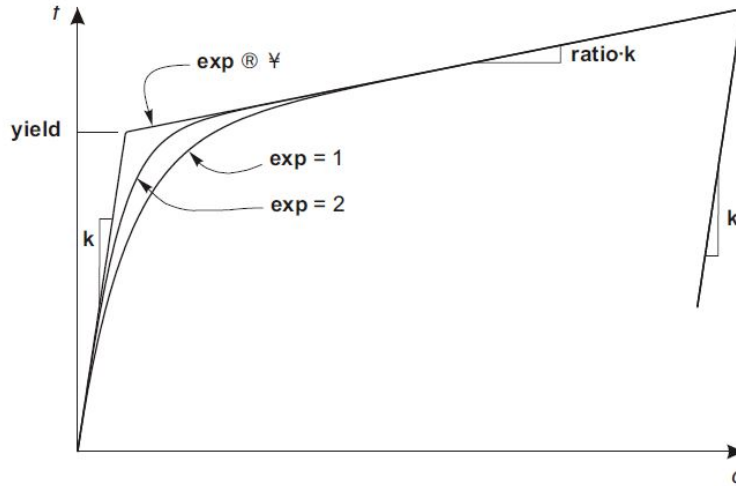
Figure 4.17: Wen hysteretic rule, [29]

The nonlinear force-deformation relationship is given by:

$$f = \mathbf{ratio} \cdot \mathbf{k} \cdot d + (1 - \mathbf{ratio}) \cdot \mathbf{yield} \cdot z \qquad (4.15)$$

where $\mathbf{k}$ is the elastic stiffness, $\mathbf{yield}$ is the yield force, $\mathbf{ratio}$ is the specified ratio of post-yield stiffness to elastic stiffness ($\mathbf{k}$), and z is an internal hysteretic variable that follows the differential equation:

$$\dot{z} = \frac{\mathbf{k}}{\mathbf{yield}} \cdot \begin{cases} \dot{d}\,(1 - |z|^{\mathbf{exp}}), & \text{if } \dot{d}z > 0, \\ \dot{d}, & \text{otherwise} \end{cases} \qquad (4.16)$$

where $\mathbf{exp}$ is an exponent greater than or equal to unity and smaller than 20. Larger values of this factor increases the sharpness of yielding.

The UFPs are therefore modeled as 5 horizontal link elements that connect the wall panels at each floor level. They are rigid in the horizontal direction, following the rigid diaphragm behavior of each floor level, while they follow the Wen hysteretic rule if subject to shear deformations. The properties of the UFP links could be summarized as:

Table 4.10: Proposed Model, UFP link parameters

Properties	Parameters			
	USCS		SI	
k	186.6	kip/in	33201.5	kN/m
yield	51.3	kips	228.2	kN
ratio	0.015		0.015	
exp	2		2	

(a)   (b)
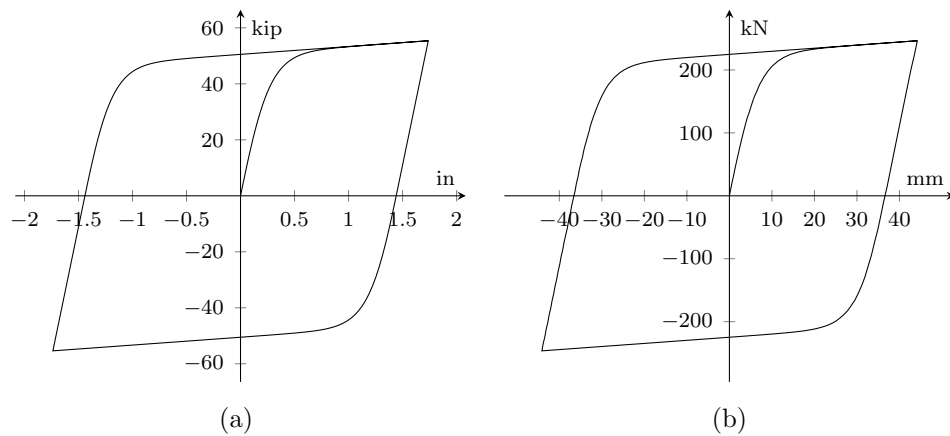
Figure 4.18: Nonlinear shear-displacement response of UFP links under cyclic loads: (a) USCS units, (b) SI units

4.4.6   Loads and Constraints

Load and global restraints are modeled as in the PRESSS model and they have been used the same values. So:

- The vertical loads are concentrated forces applied at the centers of compressions, where the foundation links are placed. They are worth $120.88\,\text{kips}$ ($537.70\,\text{kN}$) at the exterior nodes and $113.12\,\text{kips}$ ($503.18\,\text{kN}$) at the interior ones;

- Seismic masses are lumped masses of $0.545\,\text{kip}\,\text{s}^2\,\text{in}^{-1}$ ($95.444\,\text{tons}$) at the centerline of each wall panels and they work only in the horizontal

direction and not in the vertical one;

- The system is restrained in the vertical direction thanks to the springs at the base;

- The nodes in correspondence with the foundation links on the right of each wall panel that belong to the shell elements are laterally fixed.

4.4.7 Input Ground Motions

The PRESSS test building was subject to a design level input motion derived from the El Centro record obtained from the 1940 Imperial Valley earthquake. Since there isn't the possibility to use the same seismic input motion, existing acceleration time histories have been modified in order to match the design response spectrum. For this purpose *SeismoMatch* software has been used. It is an application developed and maintained by Seismosoft Ltd capable of adjusting earthquake accelerograms to match a specific target response spectrum. In pictures below it is possible to see the ground motions used in the present analysis and how their response spectra match well with the target one.

4.5 Results of the Proposed Model

Expected Behavior

The response of the proposed model reflects all the specific characteristics related to unbonded post-tensioned precast jointed walls under seismic actions. Therefore the proposed model should displays all these peculiarity, that could be analyzed through time-history analysis. Time-history analysis is a step-by-step analysis of the dynamical response of a structure to a
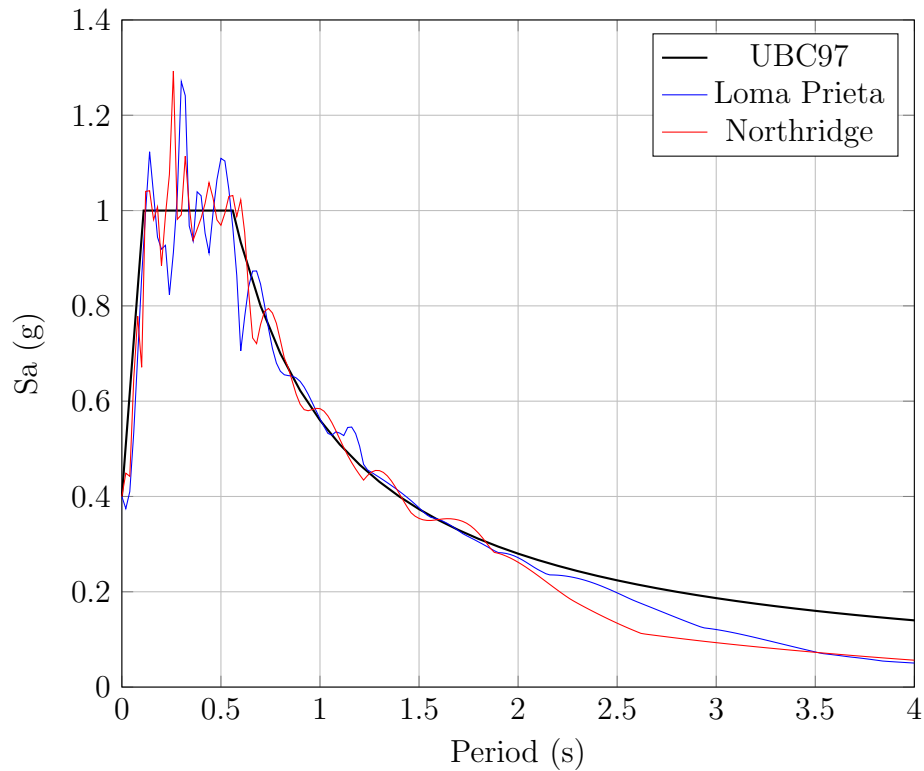
Figure 4.19: Response spectra comparison

specified loading that may vary with time, for example the ground acceleration. To find the full time history of a structural response, the dynamic equation of motion must be solved at a number of subsequent time instants. According to the proposed way to model this kind of structures, the foundation links should provide vertical resistance in compression but zero strength in tension in order to allow the formation of a gap at the joints between walls and foundation when the lateral load applies an overturning moment on the wall system. Vertical unbonded post-tensioned tendons, that close the wall lift-off and pull the structure back to its undisplaced configuration, are modeled with elasto-plastic links that should remain in the elastic range at all times during an earthquake, otherwise the structure doesn't have enough
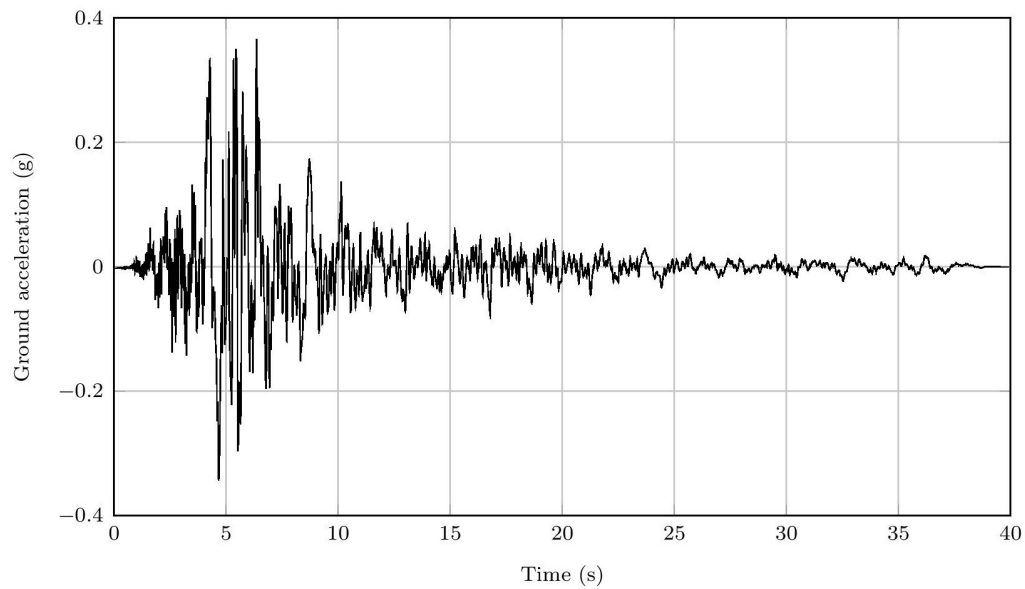
(a) Loma Prieta
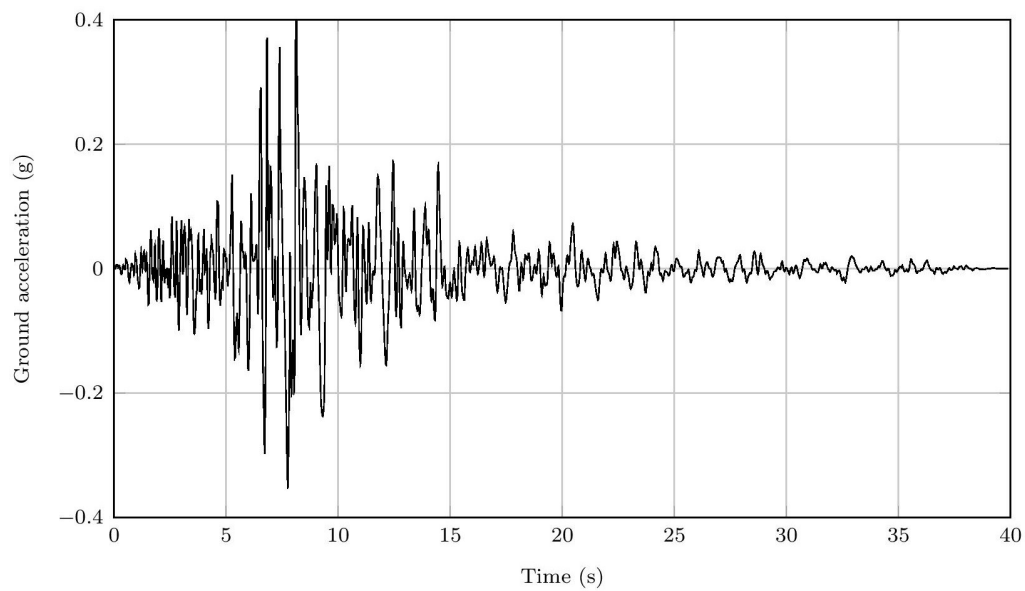
(b) Northridge

Figure 4.20: Response spectrum compatible time histories

self-centering capacity. The UFP links represent the shear connectors between the wall panels and assure the required energy dissipation. Fig. 4.21 is the exaggerated deformed shape of the proposed model under lateral load, showing the formation of the gap opening at the base. Moreover, the wall panels displace and rotate as a rigid block and remain in the elastic range, since it has been supposed the linear elastic behavior just from the beginning.

Fig. 4.22 instead shows the force-displacement relationships of the foundation links, the PT links and the UFPs links respectively when the structure is subject to the Loma Prieta spectrum-compatible earthquake as previously defined (Fig. 4.20). The components behave as expected, in accordance with the considerations made in Chapter 3.

Pushover Results

A pushover analysis is then performed since it is a valuable resource for examining a model as it slowly increments the lateral load profile allowing various mechanisms in the model to be noted. So the proposed model is subject to a lateral load distributed in an inverse triangular fashion over the height of the wall, as the displacement profile assumed in the DDBD procedure. Fig. 4.23 shows the results of a pushover analysis in terms of base moment-top displacement relationship. The first circle highlights the wall uplift that correspond to the beginning of the nonlinear behavior of structure. At the second circle the first yield of the UFP links occurs and the structural stiffness rapidly decrease. The PT links first yields in correspondence of the third circle. The maximum resisting overturning moment corresponds to the point where the second PT link undergoes a nonlinear displacement (forth circle). At this point the stiffness of the PT links suddenly decreases to k_H and this is the reason why the pushover curve starts descending.
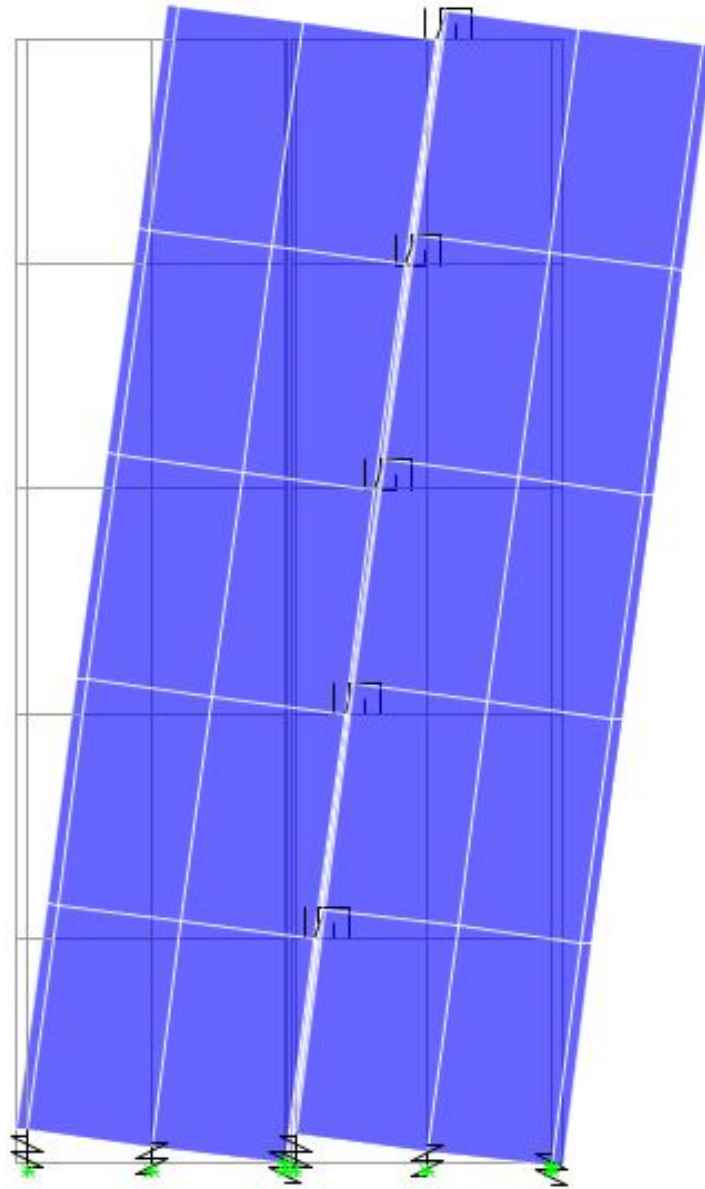
Figure 4.21: Exaggerated displaced configuration of the proposed model

The results of the proposed model can be numerically compared with the one of PRESSS analytical model, showed in Fig. 4.12, here represented for an easily comparison. The dashed line is the one performed without the
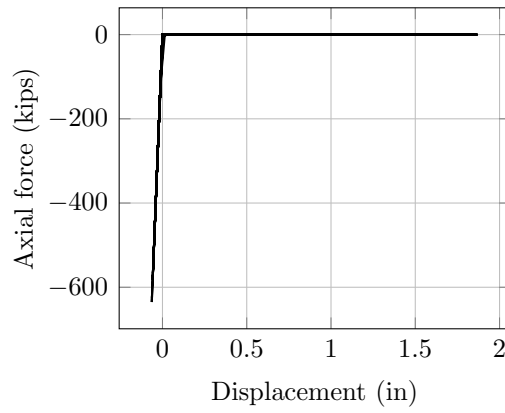
(a) Foundation Link
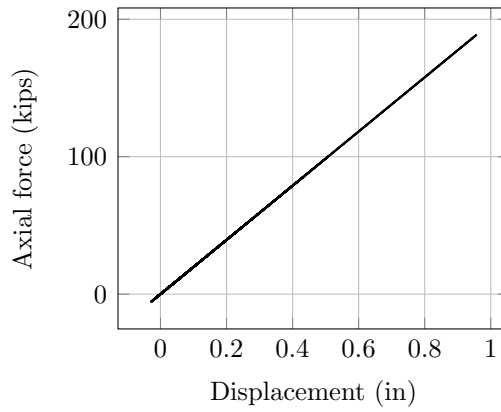
(b) PT Link
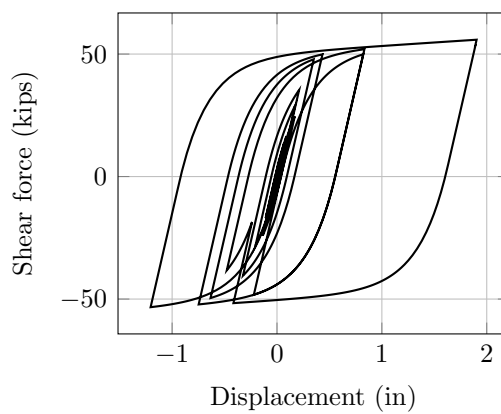
(c) UFP Link

Figure 4.22: Force-displacement relationships for different link elements in the proposed model under a simulated ground motion

additional PT column and it is our reference for validating the model. As can be seen in the picture, the two models assume the same trend under lateral forces. On the other hand, the moment resistance of the proposed model is lower than the resistance of the PRESSS model. In fact it reaches a maximum of $72\,273\,\text{kip in}$ ($6559\,\text{kN m}$) corresponding to the yield of both the PT links, roughly 90% of the one performed in the analytical model developed by the PRESSS researchers. This is due to the uncertainties in the definition of the UFP links, that don't allow a perfect reproduction of the hysteretic behavior of these elements and therefore the system doesn't carry out the same energy dissipation. The fact that for the same amount of imposed lateral displacement the overturning moment is lower depends on the lower value of energy dissipated by the UFP links respect to the UFP springs in the PRESSS analytical model.

Viscous Damping Calculation

The same problem recurs in the comparison of the calculated hysteretic viscous damping coefficient. Subsequent pushover analysis have been run in ETABS 2015 in order to reproduce a complete hysteretic loop. Firstly the wall system has been subjected to a monotonically increasing pattern of lateral forces in one direction until the design displacement. The same load distribution has been applied in the opposite direction to the deformed configuration in order to reach the same design displacement in the other direction. Finally, the structure has been pulled back to the initial position. The results could be seen in Fig. 4.24, where the red line is the computed hysteretic cycle and the blue line is the equivalent elastic response. The areas under these curves have been highlight with pattern of the same colors of the curves, in order to show respectively the dissipated energy per cycle A_h and
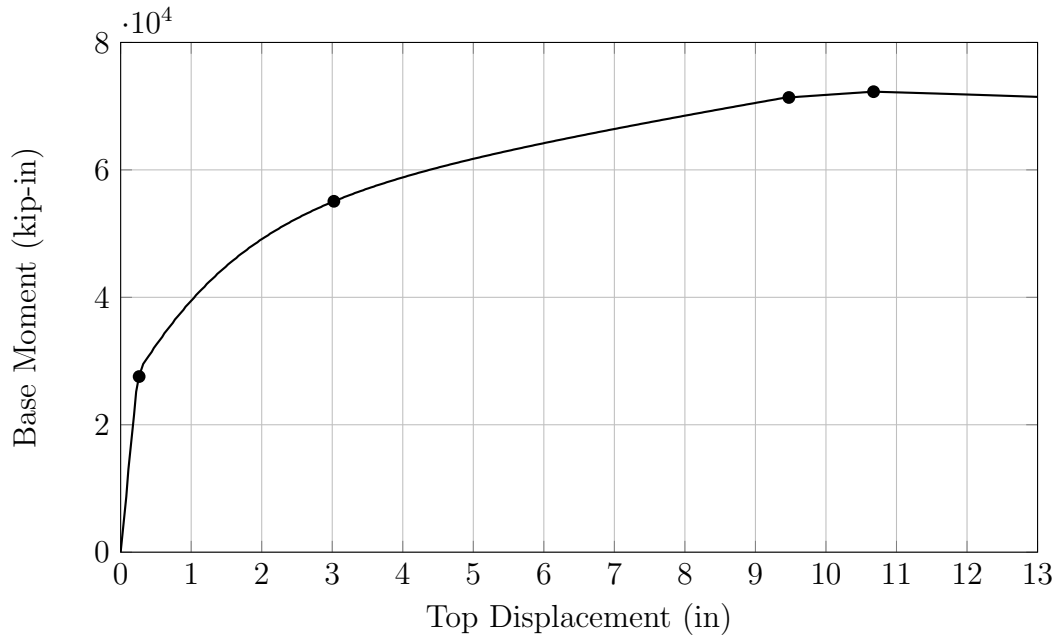
(a) *Proposed Model pushover*
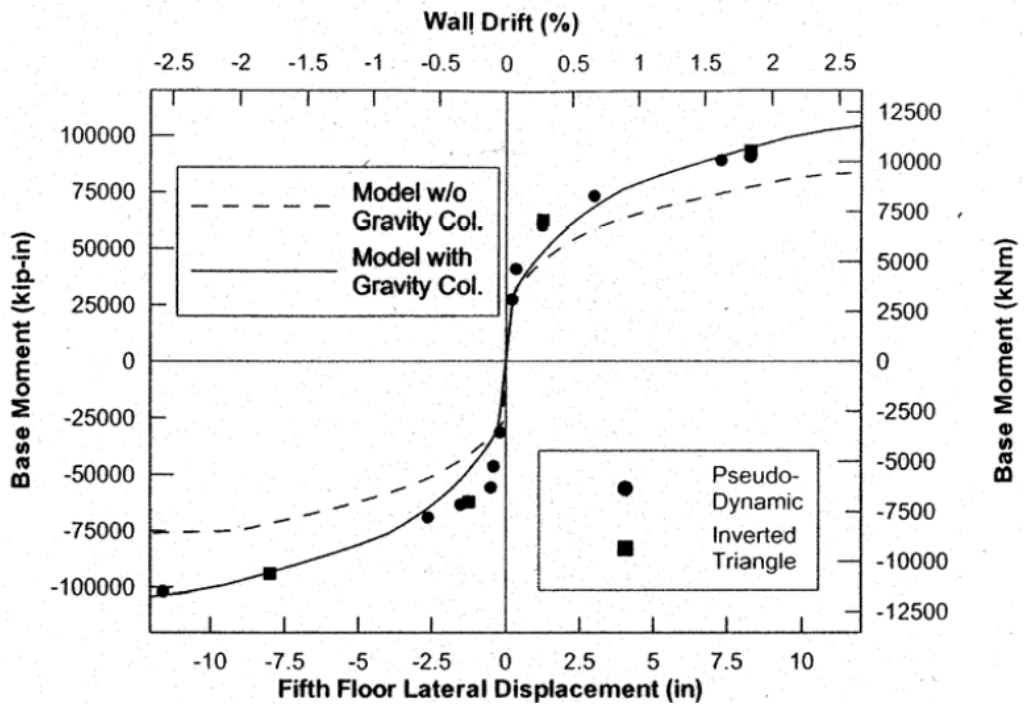
(b) *PRESSS pushover*

Figure 4.23: Proposed Model Base moment-Top displacement relationship, pushover results
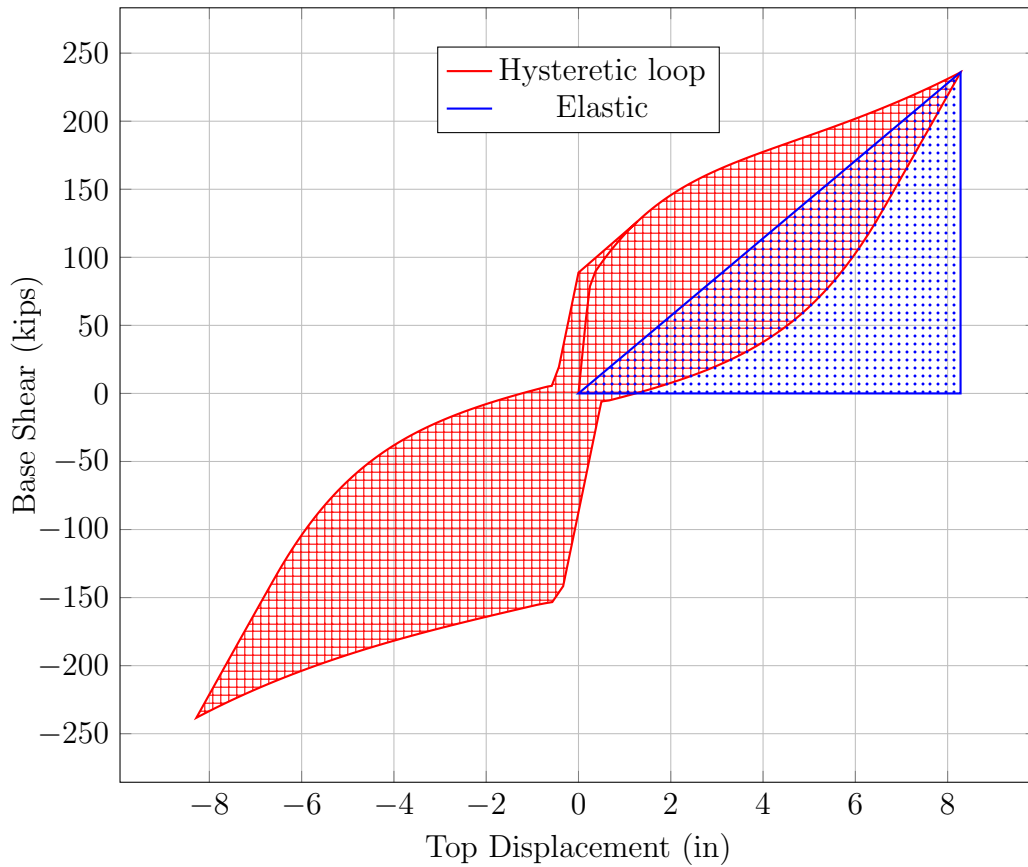
Figure 4.24: Full cycle hysteresis loop

the equivalent elastic strain energy A_e, in according to Eq. (4.12).

The computed hysteretic viscous damping coefficient is equal to 15.24%, that it is lower than the value presents in the PRESSS reports, that is 15.78%. The result is a confirm of the consideration that the energy dissipated by the UFP links in the proposed model is too small and not representative of the real problem. Lacks in PRESSS reports about them don't allow more accurate definition of the nonlinear behavior of the shear connectors. However, the resulting equivalent viscous damping coefficient remains coherent with the value assumed in the design procedure.

Results of the Time Histories

The proposed model remains a good estimator of the global behavior of the lateral load resisting system subject of study. Two design spectrum compatible ground motions, in particular the Loma Prieta earthquake and the Northridge earthquake (Fig. 4.20), have been considered. Fig. 4.25 displays the trend of the displacement in time of each floor level under these seismic excitations during the first 20 seconds, when the ground accelerations are more severe. It can be seen that the lateral displacement of the roof level is lower than the one assumed for the design, relative to 2% drift limit. In fact the maximum displacement during the Loma Prieta earthquake is 8.52 in (216 mm) and during the Northridge earthquake is 8.84 in (225 mm), while the design target displacement is 9 in (229 mm). Moreover, Fig. 4.26 shows the full time history of the top displacement during the same ground motion. When the earthquake finishes, the structure still has self-centering capacity. So the wall comes back to its initial position and the residual displacement is zero.

Finally, the base moment hysteresis loop during a simulate seismic excitation is described by Fig. 4.27. The former is the cycle when the proposed model is subject to the Loma Prieta ground motion while the second is the nonlinear behavior under the Northridge time history. The figure shows the self-centering characteristics of the split wall panel system by the "flag-shaped" hysteresis loop, according to the theoretical considerations made in Chapter 3.
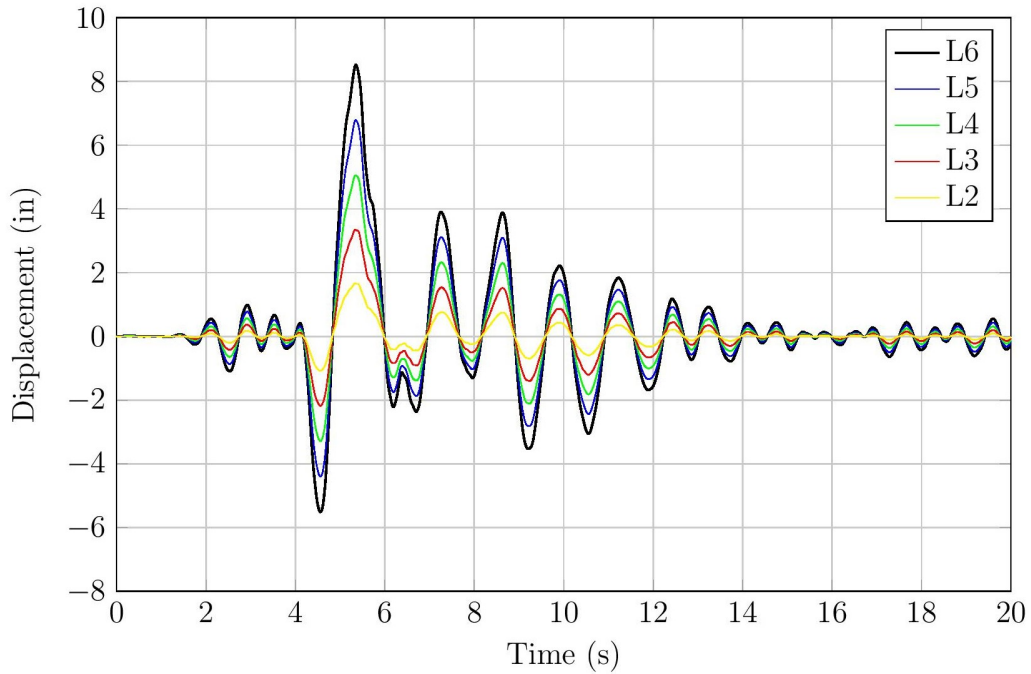
(a) *Loma Prieta Ground Motion*
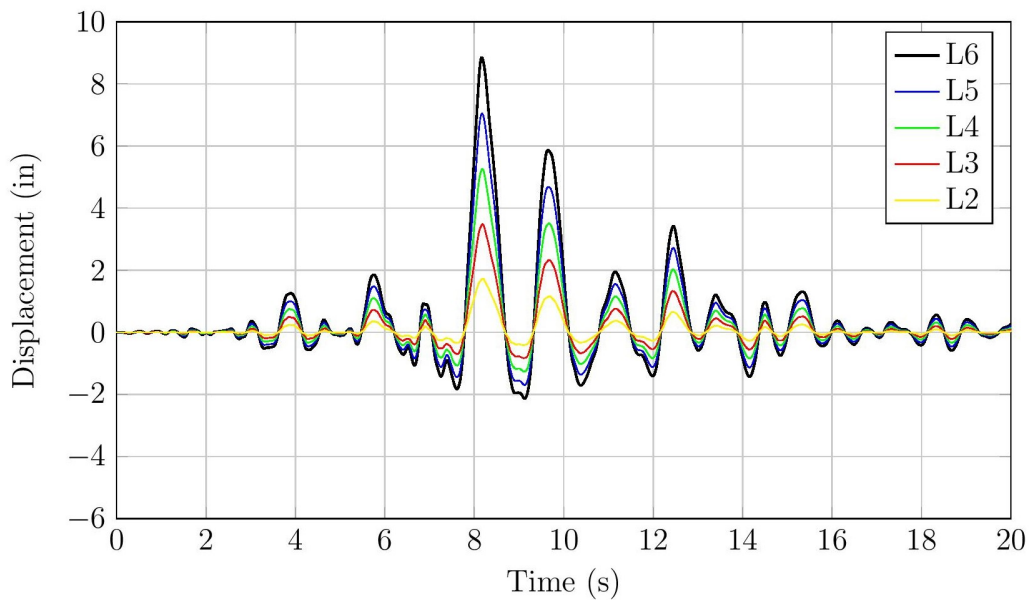
(b) *Northridge Ground Motion*

Figure 4.25: Floor Displacements time histories
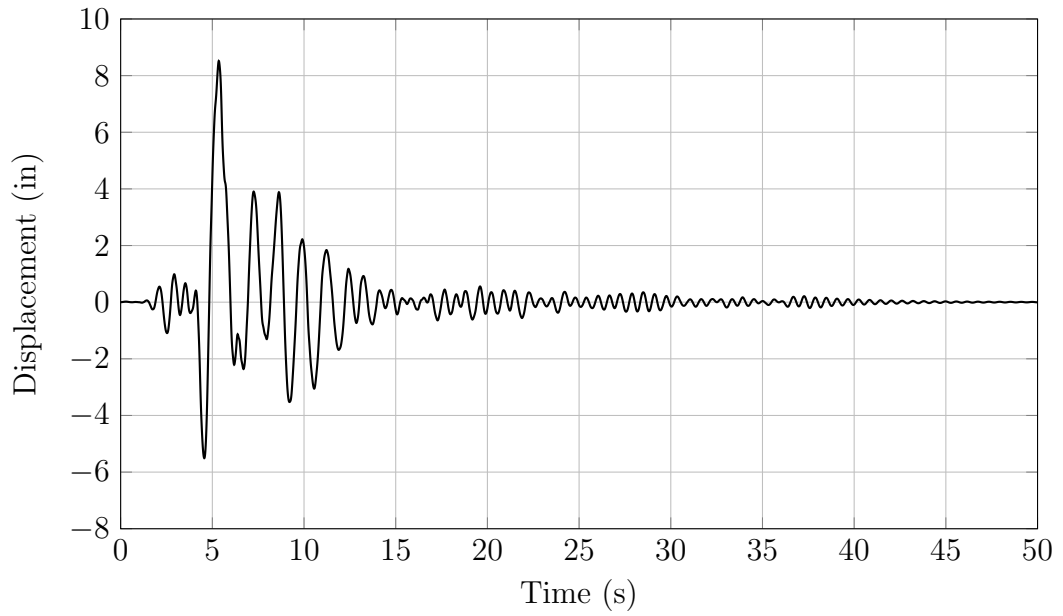
(a) *Loma Prieta Ground Motion*
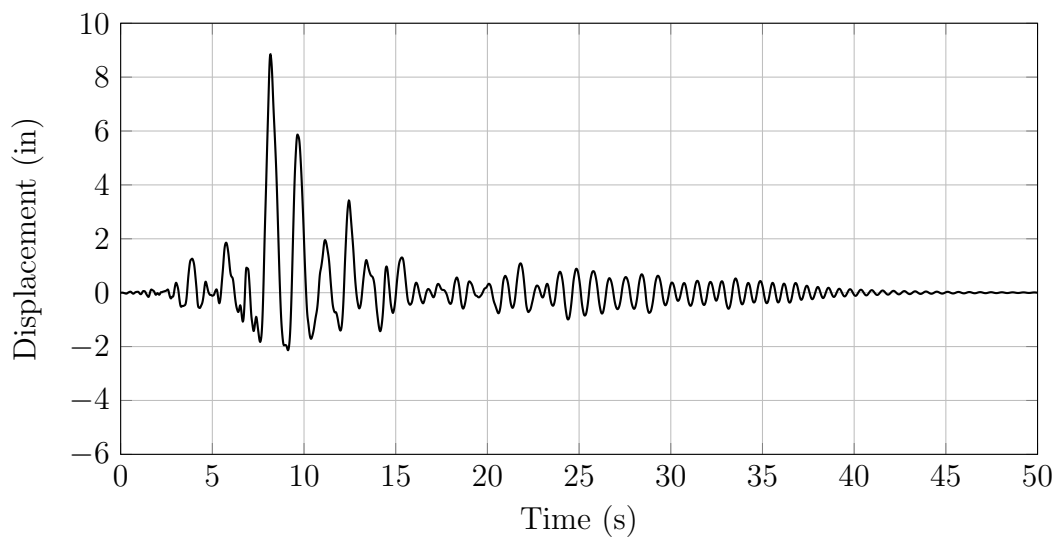
(b) *Northridge Ground Motion*

Figure 4.26: Top Displacement time history
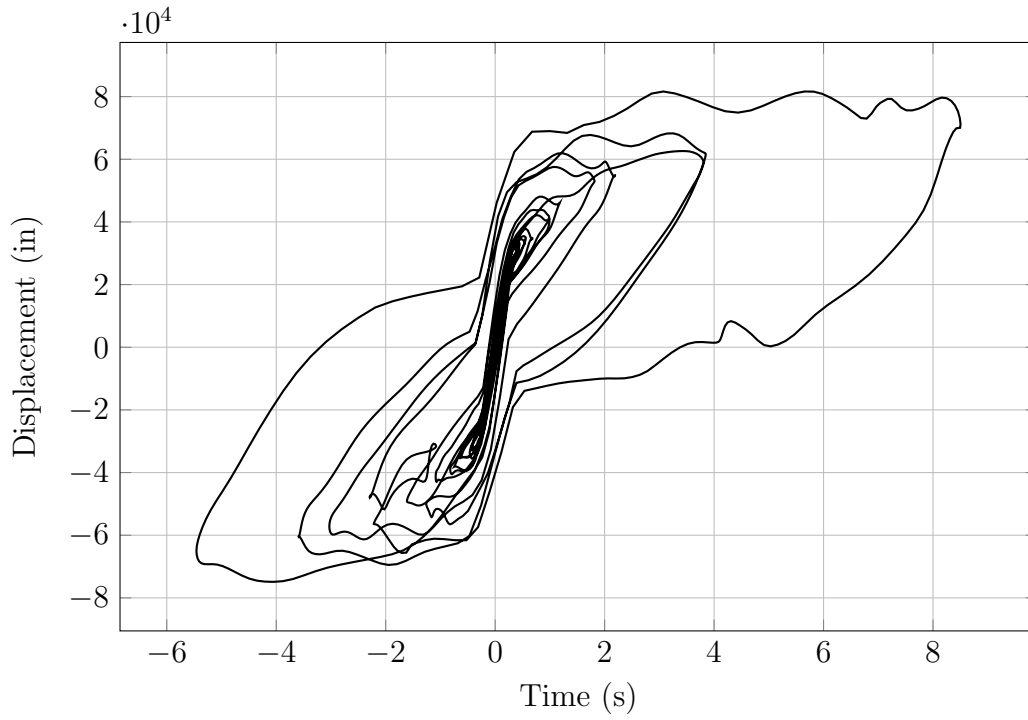
(a) *Loma Prieta Ground Motion*
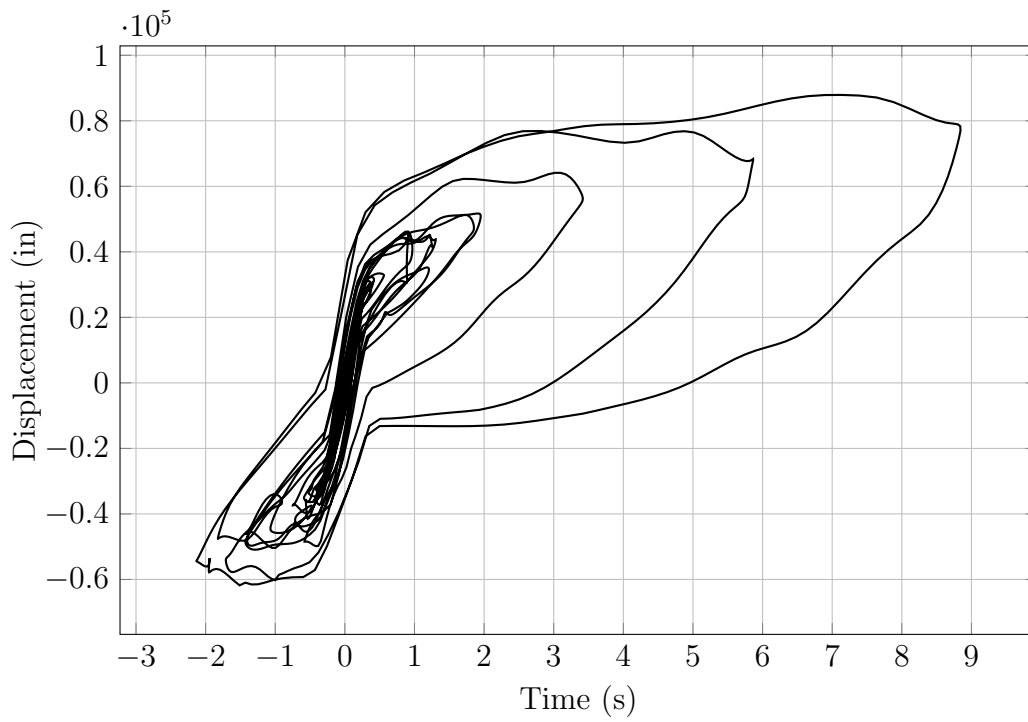
(b) *Northridge Ground Motion*

Figure 4.27: Base moment hysteresis loop

Chapter 5

Case Study: New Long Beach Civic Center

5.1 Introduction

The objective of this chapter is the application of unbonded post-tensioned
hybrid walls as lateral resisting system of the New Long Beach Civic Center
(Long Beach, California). This building is considered an essential facilities
and therefore the owner required that it should guarantee enhanced levels
of seismic performance. In fact, it should experience of few or no injuries,
the new facility must be reoccupable within a week, full functionality should
be guaranteed within 30 days after a design earthquake and it results that
financial loss due to the design earthquake would be lower than 5 %. In order
to achieve the required seismic performance the use of enhanced walls has
been explored. As it has been presented previously, this kind of wall assured
a rocking behavior that results in small or zero residual displacement after
the design earthquake. Thus, this behavior concentrates all the non-linearity
at the base of the wall and guarantees that the remainder of the wall behaves

almost linear elastic limiting damage. The self-centering behavior is provided by unbonded post-tensioned tendons, but they have to be combined with an energy dissipation system that softens the lateral displacements.

In Chapter 2, two different design procedures have been explored and the lateral seismic forces applied to the structure have been computed. These forces can be used to determine the material quantities required to provide enough strength and a certain level of performance of the building, for example in terms of drift of lateral displacement (see Chapter 3). Chapter 4 instead focuses on the development of a modeling procedure that could reproduce the expected behavior of unbonded post-tensioned concrete hybrid walls. The model variation exercise was necessary in order to verify the sectional design developed thanks to the guidelines present in Chapter 3 on the basis of the seismic forces computed according to Chapter 2.

In the following Chapter all these operations will be applied to an unbonded post-tensioned shear wall as part of the New Long Beach Civic Center. In fact moving away from the feasibility design already made by the engineers of Skidmore, Owings and Merrill LLP, new configurations have been explored and a single shear wall with different design assumptions has been studied. Initially, an unbonded post-tensioned hybrid shear wall has been considered with mild reinforcement that provides the required energy dissipation thanks to its elongation, while post-tensioned tendons running all along the wall height give a restoring force that limits the lateral displacement after the earthquake occurs. As requested by the client, the considered structure is cast-in-place and not precast as the PRESSS test building, but this difference does not imply changes in the design of the wall base, which is the more critical part for this kind of structure. Moreover, the same procedure has been applied to a conventional monolithic reinforced concrete shear

wall in order to compare the results between these two options.

5.2 New Long Beach Civic Center

The case study considered is the New Long Beach Civic Center (Long Beach, California). Fig. 5.1 shows the site plan of the whole project of renovation of the downtown of Long Beach. The project includes a new City Hall, a new Port Building for Harbor Department administration, a new and relocated Main Library, a redeveloped Lincoln Park, a residential development, and a commercial mixed use development. In total, the proposal includes six new buildings, three new parking garages, related infrastructure and landscaping, and two new public street extensions through the project site. Both the City Hall and Port buildings would be up to 11 stories in height.

Skidmore, Owings and Merrill LLP (SOM) has been involved in the design of Civic Center Block, that includes the City Hall and the Port Administration Building (Fig. 5.2). The former would be an approximately $270\,000$ gross square feet (gsf) ($25\,084\,\mathrm{m}^2$) up to 11-story concrete frame structure that includes office space for City staff and elected officials. The structure would also include Council Chambers, meeting rooms, transaction counters and other public serving components. The Port Building would be up to 11 stories, utilizing a concrete frame structure of up to $240\,000$ gsf ($22\,300\,\mathrm{m}^2$). It would be designed to house the administrative functions of the Harbor Department. The space within this building would be primarily office space. City Hall Building. Located around and between the City Hall and Port Building would be a $73\,000$ square foot (sf) ($6782\,\mathrm{m}^2$) Civic Plaza, which would include landscape elements appropriate for larger spontaneous gatherings as well as planned events. The Port and City Hall buildings would share a common
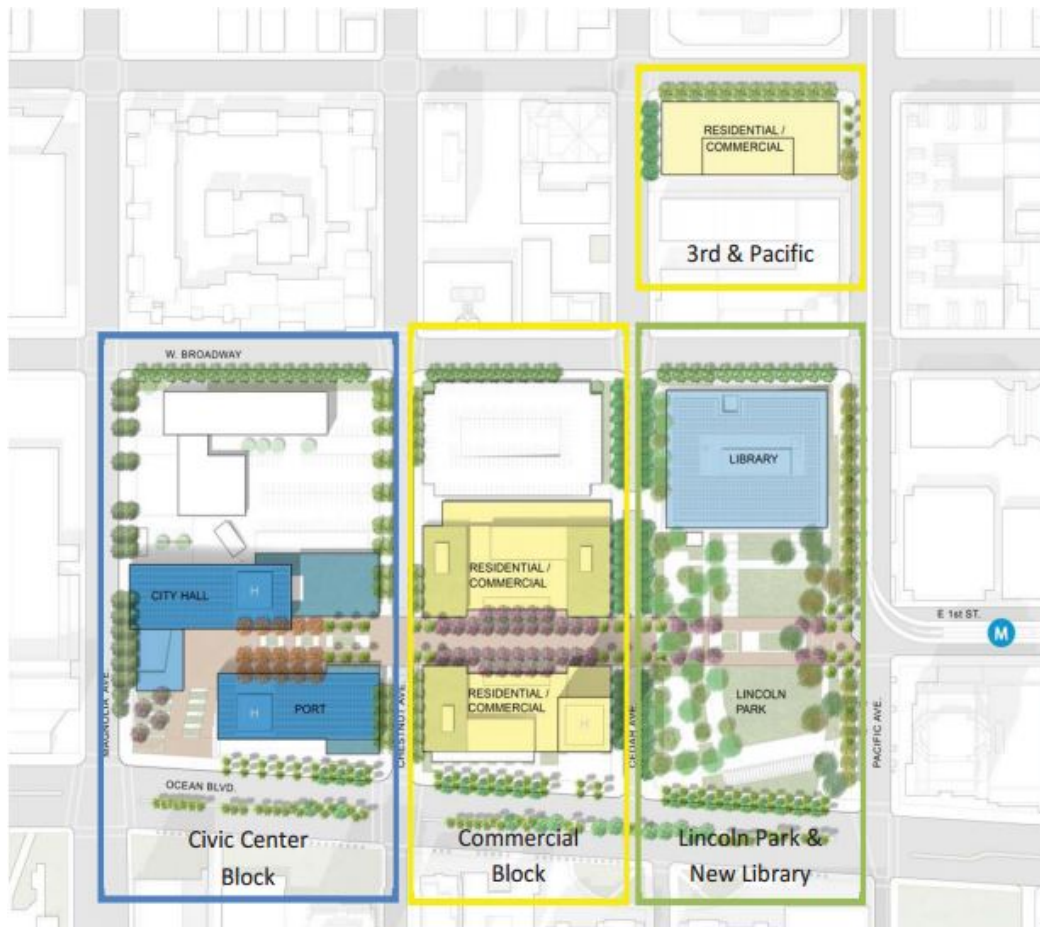
Figure 5.1: Global view of Civic Center

underground parking structure that includes shared infrastructure such as the combined central plant, common points of vehicular access and shared loading dock services.

Fig 5.3 shows the typical elevation of the building. The City Hall and the Port Building present an equal building layout, with a total height of 162.5 ft (49.53 m) above ground, while the levels below ground are in common. Also the plan of the two building is identical and the typical framing is shown in Fig. 5.4. The lateral resisting system of these building is composed by two concrete cores placed symmetrically with respect to the central axis. These

two cores contain stairs and elevators. The frame system has a typical bay of 30 ft (9.14 m) in one direction and is designed to carry only the gravity loads, with no contribution in the seismic resistance.

Figure 5.2: Global view of Civic Center

Long Beach is located in a region with high seismicity. The owner requires not only the collapse of the structure during an earthquake be prevented, but also that the structure be costly efficient as well, in terms of structural and non-structural repair and in terms of loss of business operation after the seismic event. Therefore, the design requirement for the Civic Center is that it should have a 50% confidence level that after the design earthquake occurs, the Civic Center should be able to:

- Experience few or no injuries;

- Reoccupation of the new facility within a week;
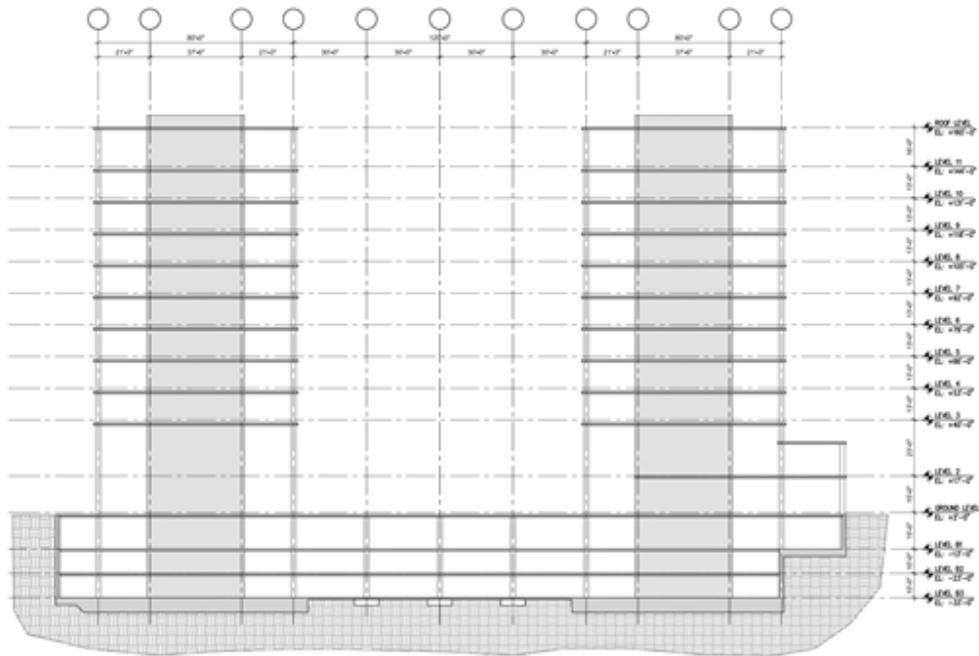
Figure 5.3: Typical system elevation
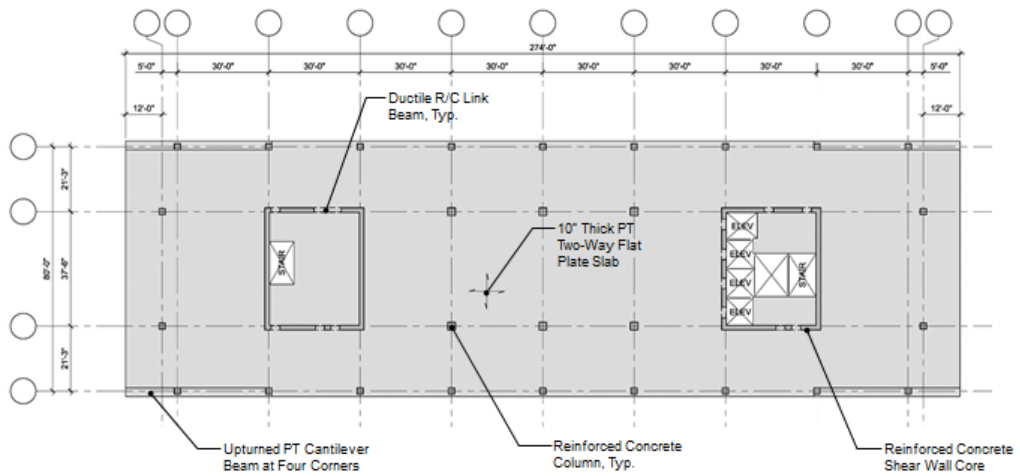
Figure 5.4: Typical tower framing plan

- Recover full functionality within 30 days;

- Experience less than 5% financial loss (as compared to the replacement value).

In order to achieve this very strict performance level superstructure and foundations have to remain remain essentially elastic during the seismic event. Moreover the relative displacements should be very low in order to limit damage of non-structural components, which however need to be designed to accommodate relative displacements. Mechanical, electrical and plumbing components and other critical systems need to be protected to make sure that they are replaced/repaired within 1 month after the earthquake. This enables normal operations to resume once utilities are restored. Following the American building code, these considerations mean that the Civic Center falls into the Risk Category IV (Table 1.5-1, ASCE 7-10), which implied a drift limit of 1% (Table 12.12-1, ASCE 7-10).

Enhanced walls that perform an almost elastic behavior are needed. In order to know the behavior of the whole structure using this kind of walls and their advantages, previously it is necessary to study the behavior of a single wall. For this reason, the present research takes into consideration one wall which runs parallel to the shorter side of the building. The interaction with the other walls composing the lateral resisting system could be a future development of this work. In order to limit the coupling between walls placed orthogonally, the plan layout has been changed, as shown in Fig. 5.5, where the red boxes are the proposed location of the walls. This is possible because the building plan is not definitive yet, giving the possibility to suggest new configurations. It is obvious that the location of the walls must be confirmed by the architects, but it is not relevant in the present research.

An independent engineering consultant carried out a geotechnical investi-
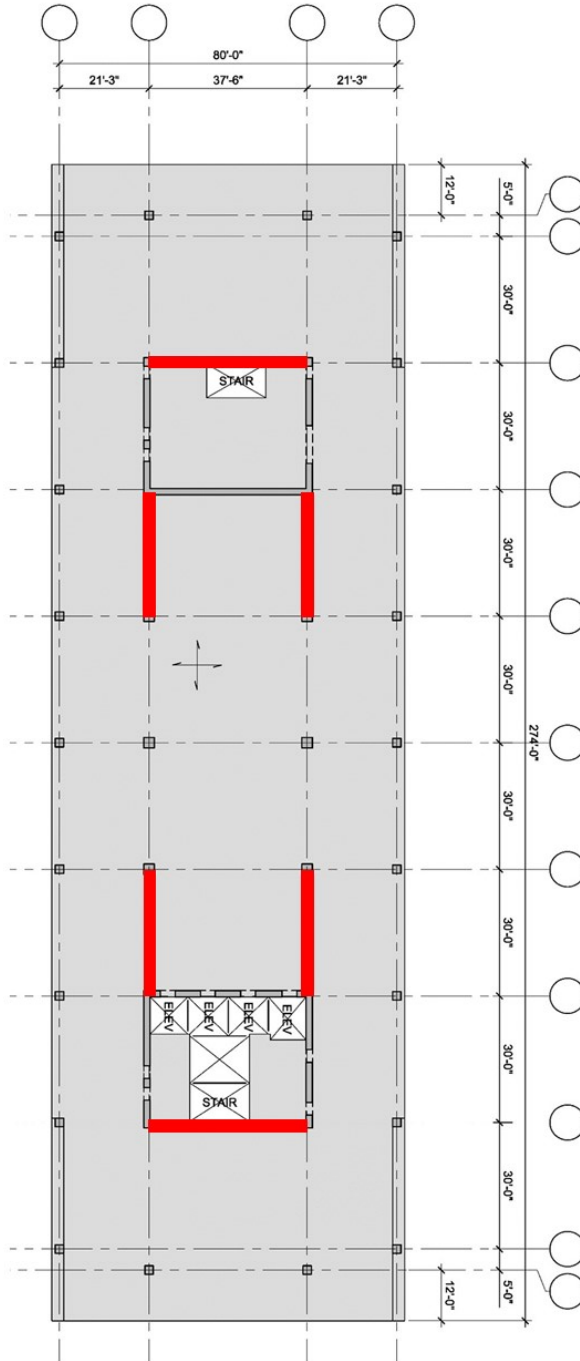
Figure 5.5: Proposed plan
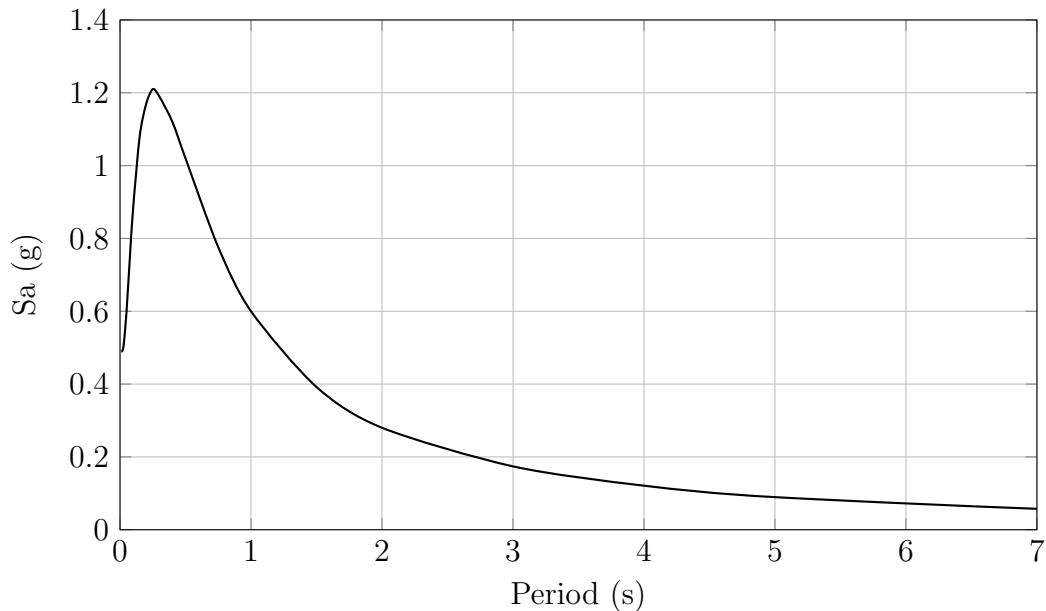
Figure 5.6: Site-Specific Response Spectrum

gation and one of the objectives was proposing a site-specific response spectrum for a better evaluation of the possible earthquake-induced loads which may be experienced by the considered building during its design life. Therefore, they have performed a Probabilistic Seismic Hazard Analyses (PSHA) and a Deterministic Seismic Hazard Analyses (DSHA) using the computer program EZ-FRISK (Risk Engineering, 2014) in order to develop site-specific response spectra in accordance with 2013 CBC and Chapter 21 of ASCE 7-10. In Fig. 5.6, it is possible to see the site-specific response spectrum used in the following analysis.

Finally, the following uniformly distributed loads have been considered at each level. The self-weight of the members is not listed because it is automatically computed by the software.

Table 5.1: Uniformly Distributed Loads

Load Name	Load Type	Value				
		USCS		SI		
Live Load	Typical Level LL	100	psf	4.8	kPa	
	Roof Level LL	150	psf	7.2	kPa	
	Partition	10	psf	0.48	kPa	
Superimpose Dead Load	Typical Level SDL	35	psf	1.7	kPa	
	Roof Level SDL	40	psf	1.9	kPa	

5.3   Wall Description

The considered wall runs parallel to the shorter side of the building (see
Fig 5.5). Since they are placed in a symmetric fashion and the torsional
effects are not considered in the present research, they are subjected to the
same actions during a seismic event. The wall is 162.5 ft (49.53 m) tall and
37.5 ft (11.43 m) wide. The effective seismic mass corresponds to half of the
mass of the building, since in that direction the lateral resistance is provided
by 2 wall placed symmetrically in plan. The gravity mass supported by
the considered wall corresponds to the sum of the weight of each floor level
corresponds to its tributary area. Thus, the effective seismic mass at each
floor level is the 50% of the total floor mass, while the tributary weight is
the 7.4% of it. As already said, the structural typology taken into account is
an unbonded post-tensioned concrete hybrid wall, whose material properties
are listed in Table 5.2.

The energy dissipation system combined with the wall system is com-
posed by mild reinforcement placed at the interface between the wall and
the foundation and debonded for a certain length inside the concrete.

Table 5.2: Material Properties

Material	Properties	Symbol	Value			
			USCS		SI	
	Nominal yield strength	f_y	60	ksi	414	MPa
Steel	Failure strength	f_{us}	90	ksi	621	MPa
	Modulus of elasticity	E_s	30458	ksi	210	GPa
Concrete	Nominal strength	f'_c	6	ksi	41.4	MPa
	Tensile strength	f_{upt}	270	ksi	1861.6	MPa
	Yield strength	f_{ypt}	245	ksi	1689	MPa
	Tendon diameter	d	0.5	in	13	mm
Tendon	Tendon area	A	0.153	in^2	98.7	mm^2
	Modulus of elasticity	E_p	28500	ksi	196.5	GPa
	Initial prestress	f_{se}	149.2	ksi	1028.5	MPa

5.4   Design Procedure

The wall has been designed with both the FBD and DDBD method. The two procedure applied to the wall are presented in the following sections.

5.4.1   Direct Displacement-Based Design

The design procedure computed with the DDBD takes into account the actual behavior of the structure. Once the design drift is set, the displacement profile along the wall follows its deformed shape. In the case study the wall behaves like a rigid block and it has to remain essentially elastic. For this reason, the profile displacement results to be linear along the height of the wall. The yield displacement reflects the high level of ductility provided by the wall that is also takes into account in the equivalent viscous damping defined for the specific hysteretic rule of the system.

Table 5.3: Design displacement at each level

Level	Height				Wall Displacement			
	USCS		SI		USCS		SI	
Top	162.5	ft	49.5	m	1.625	ft	0.495	m
Roof	158.0	ft	48.2	m	1.580	ft	0.482	m
11	142.0	ft	43.3	m	1.420	ft	0.433	m
10	129.0	ft	39.3	m	1.290	ft	0.393	m
9	116.0	ft	35.4	m	1.160	ft	0.354	m
8	103.0	ft	31.4	m	1.030	ft	0.314	m
7	90.0	ft	27.4	m	0.900	ft	0.274	m
6	77.0	ft	23.5	m	0.770	ft	0.235	m
5	64.0	ft	19.5	m	0.640	ft	0.195	m
4	51.0	ft	15.5	m	0.510	ft	0.155	m
3	38.0	ft	11.6	m	0.380	ft	0.116	m
1	0.0	ft	0.0	m	0.000	ft	0.000	m

Design Criteria Wall with unbonded prestressing will rarely be governed by strain limitations and thus the critical value is the drift at the top floor.

$$\theta_c = 0.01 \tag{5.1}$$

Design Displacement Since the design deformation is dominated by single crack at the base of the wall, the design displacement profile may be assumed to be linear along the height and it is defined through the 1% drift multiplied by the progressive height h_i corresponding to the height of each story level of the Civic Center.

$$\Delta_i = \theta_c h_i \tag{5.2}$$

The values are shown it Table 5.3.

Hence the design displacement results to be:

$$\Delta_d = \frac{\sum_{i=1}^{n}(m_i \Delta_i^2)}{\sum_{i=1}^{n}(m_i \Delta_i)} = 1.115 \, \text{ft} (0.400 \, \text{m}) \tag{5.3}$$

Yield Displacement The yield drift depends on the material sizes and structural geometry defined for the wall in

5.5 Wall Description

. It can be based on the stiffness of the uncracked wall section up the full height. For reinforced cantilever wall buildings, the maximum drift occurs at the top of the building and the yield drift can be defined through the following dimensionless yield curvature:

$$l_w \phi_y = 2.00 \epsilon_y \tag{5.4}$$

Assuming a linear distribution of curvature over the height, with $h_n = 162.5\,\text{ft}(49.53\,\text{m})$ and $l_w = 37.5\,\text{ft}(11.43\,\text{m})$, the yield drift at roof level results to be:

$$\theta_{yn} = \epsilon_y h_n / l_w = 0.0085 \tag{5.5}$$

Due to the high level of ductility provided by the system with mild reinforcement, the yield displacement of a prestressed wall can be assumed to be approximately of 40% of the one of a reinforced concrete wall. Hence, it results to be:

$$\theta_y = 0.4 \epsilon_y h_n / l_w = 0.0034 \tag{5.6}$$

Displacement Ductility Since the design displacement profile is almost linear, the displacement ductility can be approximated by:

$$\mu = \theta_c / \theta_y = 2.929 \tag{5.7}$$

Effective Mass The effective mass of the SDOF structure results from the consideration of the masses m_i computed at each floor level of the Civic

Center:

$$m_e = \sum_{i=1}^{n} \frac{m_i \Delta_i}{\Delta_d} = 21.95 \, \text{kip s}^2/\text{in}(3843.2 \, \text{ton}) \qquad (5.8)$$

Equivalent Viscous Damping The effective damping depends on the structural system and on the displacement ductility μ. As already said in Chapter 3, one of the key aspect for an efficient design of an hybrid wall is the proportioning between the yielding contribution, which is responsible for the energy dissipation of the system, and the self-centering contribution. This design criteria could be summarized as the ratio κ_d between the yielding components and the elastic restoring components. The value of this ratio determines the amount of dissipated energy and the re-centering ability of the system.

The nominal base moment strength of an unbonded post-tensioned hybrid wall can be seen as the sum of three components, M_{wn}, M_s and M_{pt}, representing respectively the contributions of applied axial loads, the wall mild steel reinforcement and PT tendons. Thus the parameter κ_d, proposed by Kurama and called "ED steel moment ratio" is defined as:

$$\kappa_d = \frac{M_s}{M_{pt} + M_{wn}} \qquad (5.9)$$

An appropriate value for κ_d should be selected for design. If the yielding contribution is too small (i.e., κ_d ratio is too small), then the system doesn't provide adequate energy dissipation. Conversely the self-centering capability of the wall may be too small and thus it may not be sufficient to close the gap opening at the base joints after the seismic event, if the κ_d ratio is too large. The values proposed for this parameter range from 0.50 to 0.80 to satisfy the required performances. The value selected in the present case is $\kappa_d = 0.75$.

The effective damping can be computed through the equation proposed by Priestley [16] for flag-shaped hysteresis, that for a generic value of κ_d and r (post-yield stiffness ratio) is given by:

$$\xi_{\text{area}} = \frac{E_{\text{hysteresis}}}{4\pi E_{\text{elastic}}} = \frac{\kappa_d(\mu - 1)}{\mu\pi(1 + r(\mu - 1))} \tag{5.10}$$

In Eq. 5.10 $E_{\text{hysteresis}}$ represents the energy dissipated and E_{elastic} represents the energy that would be stored in an equivalent purely elastic system without dissipation. These two quantities are represented in Fig. 5.7 respectively by the blue area and the red one.
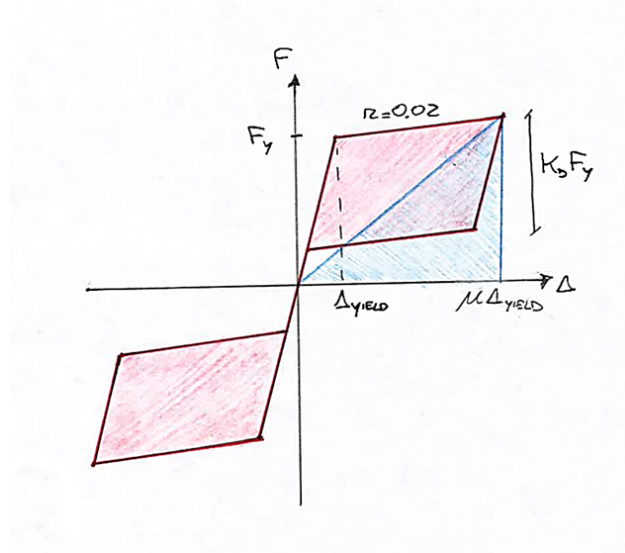
Figure 5.7: Idealized hysteretic damping calculation

The damping calculated from Eq. 5.10 has to be multiplied by the correction factor from Fig. 5.8 and has to be added to the elastic damping component. The estimate of EVD is established in [16] for hysteresis rules with specific characteristics. When the hysteresis rules have different characteristics than those presented by Priestley, the appropriate ductility/damping equations defined with inelastic time-history analysis (ITHA) have to be
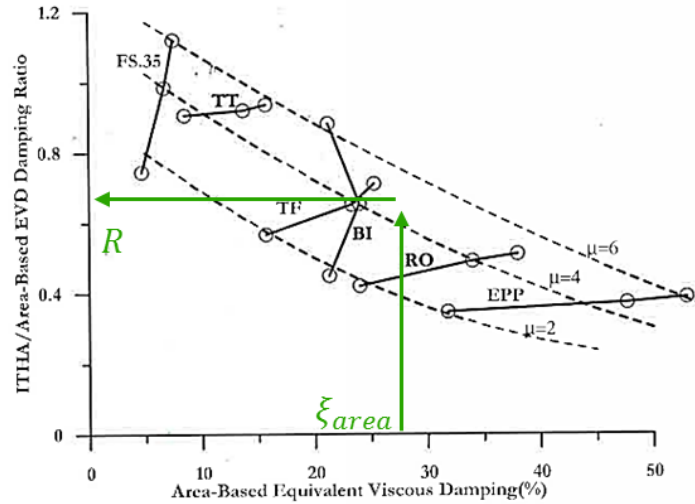
Fig.3.15:   Correction Factors to be Applied to Area-Based Equivalent Viscous
Damping Ratio (Eq.(3.10))

Figure 5.8: Correction factors to be applied to the area-based equivalent viscous
damping ratio, Priestley [16]

developed. Some correct estimates of the relationship can be obtained by
comparing the relationship between the area-based viscous damping, given
by Eq. 5.10 which can be computed for any system if the hysteretic compo-
nent is known, with the hysteretic component of viscous damping calculated
for specific level of displacement ductility. This relationship is plotted in
Fig. 5.8 for six hysteretic rules that are: elastic-perfectly plastic (EPP), bi-
linear (BI), Taketa Thin (TT), Taketa Fat (TF), Flag with $\kappa_d = 0.35$ (FS)
and Romberg-Osgood (RO).

The vertical axis is the ratio between the hysteretic component of the
equivalent viscous damping computed from ITHA and the area-based one
found from Eq. 5.10. This can be considered as an appropriate correction
factor to be applied to the area-based viscous damping and it can be com-
puted with Fig. 5.8 for a known level of displacement ductility. The three

data point are defined for each hysteresis rule for ductility levels of 2, 4 and 6. This approach represents a suitable alternative to estimate time-history analysis. In the present case the area-based EVD is $\xi_{\mathrm{area}} = 15.1\%$ and the displacement ductility is $\mu = 2.929$. Hence, this results in a correction factor $R = 0.65$.

Finally the elastic damping is estimated to be $\xi_{\mathrm{el}} = 0.05$ and thus the equivalent viscous damping results to be:

$$\xi_{\mathrm{eq}} = \xi_{\mathrm{el}} + R\xi_{\mathrm{area}} = 14.84\% \tag{5.11}$$

Design Displacement Spectra The design displacement spectrum is defined for the evaluated level of equivalent viscous damping. The displacement spectrum can be considered to be independent from the period after the corner period that can be evaluated from the moment magnitude. In the present case the corner period is computed to be $T_c = 4$ sec. The relative design displacement spectrum can be developed from the acceleration spectrum for 5 percent damping. Initially the elastic displacement spectrum is calculated and then it will be modified for the correct value of damping. The displacement spectrum for 5% of damping can be defined as:

$$\Delta_{(T,5)} = S_{(T,5)}\, g\, T^2/(4\pi^2) \tag{5.12}$$

The displacement spectra for the present level of ξ_{eq} results from:

$$\Delta_{(T,\xi_{\mathrm{eq}})} = \Delta_{(T,5)} \cdot \left(\frac{0.07}{0.02 + \xi}\right)^{0.5} \tag{5.13}$$

Both of them are represented in the graph in Fig. 5.9.

The design displacement spectrum at T_c results to be $\Delta_{(T_c,\xi)} = 15.2\,\mathrm{in}\,(0.386\,\mathrm{m})$.
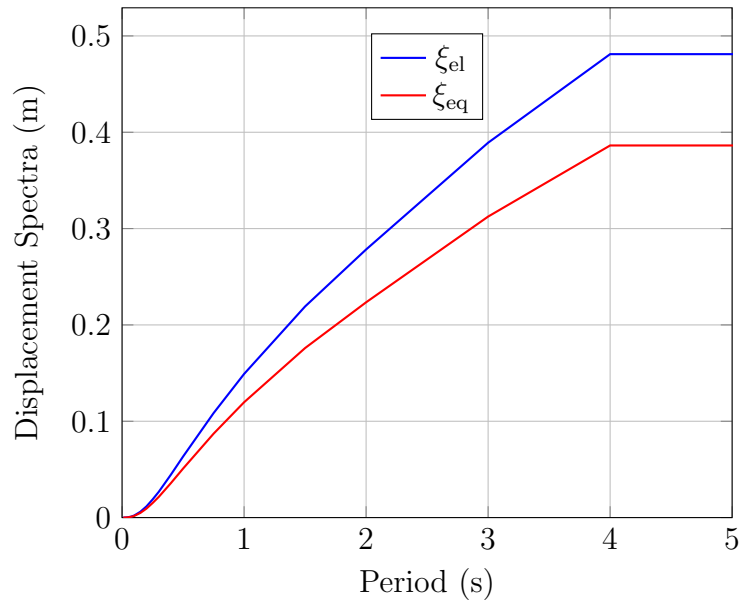
Figure 5.9: Response displacement spectra

Effective Period   The effective period corresponding to the design displacement can be found by proportion as:

$$T_e = T_c \cdot \frac{\Delta_d}{\Delta_{(T_c, \xi)}} = 3.52 \, \text{sec} \tag{5.14}$$

Effective Stiffness   The effective stiffness can be found by the effective mass and the effective period and it results to be:

$$K_e = \frac{4\pi^2 \, m_e}{T_e^2} = 69.97 \, \text{kip/in} \, (12\,254 \, \text{kN/m}) \tag{5.15}$$

Design Base Shear   The design shear at the base of the wall is defined through the design displacement and the effective stiffness. It is equal to:

$$F = V_{base} = K_e \, \Delta_d = 936 \, \text{kips} \, (4164 \, \text{kN}) \tag{5.16}$$

Moment Base Design   The evaluated base shear must be distributed as design force to the different lumped masses of the wall in proportion to their

value and displacement. In this way the design moments at plastic hinges location can be established. The design force at level i results to be:

$$F_i = V_{\text{base}} \cdot \frac{m_i \Delta_i}{\sum_{j=1}^{n}(m_j \Delta_j)} \tag{5.17}$$

The design moment at the base of the wall resulting from this distribution of forces is $M_{\text{base}} = 104.362 \, \text{kip ft} (141\,496 \, \text{kN m})$.

5.5.1 FBD Comparison

The design procedure for the unbonded post-tensioned hybrid wall has been computed also with the Force-Based Design method. The values considered a reduction factor $R = 5$, the deflector amplification factor $C_d = 5$ and importance factor $I = 1$, according to ASCE 7-10 standard. The forces resulting from FBD procedure are:

$$V_{wd} = 1939.4 \, \text{kips} \, (8627 \, \text{kN})$$

$$M_{wd} = 215\,833 \, \text{kips ft} \, (305\,424 \, \text{kN m})$$

$$N_{wd} = 2179 \, \text{kips} \, (9694.4 \, \text{kN})$$

These forces result to be much higher than those found with the DDBD method, except for the axial force that results from the tributary area of the considered wall and therefore it remains the same. In particular the base shear is around 50% higher than the one resulting from the DDBD methodology. This overestimation is compatible with the results of the PRESSS program, as shown in the previous Chapter. However, the analytical model of the wall designed with the forces of the DDBD method behave well, as proved through pushover analysis and inelastic time-history analysis proposed later. It is possible to see that the discrepancy between the methods results in a substantial increasing of required material.

5.6   Base Cross-Section Design

The design forces are the design shear $V_{wd} = 936\,\text{kips}$ (4164 kN), the design moment $M_{wd} = 104.362\,\text{kip\,ft}$(141 496 kN m) both defined in the previous section, and the value of gravity load defined through the tributary area of the wall. The value of gravity force is $N_{wd} = 2179.4\,\text{kips}$ (9694.4 kN). Once the design forces are know, the base cross-section can be designed establishing the required material quantities. This implies the definition of the amount of PT steel and ED steel, their location and the wall dimensions necessary to satisfy the wall design base forces. The wall section should have a symmetric layout and the ED and PT steel should be placed outside the confined regions at the wall toes. The analytical design procedure has been presented in Chapter 3. In this section its main aspects will be presented in order to compute the resulting material quantities.

Section Layout and Initial Assumptions   The PT tendons will be placed less eccentric than the ED bars in order to have higher deformation in the mild reinforcement than in the tendons. In the computations, the steel areas are considered lumped in two areas placed symmetrically respect to the centerline. The eccentricity of the PT tendons from the wall centerline is assumed to be $e_p = 3.28\,\text{ft}$ (1.00 m) and the one of the ED steel of $e_p = 6.56\,\text{ft}$ (2.00 m). Moreover, the initial assumption of the wall thickness is $t_w = 16\,\text{in}$ (0.41 m). The unbonded length of the PT tendons is equal to the wall height in order to distribute the strains and keep the tendons in the elastic field.

Steel Quantities Since lumped steel areas are considered in the present case, the governing equilibrium equations at the base cross section are:

$$C_d = 0.85 \, f'_c \, t_w \, \beta_1 \, x_n \tag{5.18}$$

$$C_d = N_{wd} + 2A_s \sigma_{s,m} + 2A_{pt}\sigma_{pt,m} \tag{5.19}$$

$$\frac{M_{wd}}{\phi_f} = C_d \left(\frac{l_w}{2} - \beta_1 \frac{x_n}{2} \right) \tag{5.20}$$

The design is made without iterations and the neutral axis x_n is solved directly from Eqs. (5.18) and (5.20). The steel areas are computed using Eqs. (5.19) and (5.9), after the definition of their relative strains and stresses. From the value of the neutral axis length the ED steel and PT steel elongations can be computed using the displaced configuration and the selected location of the bars (e_s) and tendons (e_p) from the wall centerline. The determination of these elongations is not based on compatibility but on kinematic. In fact when the gap opens at the base, the PT steel and the ED steel are debonded to the concrete and therefore the hypothesis of perfect adherence between steel and concrete is no more valid. It is necessary to use kinematic considerations due to base section rotation, that creates an elongation of the debonded mild reinforcement and of the unbonded PT steel. Then the stresses $\sigma_{s,l}$, $\sigma_{s,r}$ and $\sigma_{pt,m}$ are calculated with the selected unbonded length $(l_s$ and $l_{pt})$ and the selected stress-strain relationship. The required A_{pt} and A_s can be found by solving Eqs. (5.19) and (5.9) for the assigned value of κ_d. In the present research the stresses of the ED steel lumped areas have been assumed equal to the yield stress f_y and the bedonding length is then calculated as the minimum length that assure the yield elongation in the ED steel for the calculated neutral axis.

The resulting neutral axis and l_s will be:

$$x_n = 10.9 \, \text{ft} \, (3.334 \, \text{m})$$

$$l_s = 7.5\,\text{ft}\,(2.275\,\text{m})$$

The required value of A_{pt} and the respective number of tendons n_{pt} at each side results to be:

$$A_{pt} = 7.19\,\text{in}^2(4639\,\text{mm}^2)$$

$$n_{pt} = 47$$

The required value of A_s and the respective number of rebar n_s (#10 according to American standards, corresponding to a nominal diameter of 1.27 in, so 32.3 mm) at each side result to be:

$$A_s = 29.21\,\text{in}^2(18\,845\,\text{mm}^2)$$

$$n_s = 23\,\#10$$

Design Check Part of the design objectives is that, under the design level of ground motion, the PT steel remains in the linear-elastic range and that the ED steel yields during the seismic event. It is possible to verify these requirements computing the elongation and the stress level in the steel. Regarding the PT tendons, the strain and stress level has to be lower than the yielding one. On the other hand, it has to be proved that the strain and stress in the ED steel are higher than the yielding level.

In the present work the respective values of stress and strain for the two materials have been computed for their established length of debonding. It has been verified that their values respect the required limits.

An other objective is to assure that shear slip at the base horizontal joint does not occur. It is considered to be satisfied for the design earthquake but it has to be verified for the maximum considered earthquake, that is not take into consideration the present work. For this check and for the other requirement necessary to satisfy the design goals it is possible to refer to

Kurama's prescriptions [23]. Also the design of the confinement of the base cross-section can be determined referring to [23]. The confinement of the wall base is fundamental in order to have the non-linearity primarily dues to gap opening at the base and in the concrete in compression only at the wall toes.

Moreover, the direct displacement-based design method requires that the estimated hysteretic damping (computed with Eq. (5.11)) has to be compared with the energy dissipated by the structure per load cycle. It will be discussed later, in Sec.5.7.

5.7 Analytical Validation of the DDBD procedure

Once the design of the lateral load resisting system has been performed, the results must be validated. Since there is not the possibility to create a test building in order to simulate the response of the designed wall under a ground motion, an analytical model has been developed. The unbonded post-tensioned hybrid concrete wall is modeled following the procedure developed at Chapter 4. The only difference with the jointed walls is the energy dissipation device, here obtained thanks to mild reinforcement which is debonded at the base in order to allows its yielding when the earthquake occurs. In the present research the ED steel has been modeled is a similar way as the post-tensioned tendons. In fact the relative lumped areas used in the design have been modeled as link elements at the base of the wall and placed in the actual location of the designed base section. With respect to the u-shaped flexural plates, the present energy dissipation device has a well known hysteretic function and its nonlinear behavior could be assumed as
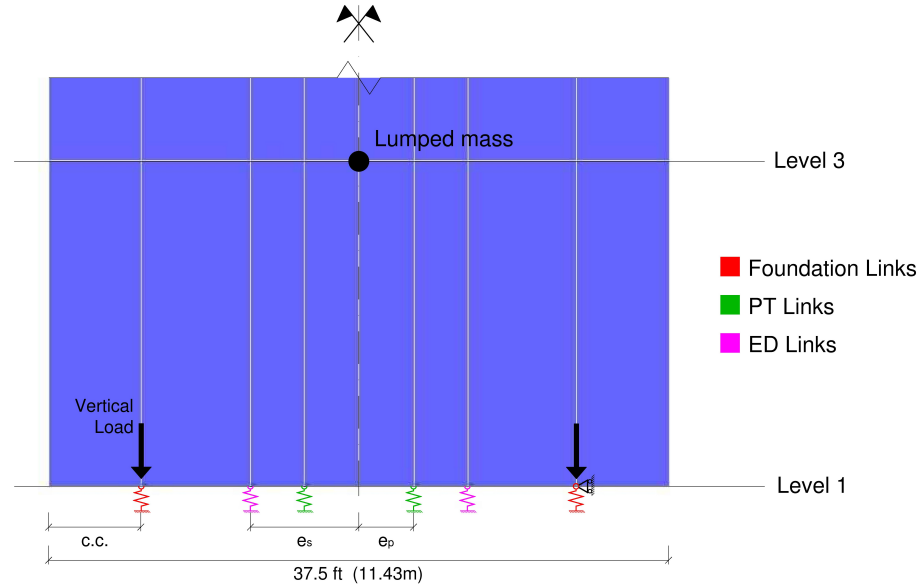
Figure 5.10: Wall base layout of the model of a hybrid wall

elastic-perfectly plastic. In a similar way of what did for the PT links, the stiffness of the ED links is:

$$k_{ED} = \frac{E_s A_s}{l_s} \qquad (5.21)$$

where E_s is the modulus of elasticity of the mild steel, A_s is the lumped areas of the link under consideration and l_s is its debonded length.

The yielding force $F_{y,ED}$ is calculated as the product of the yield stress f_s and the ED steel area A_s.

See Fig. 5.10 for the base layout of the unbonded post-tensioned hybrid wall developed in ETABS 2015.

The characteristics of all the elements that compose the analytical model are summarized in Table 5.4. Their definition follows the modeling assumptions developed in Chapter 4. The stiffness of the foundation links is 10 times higher that the one proposed in the PRESSS research program. This

Table 5.4: ETABS Model - Properties of the Components

Component	Property	Value			
		USCS		SI	
Wall Member	Elastic Mod. E_c	3605	ksi	24.855	GPa
	center of compr.	48.23	in	1.225	m
Found. Links	Stiffness k_{FL}	100 000	kip/in	17 512 684	kN/m
	Yield Force $F_{y,fl\,C}$	10 000	kips	44 482	kN
	Yield Force $F_{y,fl\,T}$	0.1	kips	0.45	kN
PT Links	Stiffness k_{PT}	2828.1	kip/in	15 393.5	kN/m
	Post-Yield Ratio	0.02		0.02	
	Yield Force $F_{y,pt\,T}$	576.91	kips	2566.24	kN
	Yield Force $F_{y,pt\,C}$	2371.23	kips	10 547.76	kN
ED Links	Stiffness k_{ED}	381 708	kip/in	2 077 679	kN/m
	Yield Force $F_{y,ED}$	1564.25	kips	6958.15	kN

value has been decided in order to minimize the initial shortening of the links due to the prestressing force. A better evaluation should be preferred in a further study and its influence in the global response of the structure could be part of a future development of the present research. The yielding force in compression of these links has been calibrated in order that they remain in the elastic range when the design top displacement is applied to the wall system.

As for the masses, the forces applied to the structure when the design earthquake occurs, the vertical loads are modeled as concentrated forces applied on the foundation links. They are symmetric and worth 1987 kips (8838 kN), calculated as half of the sum of the initial prestress equal to 1794 kips (7982 kN) and the axial force acting on the wall, equal to 2178 kips (9694 kN). Effective seismic mass at each level instead is modeled as lumped masses at the centerline of the wall and they work only in the horizontal direction and not in the vertical one. The nodes in correspondence with the
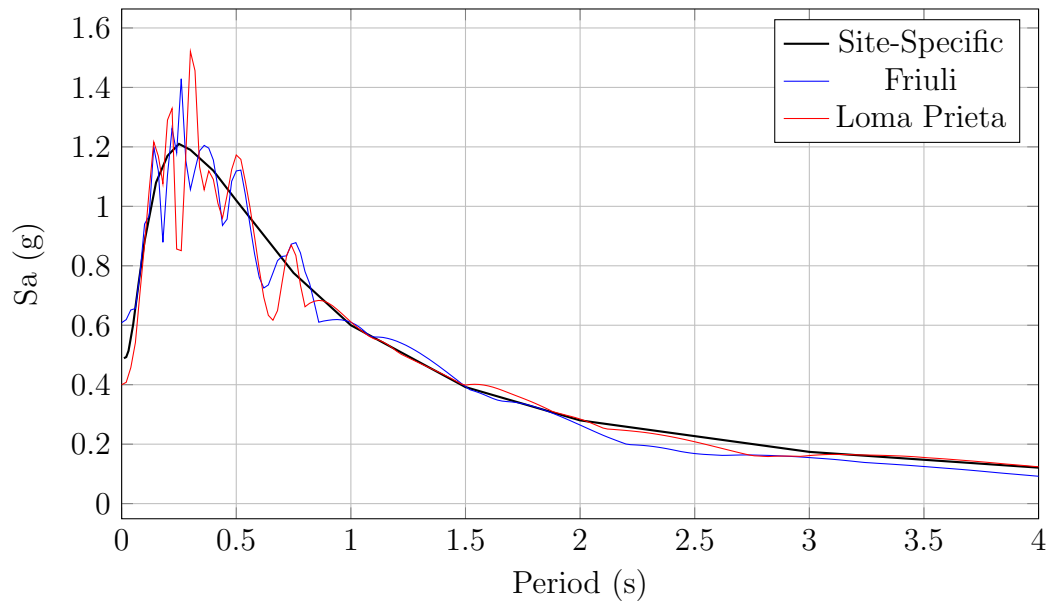
Figure 5.11: Response spectra comparison

foundation link on the right of the wall is laterally fixed, in order to avoid shear slip.

Regarding the dynamic nonlinear analysis, *Seismomatch* software has been used in order to determine ground motions that are compatible with the site-specific response spectrum, as in Chapter 4. The 2 accelerograms that better converge are the Friuli (1976)record and the Loma Prieta, California (1989) record. Their spectrum compatible ground motions are presented in Fig. 5.12, while Fig. 5.11 shows their matched response spectra in comparison with the target one.
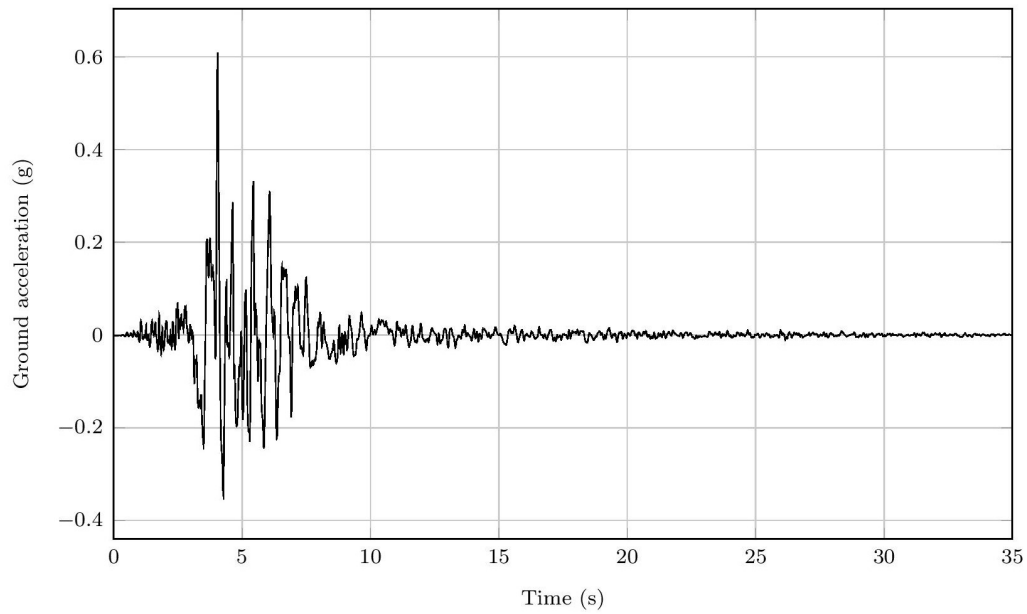
(a) Friuli
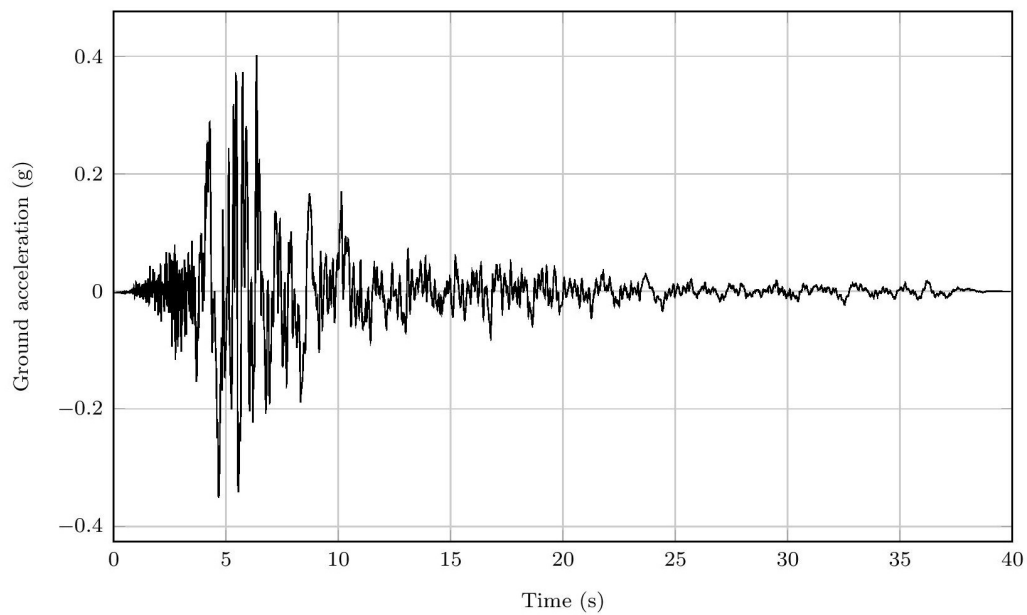
(b) Loma Prieta

Figure 5.12: Case study, response spectrum compatible time histories

5.7.1 Damping Validation

The hysteretic damping calculated during the DDBD procedure has to be compared with the energy dissipated by the structure per load cycle. The energy dissipated by the lateral resisting system under lateral loads can be determined with a cyclic pushover analysis. As in Chapter 4, the 3 subsequent nonlinear static analysis have been run controlling the top displacement: firstly till the design displacement, then back till the design displacement in the opposite direction and finally to the initial undeformed configuration. Fig. 5.13 shows on blue the result of the cyclic pushover analysis, highlighting also the area enclosed by the curve, which describes the energy dissipated by the structure. The green area instead represents the equivalent elastic strain energy. From the graph it results $\xi_{\text{hyst}} = 14.76\%$, that summed with the 5% elastic damping consists in an equivalent viscous damping much higher that the 14.84% theoretically computed.
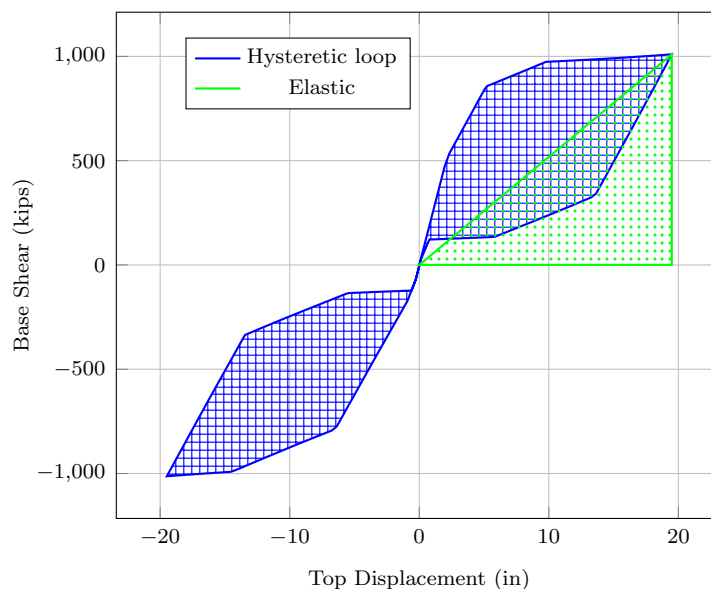
Figure 5.13: Case study, full cycle hysteresis loop, first iteration

Further iterations are therefore required. The computed hysteretic damping is used for the calculation of the forces acting on the unbonded post-tensioned hybrid wall and so in the definition of the material quantities, following all the steps presented in the previous sections. This procedure must be repeat till convergence of the hysteretic viscous damping. The final quantities are listed below, corresponding to an hysteretic damping coefficient of 12.9%. The concentrated vertical load at the center of compressions is equal to 1934 kips (8603.6 kN).

The base design forces are:

Base Shear V_{wd}: 861 kips (3829 kN)

Base Moment M_{wd}: 1 103 490 kip in (130 129 kN m)

Base Axial Load N_{wd}: 2179.4 kips (9694.4 kN)

Table 5.5: Material Quantities

		USCS		SI	
PT Tendons	A_{pt}	5.66	in²	3652	mm²
	n_{pt}	37		37	
ED Steel	A_s	26	in²	16 774	mm²
	n_s	20	#10	20	#10
	l_s	13.25	ft	4.04	m

Using those parameters of the single components in the analytical model, the computed hysteretic viscous damping is 12.45%, coherent with the 12.7% used for the design. Fig. 5.14 shows the relative hysteretic loop. Prediction results described in subsequent sections have been obtained from the analytical model with the quantities presented above. In Fig. 5.14 it is possible to see the perfect flag-shaped hysteretic loop of the designed unbonded post-

Table 5.6: ETABS Model - Properties of the Components

Component	Property	Value			
		USCS		SI	
Wall Member	Elastic Mod. E_c	3605	ksi	24.855	GPa
	center of compr.	43.11	in	1.095	m
Found. Links	Stiffness k_{FL}	100 000	kip/in	17 512 684	kN/m
	Yield Force $F_{y,fl\,C}$	10 000	kips	44 482	kN
	Yield Force $F_{y,fl\,T}$	0.1	kips	0.45	kN
PT Links	Stiffness k_{PT}	82.74	kip/in	14 489.6	kN/m
	Post-Yield Ratio	0.02		0.02	
	Yield Force $F_{y,pt\,T}$	543.04	kips	2415.55	kN
	Yield Force $F_{y,pt\,C}$	2231.99	kips	9928.40	kN
ED Links	Stiffness k_{ED}	4969.31	kip/in	872 753.4	kN/m
	Yield Force $F_{y,ED}$	1560.06	kips	6939.47	kN

tensioned hybrid wall. This is in line with the expected behavior studied in Chapter 3.
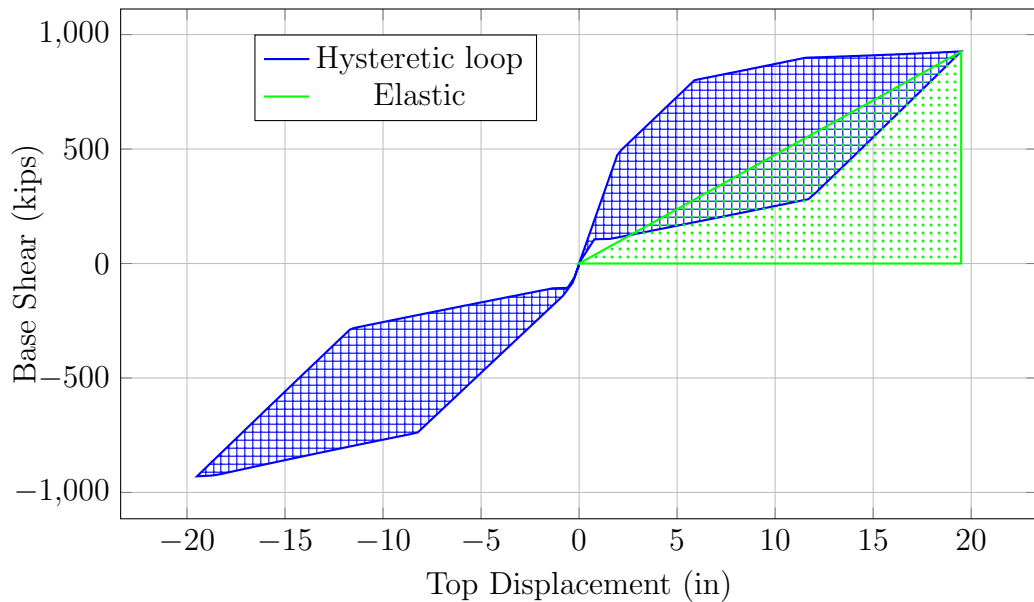
Figure 5.14: Case study, full cycle hysteresis loop, final iteration

5.7.2   Pushover Results

A nonlinear static analysis was carried out in order to show the expected structural behavior of the proposed unbonded post-tensioned hybrid wall under lateral loads. It has been performed controlling the displacement of the top level and considering an inverse triangular distribution of lateral forces over the height of the wall. It is coherent with the DDBD design procedure, that admits a linear profile of the wall displacements. The resulting base moment-top displacement relationship in shown in Fig. 5.15. The change in the structure stiffness here is more pronounced than seen for the PRESSS test building. This is due to the different hysteretic behavior of the energy dissipation device, here presented by mild steel that has been modeled with a sharp discontinuity in the stress-strain response. So at the first point the wall starts uplift, while the second and third points concern the first yield of the ED links, the left and the right one respectively. The PT tendons are not expected to yield within the 30 inches displacement limit considered in the graph, assuring an elastic behavior in the practical applications and therefore providing re-centering capability to the structure.

5.7.3   Results From Time Histories Analysis

Time histories analysis has been run in order to see the dynamic behavior of the lateral resisting system considered during a simulated earthquake. Friuli and Loma Prieta records has been used, as previously described. Fig. 5.16 shows the first 25 seconds of the behavior in time of the wall in terms of floor displacement. Level 3, 6 10 and the top level have been considered. The maximum displacement during the Loma Prieta earthquake is 16 in (407 mm) and during the Friuli earthquake is 13.62 in (346 mm). The target displacement
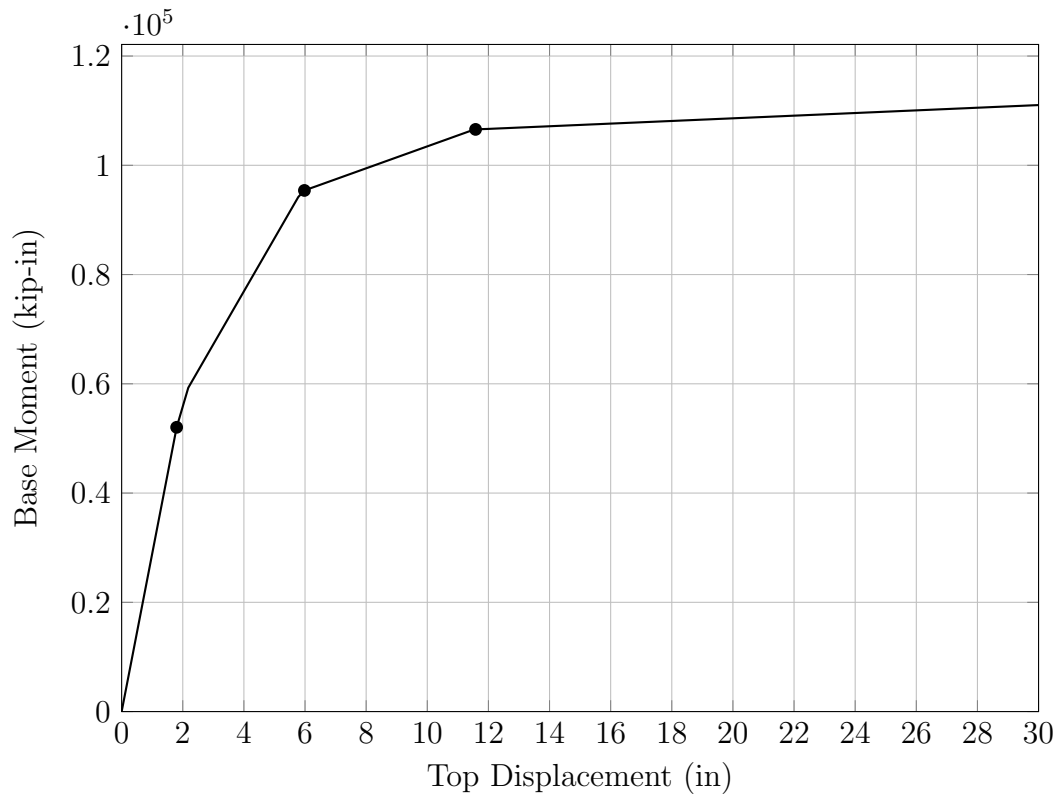
Figure 5.15: Case study, Base moment-Top displacement relationship, pushover results

considered in the design was 19.49 in (495 mm), so the predicted response is lower than the target one. Moreover, the force-displacement relationships of the different links show that the PT links remain in the elastic range and the ED links yield, providing self-centering capacity and energy dissipation, respectively. Fig. 5.17 shows the nonlinear response of those components under the Loma Prieta ground acceleration, together with the response of the foundation links, which work only in compression.

Finally, the time histories analysis show that the lateral resisting system comes back to the undeformed configuration after the earthquake occurs. In fact after 60 sec the horizontal displacement of the roof level is around

0.118 in (3 mm) during the Loma Prieta ground motion and 0.079 in (2 mm) during the Friuli ground motion.
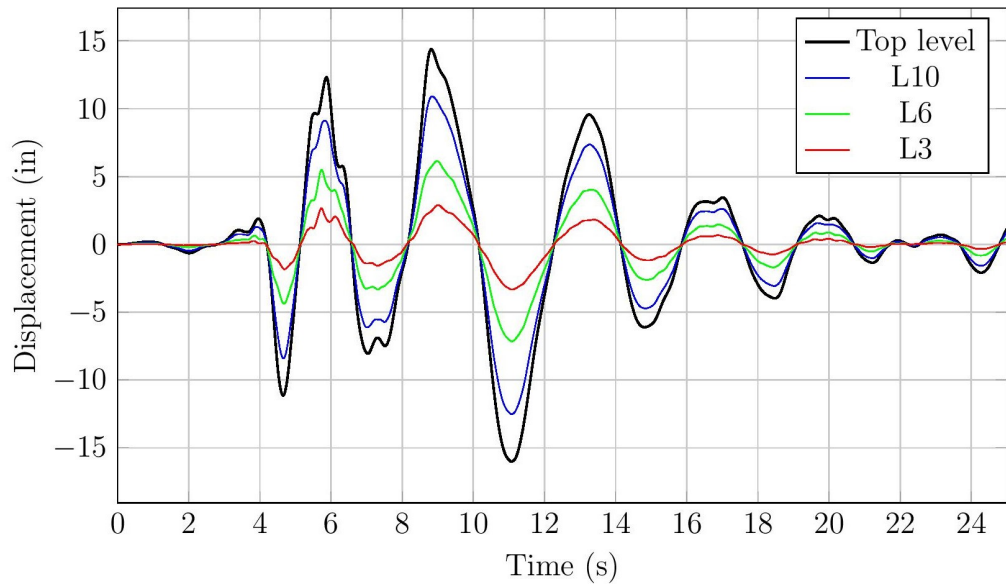
(a) *Loma Prieta Ground Motion*
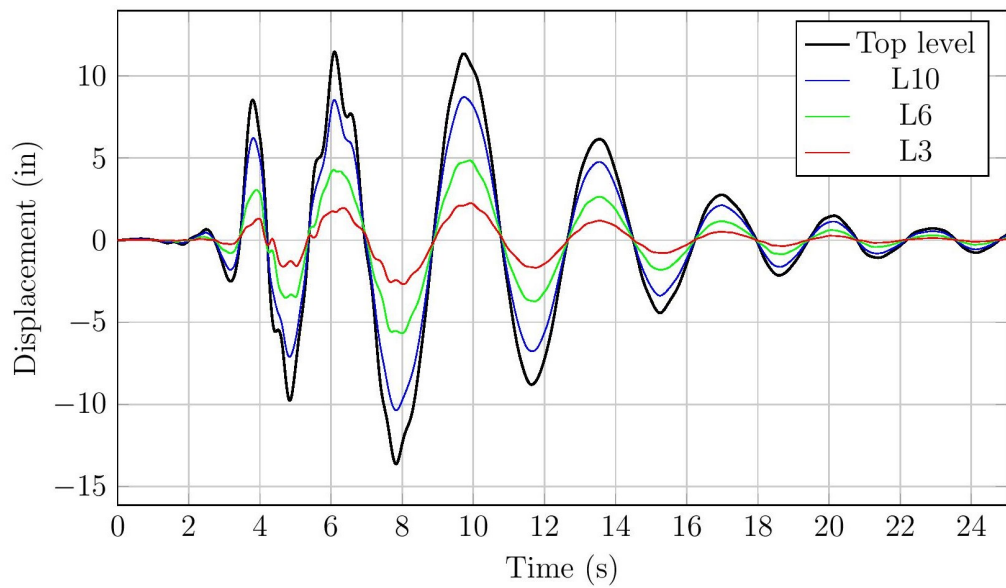
(b) *Friuli Ground Motion*

Figure 5.16: Floor Displacements time histories
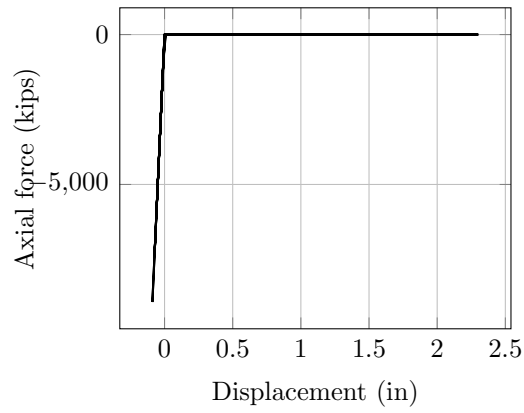
(a) Foundation Link
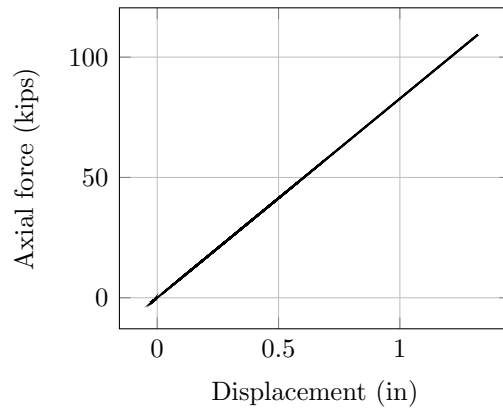
(b) PT Link
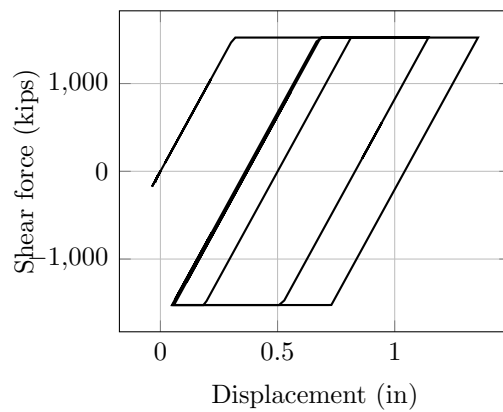
(c) ED Link

Figure 5.17: Force-displacement relationships for different link elements under the Loma Prieta ground acceleration

5.8 Comparison with a Conventional Reinforced Concrete Wall

The design procedure has been performed for the case of a conventional concrete wall too. The forces found from the DDBD and FBD methods were used to design the monolithic wall, which was then validated through inelastic time-history analysis. The purpose of this exercise is to highlight the advantages that come from the use of an unbonded post-tensioned hybrid wall. Moreover, the application of the DDBD procedure to a well known structure allows us to better understand the method and validate what it has been done for a particular lateral resisting system.

The geometrical dimensions of the wall are the same considered previously as well as the seismic mass and gravity loads, except for the wall thickness, that must be to increased to 26 in (660 mm), in order to provide the required strength. Concerning the material properties, for a cantilever concrete wall the material strengths considered are the expected one. This is due to the fact that the method considers the expected behavior of the wall identifying the location of predicted plastic hinge at the base. Since the material strength normally considered in the computations represents a conservative estimate, in the case that the strength exceeds the design values, the resisting moment developed at the plastic hinge will be greater than the design value. For this reason it is recommended to use the expected strength rather than the nominal one.

For a cantilever concrete wall the DDBD method considers the expected behavior of the wall identifying at the base the location of a predicted plastic hinge. The material strength normally considered in the computations represents a conservative estimate, so if the real strength exceeds the nominal one,

Table 5.7: Material Properties for a Cantilever Concrete Wall

Material	Properties	Symbol	Value USCS		SI	
Steel	Nominal yield strength	f_y	60	ksi	414	MPa
	Expected yield strength	$1.1\,f_y$	66	ksi	455	MPa
	Failure strength	f_{us}	90	ksi	621	MPa
	Modulus of elasticity	E_s	30458	ksi	210	GPa
Concrete	Nominal strength	f'_c	6	ksi	41.4	MPa
	Nominal strength	$1.3f'_c$	7.8	ksi	53.8	MPa

the resisting moment developed at the plastic hinge location will be greater than the design value. This means that maybe the plastic hinge does not occur in the predicted location, but somewhere else that was not designed for that. For this reason it is recommended to use the expected strength rather than the nominal one in the DDBD method. The material properties taken into consideration are listed in Table. 5.7.

5.8.1 DDBD Procedure

The DDBD procedure for a conventional reinforced concrete wall is presented below, following what already presented in Chapter 2.

Design Criteria The critical parameters for monolithic concrete walls remains the drift at the top level. Thus the design drift is defined according to ASCE 7-10, thus:

$$\theta_c = 0.01 \tag{5.22}$$

Design Displacement The design displacement profile follows the deformed shape of the wall. Since the design in governed by the code drift

Table 5.8: Wall Displacement for a Cantilever Concrete Wall

Level	Height USCS		SI		Wall Displacement USCS		SI	
Top	162.5	ft	49.5	m	1.116	ft	0.340	m
Roof	158.0	ft	48.2	m	1.071	ft	0.326	m
11	142.0	ft	43.3	m	0.912	ft	0.278	m
10	129.0	ft	39.3	m	0.785	ft	0.239	m
9	116.0	ft	35.4	m	0.663	ft	0.202	m
8	103.0	ft	31.4	m	0.546	ft	0.166	m
7	90.0	ft	27.4	m	0.436	ft	0.133	m
6	77.0	ft	23.5	m	0.335	ft	0.102	m
5	64.0	ft	19.5	m	0.244	ft	0.074	m
4	51.0	ft	15.5	m	0.165	ft	0.050	m
3	38.0	ft	11.6	m	0.100	ft	0.030	m
1	0.0	ft	0.0	m	0.000	ft	0.000	m

limit, the design displacement at each level can be evaluated thanks to:

$$\Delta_i = \Delta_{y_i} + (\theta_c - \theta_{yn})H_i = \frac{\varepsilon_y}{l_w} H_i^2 \left(1 - \frac{H_i}{3H_n}\right) + \left(\theta_c - \frac{\varepsilon_y H_n}{l_w}\right) H_i \quad (5.23)$$

In order to evaluate this profile, it is necessary to define the yield drift at roof level, that results to be:

$$\theta_{yn} = \epsilon_y h_n / l_w = 0.0094 \quad (5.24)$$

The values are listed it Table 5.8.

Hence the design displacement results to be:

$$\Delta_d = \frac{\sum_{i=1}^{n}(m_i \Delta_i^2)}{\sum_{i=1}^{n}(m_i \Delta_i)} = 0.709 \, \text{ft}(0.216 \, \text{m}) \quad (5.25)$$

Yield Displacement   The yield displacement of the SDOF substitute structure is determined at its effective height H_e. So:

$$H_e = \frac{\sum_{i=1}^{n}(m_i \Delta_i H_i)}{\sum_{i=1}^{n}(m_i \Delta_i)} = 118.9 \, \text{ft}(36.24 \, \text{m}) \quad (5.26)$$

$$\Delta_y = \frac{\varepsilon_y}{l_w} H_e^2 \left(1 - \frac{H_e}{3H_n}\right) = 0.618 \, \text{ft}(0.188 \, \text{m}) \quad (5.27)$$

Displacement Ductility The displacement ductility factor is:

$$\mu = \Delta_d/\Delta_y = 1.15 \tag{5.28}$$

Effective Mass The effective mass of the SDOF structure comes from consideration on the participating mass of the first inelastic mode:

$$m_e = \sum_{i=1}^{n} \frac{m_i \Delta_i}{\Delta_d} = \text{kip s}^2/\text{in} (3647.3\,\text{ton}) \tag{5.29}$$

Equivalent Viscous Damping The equivalent viscous damping coefficient ξ_{eq} can be defined through:

$$\xi_{\text{eq}} = 0.05 + 0.444 \left(\frac{\mu - 1}{\mu \pi} \right) = 6.81\% \tag{5.30}$$

Design Displacement Spectra The design displacement spectrum is defined for the evaluated level of equivalent viscous damping in the same way of the previous case. Thus, the corner period is computed to be $T_c = 4$ sec and the displacement spectrum can be developed from the acceleration spectrum for 5 percent damping through Eq. 5.12 and Eq. 5.13. They are represented in Fig. 5.18.

The design displacement spectrum at T_c results to be $\Delta_{(T,\xi)} = 0.454\,\text{m}$.

Effective Period The effective period corresponding to the design displacement can be found by proportion as:

$$T_e = T_c \cdot \frac{\Delta_d}{\Delta_{(T_c,\xi)}} = 1.90\,\text{sec} \tag{5.31}$$

Effective Stiffness The effective stiffness can be evaluated from the effective mass and the effective period, thus:

$$K_e = \frac{4\pi^2 m_e}{T_e^2} = 226.28\,\text{kip/in}\,(39\,741\,\text{kN/m}) \tag{5.32}$$
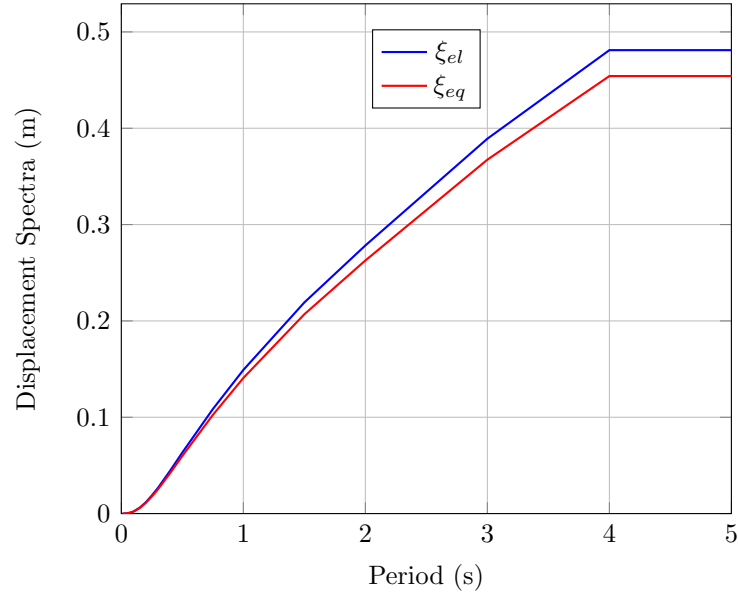
Figure 5.18: Response displacement spectra

Design Base Shear   The design base shear is defined through the design displacement and the effective stiffness. It is equal to:

$$F = V_{\text{base}} = K_e \, \Delta_d = 1931 \, \text{kips} \, (8589 \, \text{kN}) \tag{5.33}$$

Moment Base Design   The design force at level i results to be:

$$F_i = V_{\text{base}} \cdot \frac{m_i \Delta_i}{\sum_{j=1}^{n} (m_j \Delta_j)} \tag{5.34}$$

The design moment at the base of the wall resulting from this distribution of forces is $M_{\text{base}} = 229\,575 \, \text{kip ft} \, (311\,263 \, \text{kN m})$.

5.8.2   Capacity Design for Cantilever Walls

According to Chapter 2, the forces for the wall design result from considering an amplification that takes into account an overstrength factor and the dynamic influence of higher mode of vibration. The overstrength moment at
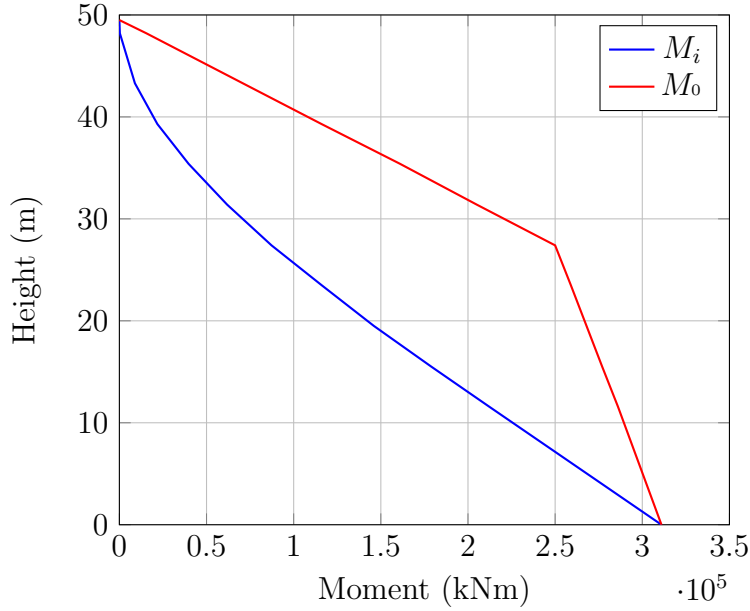
Figure 5.19: Amplified moment along the height

mid-height $M^0_{0.5Hn}$ is found from the overstrength base moment, $\phi^0 M_{\text{base}}$, by the relationship:

$$M^0_{0.5Hn} = C_{1,T}\,\phi^0\,M_{\text{base}} = 185\,919\,\text{kip ft}\,(252\,073\,\text{kN m}) \tag{5.35}$$

where $C_{1,T}$ is equal to:

$$C_{1,T} = 0.4 + 0.075\,T_i\left(\frac{\mu}{\phi^0} - 1\right) = 0.421 \geq 0.4 \tag{5.36}$$

The overstrength factor used for the moment calculation is $\phi^0 = 1$ and the initial (elastic) cracked-section period of the structure $T_i = 1.909\,\text{sec}$. The resulting profile of the amplified moment along the height is shown in Fig. 5.19.

The envelope of the shear force capacity-design is defined by a straight line that goes from the base to the top of the wall. The design base shear is evaluated through the following equation:

$$V^0_{\text{base}} = \phi^0\,\omega_V\,V_{\text{base}} = 3810.83\,\text{kips}\,(16\,951.4\,\text{kN}) \tag{5.37}$$

where ω_V is the dynamic amplification factor defined as:

$$\omega_V = 1 + \frac{\mu}{\phi^0}\, C_{2,T} = 1.579 \tag{5.38}$$

and $C_{2,T} = 0.067 + 0.4(T_i - 0.5) = 0.631 \le 1.15$

The overstrength factor ϕ^0 used for the shear calculation was found computing moment curvature analysis, that was performed thanks to S-CONCRETE software (S-FRAME Sofware Inc.), a software that executes code checks of reinforced concrete beams, columns and walls with code. Moreover, this software incorporates seismic design and ductility provisions. Through these analysis it has been possible to evaluate the value of the moment at the design curvature. The design curvature is:

$$\phi_{des} = \phi_{\text{yield}} + \phi_{\text{plastic}} = 0.001\,906\,\text{rad/m} \tag{5.39}$$

The overstrength factor is the ratio between the moment at ϕ_{des} found with the analysis taking into account the material overstrength $M_{\text{overstrength}}$, i.e considering the $1.7\,f'_c$ for the concrete and $1.3\,f_y$ for the steel, and the moment at ϕ_{des} with the nominal design strength of the materials M_{design}. The resulting value of the overstrength factor is $\phi^0 = 1.25$. The value of $M_{\text{overstrength}}$ and M_{design} can be determined following what illustrated in Fig. 5.20.

Once the design base shear is computed, the design shear force at the top of the wall is:

$$V_n^0 = C_3\, V_{base}^0 = 5545.4\,\text{kN} \tag{5.40}$$

where $C_3 = 0.9 - 0.3\,T_i = 0.327 \ge 0.3$ The resulting profile of the shear force along the height of the wall is shown in Fig. 5.21.

(a)   (b)
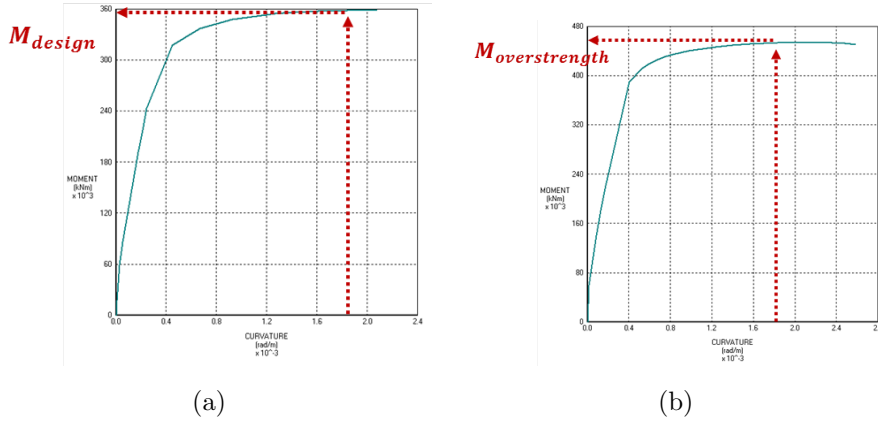
Figure 5.20: Moment curvature analysis: **(a)** nominal strength, **(b)** overstrength

5.8.3   Cross-Sections Design and Comparison with FBD

Once the design base forces are known, it is possible to design the section. The cross-section was designed with the software S-CONCRETE. The required thickness of the base cross-section results to be $t_w = 28\,\text{in}\,(0.71\,\text{m})$ and the reinforcement ratio is $\rho = 1.15\%$. The design was developed using the FBD method considering $R = 5$, $C_d = 5$, and $\Omega_0 = 2.5$. The forces resulting from FBD procedure are:

$$V_{wd} = 2198\,\text{kips}\,(9778\,\text{kN})$$

$$M_{wd} = 255\,315\,\text{kips ft}\,(346\,161\,\text{kN m})$$

$$N_{wd} = 2179\,\text{kips}\,(9694.4\,\text{kN})$$

Considering the same wall thickness at the base of $t_w = 28\,\text{in}\,(0.71\,\text{m})$, the required reinforcement ratio is $\rho = 1.21\%$.

The comparison with the Force-Based Design method was conducted also designing the upper sections. The average of steel percentage in the upper sections with the DDBD is $\rho = 0.85\%$ and with the FBD is $\rho = 0.45\%$.

In conclusion, it can be seen that at the base the DDBD forces results in an amount of steel lower at the base than that found with the FBD forces.
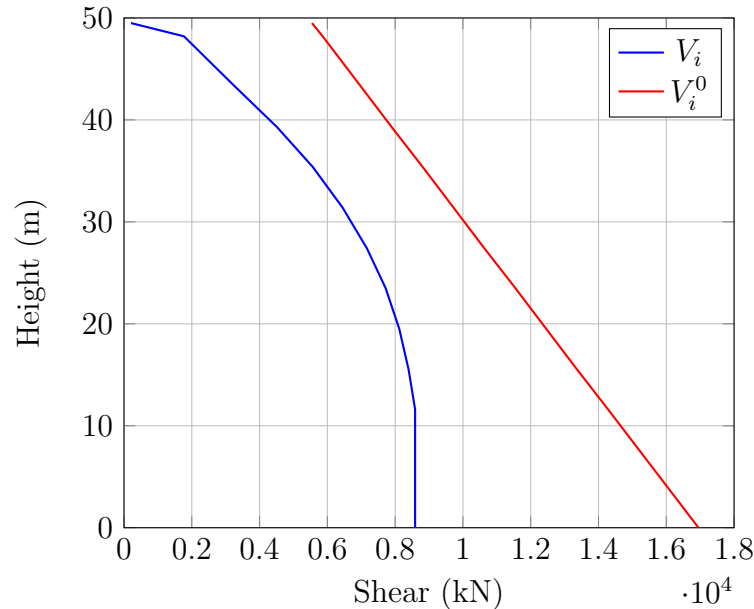
Figure 5.21: Amplified shear along the height

Whereas, the steel quantity determined by the DDBD forces in the upper sections is higher in comparison with the one determined with the FBD forces. This is in line with the fact that the DDBD method identifies the location on the plastic hinge at the base of the wall ensuring there an high level of displacement ductility and increase the force level in the other sections in order to avoid plastic hinges formation in undesired places. These results highlight the differences of the two methods: the FBD method comes from the general consideration for concrete structure, while the DDBD method considers the expected behavior of the structure, thank to experimental studies. Moreover, the application of the DDBD method to a conventional cantilever concrete wall is useful in order to well understand and validate the modification done in order to make it suitable for the case of an enhanced wall.

The unbonded post-tensioned hybrid wall allow to reduce the structural dimensions, if compared to a monolithic cast-in-place wall. In fact the use

of the enhanced lateral resisting system allow to reduce its thickness to 16 in (407 mm), while the conventional wall is 28 in (0.71 m) thick in order to reach the same seismic performance target. In-depth studies could be performed in order to understand the increase costs, in terms of material quantities and in-site labour, in comparison with the benefits provided by that self-centering structures.

Chapter 6

Conclusions and Future Developments

6.1 Introduction

The present research project studies the design and the analytical validation of unbonded post-tensioned hybrid concrete walls. The objective is to design structures that reach a specific target level of seismic performance, which requires not only that the collapse of a structure during an earthquake is prevented, but that the structure would be costly efficient as well, in terms of structural and non-structural repair and in terms of loss of business operation after the seismic event. In order to achieve this very strict performance level, superstructure and foundations have to remain essentially elastic during the seismic event. Moreover, the differential displacements should be small in order to limit damage of non-structural components, that however need to be designed to accommodate relative displacements. All these requirements imply the use of enhanced walls that perform an almost elastic behavior. One of them is the unbonded post-tensioned concrete walls with

mild reinforcement, studied into details in this project. However, alternative self-centering lateral resisting systems can be obtained. The common factor leading the design is the presence of post-tensioned tendons that elongate thanks to gap openings at the wall base. A configuration with post-tensioned tendons placed symmetrically in the wall combined with a bearing at the center of the wall could be interesting. Energy dissipation would be provided by lateral dampers devices, such as viscous dampers or friction dampers. This option will be explained and analyzed in a preliminary study in the following section.

Other possible configurations can be object of future developments of the present research.

6.2   Unbonded Post-Tensioned Concrete Wall With Central Bearing

Recent studies in earthquake engineering tried to limit permanent damage of structures and to ensure as fast as possible building reoccupation after the seismic event. As mentioned above, this requires an essentially elastic behavior of superstructure and foundation, and can be achieved with the employment of self-centering concrete wall. An interesting configuration is the one that combined the use of prestressed tendons placed symmetrically in the wall with a bearing at the center. The bearing constrains the translations of the wall while allows the rotations in all directions. In this way it fixes the center of rotation of the wall and consents to place the PT tendons in the outsider region of the wall. This layout avoids the problem of congestion at the base of the wall because the concrete doesn't react and therefore the confinement is no more required as well as the ED rebars at the base are
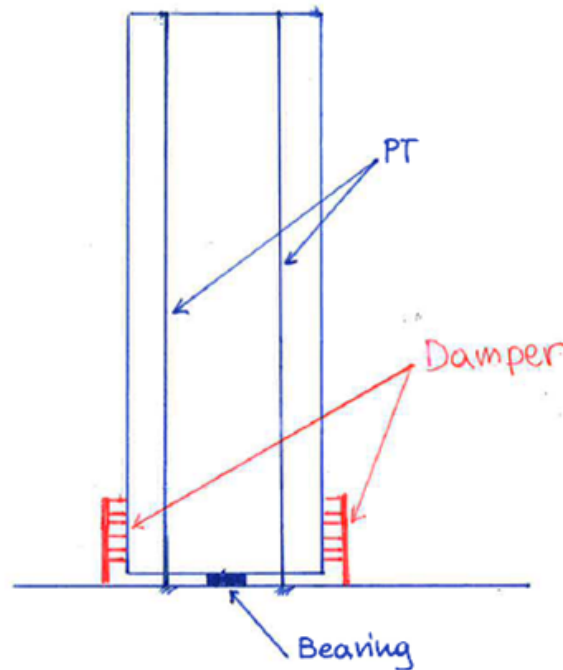
Figure 6.1: Configuration of unbonded post-tensioned concrete wall with central bearing

not needed. The arrangement of the PT tendons is more free and a more eccentric position from the center of the wall produces an higher self-centering capacity with respect to the eccentricity of $e_p = 3.28 \, \text{ft} \, (1.00 \, \text{m})$ previously taken into consideration. On the other hand, the presence of the bearing at the wall centerline constrains the length of the neutral axis to be equal to half of the total wall length, decreasing the deformation of the PT steel. In this way the possibility to yield is avoided, but more tendons are maybe required to provide enough clamping force.

The proposed wall configuration is illustrated in Fig. 6.1.

The dimensions of the wall taken into consideration are similar to what

considered previously, that are: wall height $h_w = 162.5\,\mathrm{ft}(49.53\,\mathrm{m})$, wall width $l_w = 37.5\,\mathrm{ft}(11.43\,\mathrm{m})$ and wall thickness $t_w = 26\,\mathrm{in}\,(0.66\,\mathrm{m})$. The PT tendons are placed at $11.8\,\mathrm{ft}$ ($3.6\,\mathrm{m}$) from the wall centerline.

6.2.1   Viscous Damper Design

In the previous chapter it was demonstrated that the DDBD method allows an optimization in the design of the wall. According to this seismic design procedure, a key parameter for the evaluation of the base forces is the estimate of the damping amount. In this case the wall behaves as previously like a rigid block, resulting in a linear design displacement profile that can still be defined with geometrical considerations assuming a new position of the center of rotation. As it will be presented later, the energy dissipated by the viscous damping devices (VDDs), and therefore the damping coefficient, depends on their specific characteristics. The definition of the level of damping provided by the VDDs follows the recommendations of [21]. Since our intent is to determine the suitable damper for our case study, the inverse procedure is conducted. The level of damping is estimated according to the results of Chapter 5 using the DDBD procedure and it is the starting point for the definition of the required properties of the VDDs.

The function of a viscous damping device is to absorb earthquake energy, and thus it reduces or eliminates damage to the building when an earthquake occurs. A viscous damper is a mechanical device which softens the imposed displacement, turning it into a viscous friction. The resulting viscous force is proportional to the relative velocity between the two ends of the dampers, and it has opposite sign to the applied force. The output force can be either traction or compression. The resultant force will be smaller than the force applied to the device, and consequently the motion decreases. The force in

the VDD is determined by the equation $F = Cv^\alpha$, where C is the damping coefficient and α is the damping exponent. They are both properties of the VDD element.

The damping coefficient ξ_{eq} of a structure can be calculated with the equation:

$$\xi_{eq} = \frac{E_D}{4\pi E_{S0}} \tag{6.1}$$

where E_{S0} is the total available potential energy and E_D is the dissipated energy in one cycle under cyclic displacement.

For a multistory structure with multiple VDDs Eq. 6.1 becomes:

$$\xi_{eq} = \frac{\sum_i (E_D)_i}{4\pi \sum_j (E_{S0})_j} \tag{6.2}$$

where $(E_D)_i$ is the energy dissipated by the $i-th$ VDDs under one cycle of modal displacement and $(E_{S0})_j$ is the total potential energy of the $j-th$ floor.

The maximum potential energy can be calculated as equal to the maximum kinematic energy, and thus at each level it results to be:

$$E_{S0} = \frac{1}{2}M\dot{\phi}_{XY}^2 \quad \text{for translational mode shape}$$

$$E_{S0} = \frac{1}{2}I_{CM}\dot{\phi}_R^2 \quad \text{for rotational mode shape}$$

where M is the mass of the story diaphragm, I_{CM} is the mass moment of inertia of the story diaphragm about the center mass, $\dot{\phi}_{XY}$ is the modal translational velocity of diaphragm and $\dot{\phi}_R$ is the modal angular velocity of the diaphragm.

In detail, from the previous equations:

$$\dot{\phi}_{XY} = \omega\phi_{XY}$$

$$\dot{\phi}_R = \omega\phi_R$$

where $\omega = 2\pi/T$ with T in the period of the mode considered, ϕ_{XY} is the modal translation displacement of diaphragm and ϕ_R is the modal rotation of diaphragm.

The dissipated energy in a VDD can be calculated by:

$$E_D = \pi C \omega \phi^2 \tag{6.3}$$

where ω is the modal deformation of VDD.

As previously said, in the present case study we start from the estimate of the equivalent viscous damping and with it the required characteristics of the VDD are identified. The value of EVD coefficient was estimate to be equal to the one provided earlier by the ED steel and thus equal to $\xi_{eq} = 12.44\%$, that take into account the hysteretic damping.

The same area of PT steel needed for the previous case (Chapter 5) is considered, i.e. $A_{pt} = 5.66 \, \mathrm{in}^2 \, (3652 \, \mathrm{mm}^2)$ at each side that results in 37 tendons. With this assumption on the PT area, it is possible to build an analytical model of the wall with ETABS 2015 which resembles the model defined in Chapter 5. The model will be briefly described later and allows to compute the fundamental period of the wall and the modal translational displacement. In a first analysis it is possible to compute the displacement that should be softened by the dampers placed at each side of the wall. With all these information it is possible to define the damping coefficient C inverting the equation proposed by [21]. The value of the calculated damping coefficient is $C = 199.24 \, \mathrm{kip \, s/in} \, (34\,891.88 \, \mathrm{kN \, s/m})$.

Table 6.1: ETABS Model Enhanced Wall- Properties of the Components

Component	Property	Value			
		USCS		SI	
Wall Member	Elastic Mod. E_c	3605	ksi	24.855	GPa
	center of compr.	84.375	in	2.143	m
PT Links	Stiffness k_{PT}	82.74	kip/in	14 489.6	kN/m
	Post-Yield Ratio	0.02		0.02	
	Yield Force $F_{y,pt\,T}$	543.04	kips	2415.55	kN
	Yield Force $F_{y,pt\,C}$	2231.99	kips	9928.40	kN
VDD Links	Stiffness k_{vdd}	10 000	kip/in	1 751 268	kN/m
	Damping C	199.24	kip.s/in	34 891.88	kN.s/m

6.2.2 Analytical Model

The analytical model already developed in the previous section has been implemented for unbonded post-tensioned concrete walls with central bearing. The differences are that the ED links are no more presents and the foundation links are substituted with a restrain placed at the wall centerline that fixes vertical and horizontal displacements. The VDD is modeled with the ETABS link properties of "damper exponential". These links are vertically placed outside the wall panel and they are connected to the wall member thanks to rigid links that extend horizontally from the wall. To be more clear, the characteristics of all the elements that compose the analytical model are summarized in Table 6.1. The masses and the ground accelerations have been taken into consideration making reference to Chapter 5. The stiffness of the VDD links is evaluated so that the loop during a ground motion tends to be a perfect ellipse. In this way the absence of storage stiffness makes that the natural frequency of a structure incorporated with the damper remain the same. This advantage simplifies the design procedure for a structure with supplemental viscous damping devices.

The proposed analytical model has been used for the calculation of the required damping C that the viscous damping devices should provide during the ground motion in order to soften the structural response. Nonlinear time-history analysis have been performed in order to evaluate the global behavior of the lateral resisting system, in terms of evolution in time of the horizontal displacement of the top level. Fig. 6.2 shows the top displacement without any dissipating devices (solid line) and the with the VDDs previously designed (dashed line), during the Loma Prieta ground motion. It is possible to see that the VDDs soften the global response. In fact:

- the maximum displacement is reduced from 28.73 in (730 mm) to 19.26 in (489 mm), that is below the target limit of 19.49 in (495 mm);

- after 36 sec (when the earthquake stops) the top displacement with the devices is negligible, while in the other case it is considerable and it continues oscillating around zero. This means that without VDDs the system doesn't have enough dissipation.

However, it must be specify that there is no possibility to validate the results since there aren't any previous researches on unbonded post-tensioned walls with central bearing. For the moment it is a good estimate for the definition of C and the predicted roof displacements during a ground motion, but it could not be considered reliable for more detailed analysis. The validation of an analytical model for the study of this design option could be part of further studies.
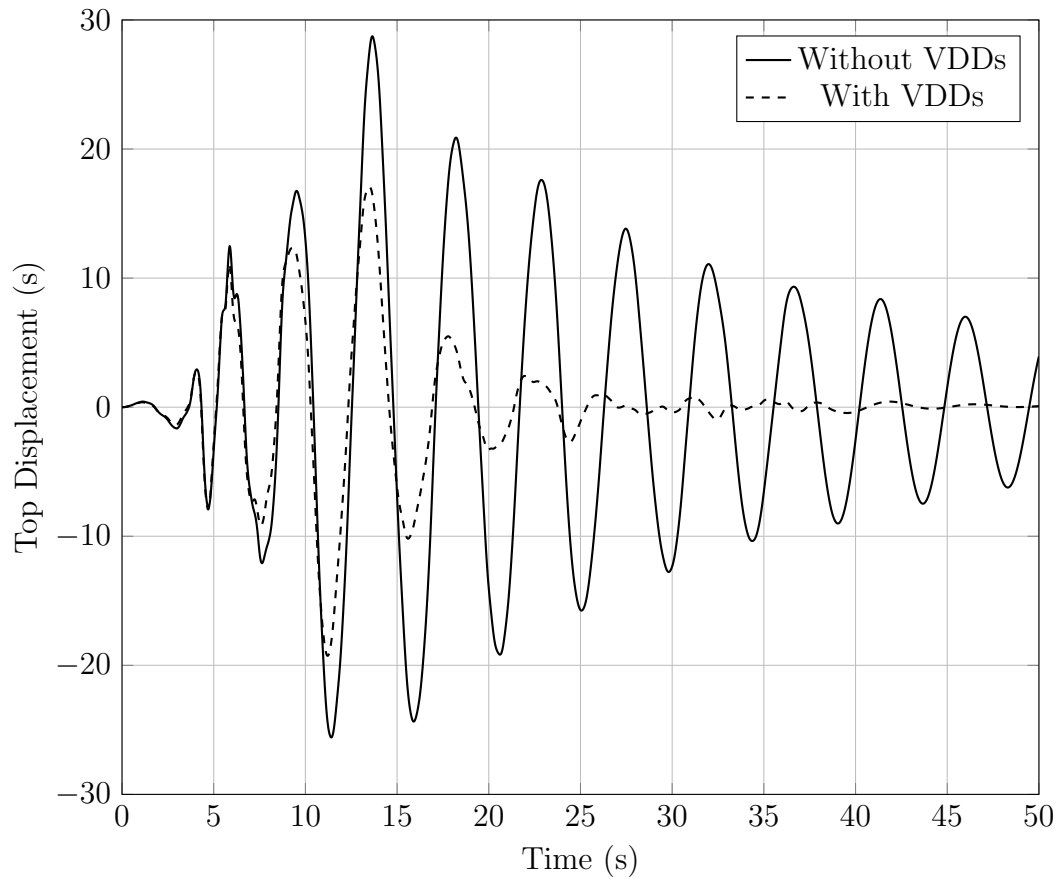
Figure 6.2: Influence of viscous dampers in the displacement response

6.3 Conclusions

The present work allows to make some considerations about the seismic design and behavior of the self-centering walls. First of all it is possible to see that the Direct Displacement-Based Design takes into account the characteristics of the system and thus it seems to be more suitable in case of particular structural systems. Moreover, it allows an optimization of the wall design since it produces design forces that are lower than those resulting from the Force-Based Design.

Another conclusion comes from considerations on the family of self-centering

walls. For this kind of wall a key aspect is to have a rocking behavior ensuring the permanence of the wall in the elastic field. On the other hand, the structure does not provide any dissipation of the energy produced by an earthquake, that need to be softened. This implies the presence of additional energy dissipation devices that can consist in mild reinforcement or external viscous dampers as seen in the present work. The rocking behavior is ensured by the PT tendons and the self-weight of the wall, which provide the self-centering forces. In order to obtain the expected performance of the wall, it is fundamental that the PT steel do not yield and thus that it is not subjected to excessive elongations. On the other hand, if the location of the PT tendons is close to the extremity of the wall, the self-centering capacity of the structure is improved. Another fundamental aspect is the confinement of the wall base, especially of the wall toes, in order to prevent nonlinear crushing of concrete and limit the nonlinearity at the gap opening at the base.

Where mild reinforcement is used as energy dissipation system, this soften the wall response through its deformation and so it needs to be placed with the adequate eccentricity from the center in order to dissipate the required energy. This requirement introduces the problem of steel congestion at the base and thus constraints the locations the PT and ED steel. Whereas the employment of lateral viscous dampers remove this issue and gives more freedom in the location of the PT steel. The combination of the viscous dampers with a bearing at the center of the wall allows the location of the tendons in the outer part of the wall providing an high degree of re-centering force. However, the design of this kind of bearing could be impracticable, since it should support the whole shear force and axial force applied at the base of the wall. It should be part of more detailed analysis of this kind of

structures.

Making a cost comparison, the configuration with PT and mild reinforcement is a well known construction typology and results to be more economic. It is largely investigated and a defined design procedure has been developed. In the Direct Displacement-Based Design the structural system of hybrid wall or hybrid frame was empirically studied, providing specific equations for the calculation of the equivalent viscous damping coefficient. Whereas, configurations with damper devices, such as the PRESSS test building, need the estimate of the required level of damping, that has to be verified with non-linear analysis.

Concerning the analytical validation of the resisting system, it has been proved that it can be modeled using ETABS 2015, a well-known and commercially available finite element software. In fact, the model created in order to reproduce the results obtained from the PRESSS research project meets this objective with a good approximation. The pushover analysis reproduces the strength of the system at design displacement with 10 percent of approximation. This is due to uncertainties related to the definition of the properties of the U-shaped flexural plates from the PRESSS reports. This result can be considered highly satisfactory. Later, the application of these modeling assumptions to an unbonded post-tensioned hybrid wall is able to reproduce its expected behavior of the structure and to verify the damping level resulting from the DDBD that is a key aspect of the DDBD procedure. Inelastic time history analysis show a negligible residual displacement after the seismic event that proves the self-centering capacity of the wall. It can be seen through the evolution in time of the lateral displacement or the hysteretic loop, that shows the expected flag shape behavior with no residual displacement.

6.4   Future Developments

The investigation of self-centering walls introduces some questions that wasn't taken into consideration in this research study. Here it was considered the behavior of a single structural wall. When this single wall is integrated in the entire building, its behavior is influenced by the interaction with the other components, like walls and flooring systems. Since the wall displaces in the earthquake direction, it is important to study torsional effects that come from the interaction with walls that form the lateral resisting system in the orthogonal direction. It could be interesting to study how to develop this technology to core-shaped lateral load resisting systems. It could be necessary to create a joint between the walls that unconstrains the relative displacement between them. Another tricky aspect is to ensure that the floor system do not cracks during the wall displacement due to the uplift.

Furthermore, the influence of the foundation behavior on the wall response as well as the prevention of shear slip was neglected in the present work and need future investigations. In particular, the prevention of shear slip that is a basic feature of the proper operation of the gap opening at the wall base. The employment of shear keys could be an interesting way to avoid this phenomenon, but it has to be studied into details in order to understand how to design them and how to avoid their crushing during the seismic events. The design concept for this configuration is shown in Fig. 6.3.

The study of other wall configurations can be explored in future projects. In fact, the self-centering walls can be combined with various kind of damping devices and they can be built in different configuration. An example is presented in Sec. 6.2, even if the design of the bearing at the wall base should be object of further investigations. Another possibility could be the coupling
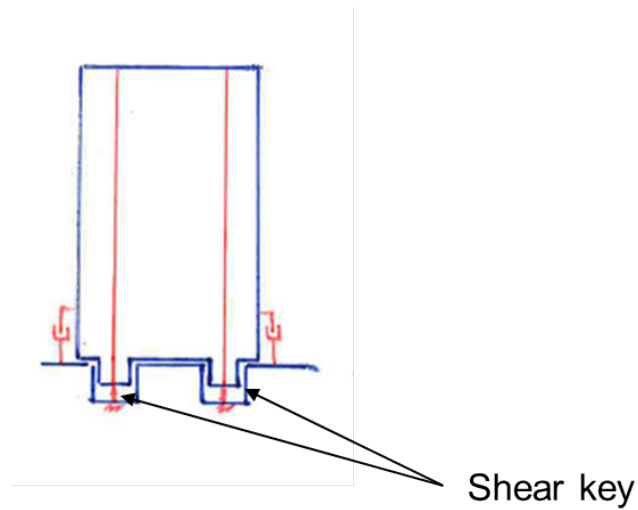
Figure 6.3: Self-centering wall with shear keys

of two adjacent walls through link beams, designed to dissipate energy (see
Fig. 6.4). For the coupled walls, the energy dissipation is provided by the
formation of plastic hinges at the ends of the beams. Moreover, the presence
of two walls implies a small eccentricity of the PT steel avoiding excessive
elongations and producing two re-centering moments instead of one. This
kind of self-centering wall has been already studied in literature and it could
be interesting to see their application to the present case study in order to
understand which configuration could be the most suitable.

Finally, only the preliminary design of self-centering lateral resisting sys-
tems has been investigated in this research and all the problems related to
their realization are avoided. For example, the compressive strains at the wall
toes are very high because when the gap opens the entire value of axial load
is supported by them. The confinement should be designed in detail, check-
ing that it is feasible for the high congestion of tendons and rebars present
at the base. Finally, even if the proposed shearwalls lead to better results

than those of a conventional reinforced concrete wall, with a cost comparison it could be interesting to understand if they are a valid alternative in the design phase.

Figure 6.4: Coupled self- centering walls

List of Figures

List of Tables

Bibliography

[1] Baird A., Smith T., Palermo A., Pampanin S., *Experimental and numerical Study of U-shape Flexural Plate (UFP) Dissipators*, Conference of New Zealand Society For Earthquake Engineering (NZSEE), Aukland, Paper No P2, 2014.

[2] Chancellor N.B., Eatherton M.R., Roke D.A., Akbas T., *Self-Centering Seismic Lateral Force Resisting Systems: High Performance Structures for the City of Tomorrow*, Buildings Journal, 18/09/2014.

[3] Conley J., Sritharan S., Priestley M.J.N., *Precast Seismic Structural Systems PRESSS-3: the Five-Story Precast Test Building vol. 3-j: Wall Direction Response*, University of California San Diego, Final Report Submitted to the Precast/Prestressed Concrete Institute, July 2002.

[4] Henry R.S., *Self-centering Precast Concrete Walls for Buildings in Regions with Low to High Seismicity*, PhD Thesis, Department of Civil and Environmental Engineering, The University of Auckland, 2011.

[5] Kurama Y.C., *Seismic Analysis, Behavior and Design of Unbonded Post-Tensioned Precast Concrete Walls*, PhD Thesis, Department of Civil and Environmental Engineering, Lehigh University (Bethlem, Pennsylvania), 1997.

[6] Kurama Y.C., Pessiki S., Sause R., *Seismic Behavior and Design of Unbonded Post-Tensioned Precast Concrete Walls*, PCI JOURNAL, May-June 1999, pp. 72-89.

[7] Kurama Y.C., *Unbonded Post-Tensioned Precast Concrete Walls With Supplemental Viscous Damping*, ACI Structural Journal, vol 97, 2000, pp. 648-658.

[8] Kurama Y.C., *Hybrid Post-Tensioned Precast Concrete Walls For Use in Seismic Regions*, PCI JOURNAL, September-October 2002, pp. 36-59.

[9] Kurama Y.C., *Seismic Design of Partially Post-Tensioned Precast Concrete Walls*, PCI JOURNAL, July-August 2005, pp. 100-125.

[10] Nakaki S.D., Stanton J.F., Sritharan S., *An Overview of the PRESSS Five-Story Precast Test Building*, PCI JOURNAL, March-April 1999, pp. 26-39.

[11] Nicknam A., Filiatrault A., *Direct Displacement-Based Seismic Design of Propped Rocking Walls*, Earthquake Spectra, vol 31 No. 1, 2015, pp. 179-196.

[12] Panian L., Steyer M., Tipping S., *Post-Tensioned Concrete Walls For Seismic Resistance*, PTI JOURNAL, vol 5 No.1, July 2007, pp. 7-16.

[13] Panian L., Steyer M., Tipping S., *Post-Tensioned Shotcrete Shearwalls*, American Concrete Institute, vol 29 No.10, October 2007, pp. 43-49.

[14] Priestley M.J.N., *Performance-Based Seismic Design*, 12th World Conference on Earthquake Engineering, Aukland, No. 2831, 2000.

[15] Priestley M. N., Amaris, A. D., *Dynamic Amplification of Seismic Moments and Shear Forces in Cantilever Walls*, IUSS Press, 2002.

[16] Priestley M.J.N., *Direct Displacement-Based Design of Precast/Prestressed Concrete Buildings*, PCI JOURNAL, November-December 2002, pp. 66-79.

[17] Priestley M.J.N., Calvi G.M., Kowalsky M.J., *Displacement-Based Seismic Design of Structures*, IUSS Press, Pavia, 2007.

[18] Rahman M.A., *Performance-Based Seismic Analysis And Design Improvements Of Two Precast Concrete Structural Systems*, Retrospective Theses and Dissertations, Iowa State University, 2008.

[19] Rahman M.A., Sritharan S., *Force-Based vs. Displacement-Based Design of Jointed Precast Prestressed Wall Systems*, Civil, Construction and Evironmental Engineering Technical Report, Paper No. 6, Iowa State University, 2011.

[20] Reitherman R.K., *Five Major Themes In the History of Earthquake Engineering*, 15th World Conference on Earthquake Engineering, Lisbon, Portugal, 2012.

[21] Sarkisian M., Lee P., Garai R., Tsui A., *Controlling Wind in Tall and Flexible Structure With Viscous Damping Devices*, SEAOC 2015 Convention Proceedings, 2015.

[22] Smith R.S.H, Tso W.K., *Inconsistency of Force-Based Design Procedure*, JSEE, Vol.4 No.1, 2002.

[23] Smith B.J., Kurama Y.C., McGinnis M.J., *Hybrid Precast Wall Systems For Seismic Region*, Structural Engineering Research Report, University of Notre Dame (Notre Dame, Indiana), 2012.

[24] Smith B.J., Kurama Y.C., McGinnis M.J., *Seismic Design Guidelines for Special Hybrid Precast Concrete Shear Walls*, Structural Engineering Research Report, University of Notre Dame (Notre Dame, Indiana), 2012.

[25] Sritharan S., Priestley M.J.N., Seible F., Igarashi A., *A Five-Story Precast Concrete Test Building For Seismic Conditions - An Overview*, 12th World Conference on Earthquake Engineering, Aukland, No. 1299, 2000.

[26] Sritharan S., Pampanin S., Conley J., *Precast Seismic Structural Systems PRESSS-3: the Five-Story Precast Test Building vol. 3-03: Design Verification, Instrumentation & Test Procedures*, Final Report Submitted to the Precast/Prestressed Concrete Institute, December 2002.

[27] Stanton J.F., Nakaki S.D., *Precast Seismic Structural Systems PRESSS-3: the Five-Story Precast Test Building vol. 3-09: Design Guidelines For Precast Concrete Seismic Structural Systems*, The University of Washington and The Nakaki Bashaw Group, Inc., February 2002.

[28] Stevenson M., Panian L., Korolyk M., Mar D., *Post-Tensioned Concrete Walls and Frames for Seismic-Resistance A Case Study of the David Brower Center*, SEAOC 2008 Convention Proceedings, 2008.

[29] *CSI Analysis Reference Manual For SAP2000, ETABS, SAFE and CSiBridge*, Computer & Structures Inc., Berkeley (California), 2015.

[30] ASCE 7-10. *ASCE/SEI 7-10: Minimum Design Loads For Buildings and Other Structures*, American Society of Civil Engineers, 2010.

[31] EN 1998. *Eurocode 8: Design of structures for earthquake resistance*, European Committee for Standardisation (CEN), 2005.